UNIVERSITÀ DEGLI STUDI DI PADOVA

Università degli Studi di Padova

Dipartimento di Ingegneria Industriale DII

Corso di Laurea Magistrale in Ingegneria Meccanica

Comparative analysis of Ski Edge Load Distribution in different Slalom disciplines and correlation with real skiing loads

Relatore

Prof. Nicola Petrone

Co-relatori

Prof Vittorio Quaggiotti

Ing. Giuseppe Zullo

Laureando

Leonardo Barioli

2018711

Anno accademico 2022/2023

Abstract

As a skier makes his way down the mountain, an intense load interaction takes places between the snow and the skis and between the skis and the skier. All these loads are generated to counterbalance the skier weight and the inertial forces that occurs during the descent. This study aims to explore the loads acting while skiing at the snow - ski interface and at the ski - leg interface with a combination of laboratory-based experiments and field-based Slalom and Giant Slalom measurements. Through a dedicated testbench, the Edge Load Profile of different skis will be determined and confronted. Then In field data will be analyzed with a general method and the global Ground Reaction forces and the Center of Pressure trends will be determined. Finally, the real skiing loads measured during Slalom and Giant Slalom in field test sessions will be confronted with the loads applied at the testbench to see if there is correlation between the two.

Index

1. Introduction

Skiing is a popular winter sport that has been enjoyed by people around the world for decades. It is also a competitive sport that has been featured in the Winter Olympics since 1924. As a skier makes his way down the mountain, an intense load interaction takes places between the snow and the skis and between the skis and the skier. All these loads are generated to counterbalance the athlete's weight and the inertial forces that occurs while skiing.

Given the popularity of skiing, it is important to better understand these mechanisms of load transferring. Especially in a competitive environment, a better understanding of these mechanism can contribute to improve the skis characteristics and the athlete's training program. If the loads acting on the ski length are known, the ski construction can be modified to better suit the athlete's needs, stiffening it in some places and softening it in other. On the other hand, the loads between the skis and the athlete are related to the engagement of the quadriceps femoris. The knowledge of these loads can highlight any asymmetry among the two legs or the same leg in left and right turns. This can be used to improve the athlete's preparation, by identifying areas of strength and weakness and by creating specific training programs aimed to reduce these asymmetries.

This study aims to explore the entity and the distribution of the loads acting while skiing between the snow and the skis and between the skis and the athlete's leg.

Load measurement at the ski - snow interface was done using the Edge Load Profile testbench in the University of Padova laboratory. Through the testbench the edge load distribution of the ski at different ski inclinations and applied loads can be determined. This allows to see how a ski transfers the load to the ground. Different skis were tested on the ELP testbench at variable angles and corresponding loads that match real skiing loads. The results will be compared to understand how the inclination, the geometry and the construction affects the ski Edge Load Distribution.

The loads at the ski - leg interface were measured with loadcells placed between the skis and the front and rear bindings. Three in vivo outdoor test sessions were performed.

In these test sessions, professional athletes skied on different Slalom and Giant Slalom courses. Collected data was then analyzed with a general method that will be presented in chapter 4. With this method the Global Ground Reaction Forces and the Center of Pressure trends were determined. By comparing the results of the different test sessions, this study will provide insights into the forces involved in different slalom disciplines.

The combination of laboratory-based experiments and field-based measurements will provide interesting information on the way the ski and the skier behaves during the performance. This information will confirm or deny conclusions based on skiing experience and perceptions.

Ultimately, the real skiing loads measured during Slalom and Giant Slalom in-field test sessions will be confronted with the loads applied at the testbench to see if there is correlation between the two. This will establish if the Edge Load Profile measured at the testbench is representative or not of the ski conditions during the competitive performance.

The findings of this study will be relevant not only to athletes and ski instructors but also to ski manufacturers and researchers in the fields of sports biomechanics, sports medicine, and performance enhancement.

2. Materials and instrumentations

Different skis, loadcells and acquisition systems were used for the study. The combination of these three elements brought to multiple configurations used to run the in vivo and in vitro tests. In this chapter all the different setup configurations will be presented and validated.

2.1. Skis and bindings

Two pair of skis were used for the study. These were the *Blizzard Firebird GS* 188 cm skis for the Giant Slalom (2.1) and the *Nordica Dobermann SLWC* 165 skis for the Slalom (Figure). Both skis were equipped with *Marker WC PC* interface plate (Figure 2.3) and *Marker Comp 20.0 EPS* bindings (Figure).

Figure 2.1. Blizzard Firebird GS 188 cm skis with Marker WC PC interface plate

Figure 2.2. Nordica Dobermann SLWC 165 skis with Marker WC PC interface plate

Figure 2.3. Marker WC PC interface plate

Figure 2.4. Marker Comp 20.0 EPS bindings

The technical specifications of the 2 pair of skis and of the plates are reported on *Table 2.1*.

	Discipline	*Length [cm]*	*Sidecut/Width [cm]*	*Construction*	*Turn Radius [m]*
Blizzard Firebird GS	Giant Slalom	188	100.5 - 65.5 - 87	Sandwich Compound Sidewall (R.&D.)	>30
Nordica Dobermann SLWC	Slalom	165	115 - 66 - 102	Energy 2 TI	>11.8 on front >12.1 on rear
Marker WC PC	Any	54.2	5.9	/	/

Table 2.1. Technical specifications of skis and interface plate

Moreover, along this study another pair of skis was used. These skis were a Nordica prototype whose specifications are not available (*Figure 2.5*). A wood superstructure designed by Professor Vittorio Quaggiotti is hinged on one of the two skis (*Figure 2.6*). This superstructure, on which the frontal binding is mounted, modifies the load distribution on the ski edge providing support along the whole ski length. As a result, the behavior of the ski during turns improves. All of this will be further seen in Chapter 4.

Figure 2.5. Nordica prototypes. On the top the standard unmodified ski, on the bottom the modified ski

Figure 2.6. Close up on the superstructure of the modified ski.

2.2. Load cells

Four M3564F1 loadcells by *Sunrise Instruments* were used to measure the loads acting between the bindings and the ski interface plate. These are low-profile 6 axis circular force and torque load cell. Geometrically, each load cell is shaped like a steel cylinder with a diameter of 65 mm, height of 10 mm and a weight of 0.190 kg. The three components of forces and moments are measured with reference to the cylinder axis (Z) and two radial orthogonal axes (X, Y). The selected load transducer has full scale force of 2500 N in X, Y axes and 5000 N in Z axis, full scale moment of and 200 Nm in X, Y axes and 100 Nm in Z axis. The data sheet of the load cell is reported in *Figure 2.7*.

The 4 loadcells used in the study are:

- Serial N° SN13827;
- Serial N° SN13828;
- Serial N° SN13829;
- Serial N° SN15029.

Each load cell provides output from 6 independent full Wheatstone bridges. In order to obtain the forces and moments in the reference system of the transducer, these signals, collected in mV, are firstly divided by the voltage of the power supply which typically is 5 V. This operation changes the unit of measure of the 6 channels from mV to mV/V. The channels in mV/V are then multiplied by the calibration matrix to obtain F_X, F_Y, F_Z [N] and M_X, M_Y, M_Z [Nm] in the reference system of the cell. The relation to use is the following, assuming that ch_i and F_i, M_i are column vectors containing an element for each collected sample:

$$[F_X \quad F_Y \quad F_Z \quad M_X \quad M_Y \quad M_Z] = ([C] \cdot [ch_1 \quad ch_2 \quad ch_3 \quad ch_4 \quad ch_5 \quad ch_6]^T)^T$$

The calibration matrices $[C]$ are provided by the manufacturer and are reported in the following pages. The loadcell SN13828 was damaged and later repaired by the manufacturer which recalibrated it and provided the new calibration matrix. For data acquired before the 11th of March 2022, $[C_{SN13828}]$ calibration matrix must be used. For data acquired later $[C_{SN13828}]^*$ must be used.

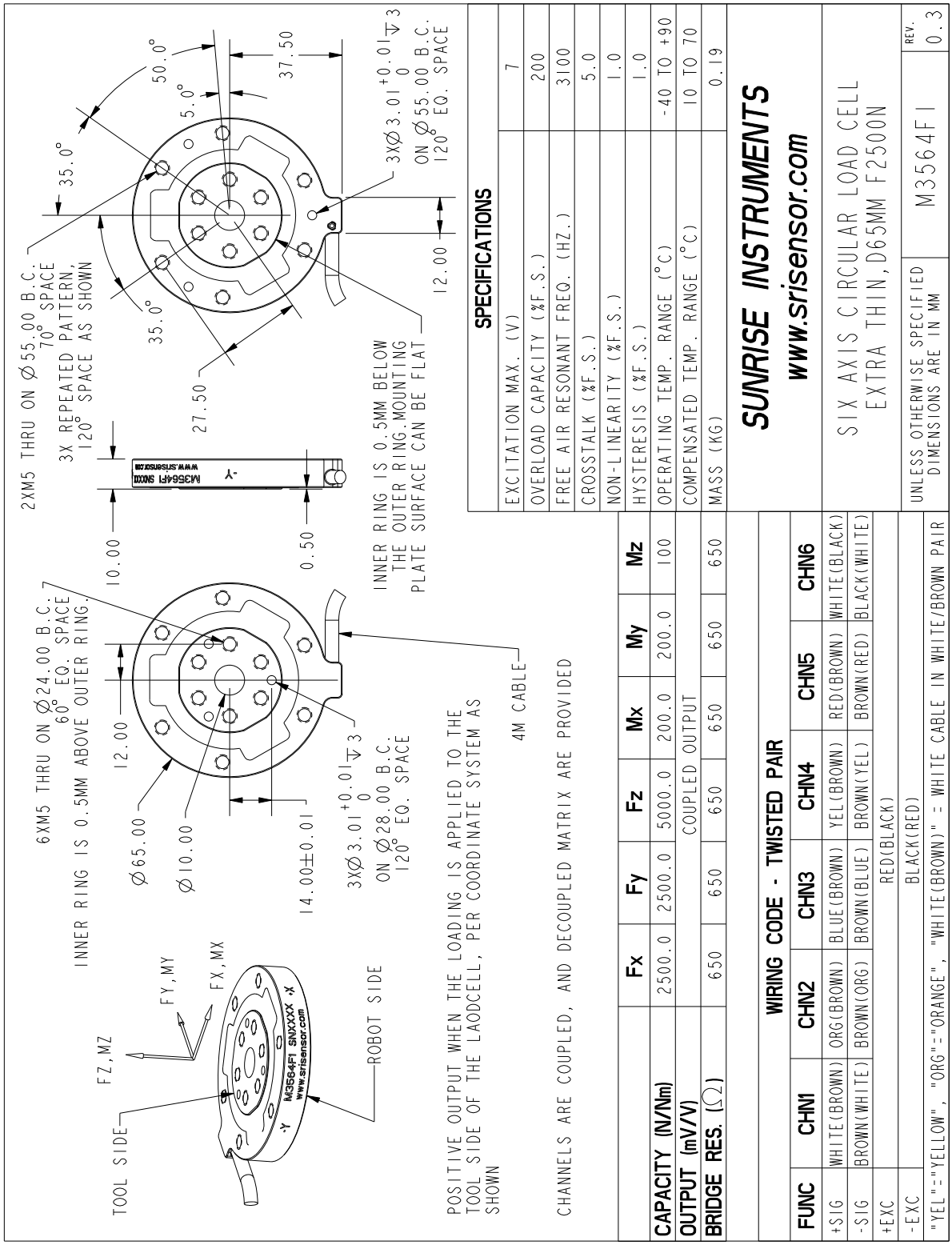

Figure 2.7. Data sheet of M3564F Load cells by Sunrise Instruments

SN13827 calibration matrix

$$[C_{SN13827}] = \begin{bmatrix} 10.2812 & -1.3081 \cdot 10^3 & 18.9952 & 15.8939 & -12.3145 & 1.2892 \cdot 10^3 \\ -33.8824 & 746.4845 & -11.2234 & -1.5265 \cdot 10^3 & 20.3664 & 754.1553 \\ -816.7397 & -10.8262 & -799.6647 & -4.0241 & -816.4005 & -6.5547 \\ 16.6526 & 0.0499 & 0.1775 & 0.0045 & -16.6111 & -0.3466 \\ -9.4654 & 0.1781 & 19.6322 & 0.0939 & -9.6619 & -0.0027 \\ -0.1165 & -20.2448 & 0.0059 & -20.6359 & 0.1055 & -20.7037 \end{bmatrix}$$

SN13828 calibration matrix

$$[C_{SN13828}] = \begin{bmatrix} 16.1339 & -1.3179 \cdot 10^3 & 11.9077 & 34.5778 & 0.5781 & 1.3000 \cdot 10^3 \\ -29.7976 & 775.8834 & -10.5230 & -1.5369 \cdot 10^3 & 31.6552 & 763.1357 \\ -805.8461 & -8.3500 & -828.3296 & -5.9820 & -823.3692 & -8.9155 \\ 16.7871 & 0.5249 & 0.1148 & -0.0658 & -16.9362 & -0.0709 \\ -9.5992 & -0.2174 & 20.0961 & 0.0453 & -9.6538 & -0.1043 \\ -0.1225 & -20.4818 & 0.2201 & -20.7976 & -0.2238 & -21.7562 \end{bmatrix}$$

SN13828 calibration matrix after repair

$$[C_{SN13828}]^* = \begin{bmatrix} 12.3775 & -1.3333 \cdot 10^3 & 10.5391 & 34.4201 & -8.8761 & 1.3082 \cdot 10^3 \\ -39.9064 & 798.4357 & -24.7122 & -1.5519 \cdot 10^3 & 22.8368 & 756.8341 \\ -810.0989 & -12.8909 & -835.7341 & -19.5988 & -832.7382 & 9.6856 \\ 16.4570 & 0.6791 & -0.1002 & -0.2487 & -17.3094 & 0.1688 \\ -9.4205 & 0.7183 & 20.0769 & 0.3110 & -9.7096 & -0.4014 \\ -0.2979 & -19.7793 & 0.1593 & -20.5523 & -0.0337 & -22.2419 \end{bmatrix}$$

SN13829 calibration matrix

$$[C_{SN13829}] = \begin{bmatrix} -5.1523 & -1.3299 \cdot 10^3 & 33.2533 & 24.2635 & -14.7065 & 1.2919 \cdot 10^3 \\ -29.6251 & 776.3958 & -6.4696 & -1.5311 \cdot 10^3 & 27.5223 & 756.4022 \\ -837.3353 & -20.0323 & -856.3873 & -9.4932 & -844.1284 & -5.3031 \\ 17.4557 & 0.3459 & 0.1831 & 0.0623 & -17.2548 & -0.2138 \\ -9.9916 & -0.1069 & 20.5139 & 0.2228 & -10.0826 & -0.0439 \\ -0.1535 & -20.4533 & -0.0695 & -20.5234 & -0.1822 & -21.1902 \end{bmatrix}$$

SN15029 calibration matrix

$$[C_{SN15029}] = \begin{bmatrix} -1.1694 & -1.4425 \cdot 10^3 & 38.9476 & 14.5324 & -14.2321 & 1.4351 \cdot 10^3 \\ -38.0291 & 832.5339 & -18.3823 & -1.7103 \cdot 10^3 & 33.9218 & 840.6121 \\ -853.2351 & -12.0894 & -868.3247 & -7.7220 & -856.4831 & -10.2401 \\ 17.0836 & 0.5417 & -0.1902 & -0.7417 & -17.7276 & 0.0064 \\ -9.7937 & -0.1698 & 21.1459 & 0.0694 & -9.8204 & 0.1270 \\ -0.2703 & -21.0196 & -0.0175 & -21.5452 & -0.1166 & -22.2918 \end{bmatrix}$$

When the physical channels of the cell are multiplied by the calibration matrix, a 6 columns matrix is obtained in which:

- column 1 contains F_X values;
- column 2 contains F_Y values;
- column 3 contains F_Z values;
- column 4 contains M_X values;
- column 5 contains M_Y values;
- column 6 contains M_Z values.

These are the load components in the reference system of each cell.

Along the study also a reduced system with 3 channels for each cell was used (chapter 5, subchapter 5.4). As will be seen in chapter 5: F_Z, M_X and M_Y load components are significantly higher than F_X, F_Y and M_Z. This, combined with the limit of the maximum channels simultaneously acquirable by the acquisition system, led to give up acquiring all physical channels and collecting only the ones responsible for F_Z, M_X and M_Y (channels 1, 3 and 5). In order to do this, the calibration matrix of every load cell was modified by replacing with zeros the values that define F_X, F_Y, M_Z and appropriately recalibrating the other values. This reduced system was used with data acquired after the repair of the SN13828 load cell so only the new calibration matrix was reduced.

SN13827^{RED} calibration matrix

$$[C_{SN13827}]^{RED} = \begin{bmatrix} 0 & 0 & 0 \\ 0 & 0 & 0 \\ -815.7812 & -798.4152 & -816.7704 \\ 16.5353 & 0.2390 & -16.7511 \\ -9.5146 & 19.6278 & -9.6941 \\ 0 & 0 & 0 \end{bmatrix}$$

SN13828^{RED} calibration matrix after repair

$$[C_{SN13828}]^{*\ RED} = \begin{bmatrix} 0 & 0 & 0 \\ 0 & 0 & 0 \\ -804.3546 & -826.3423 & -823.1831 \\ 16.6800 & 0.1566 & -17.0301 \\ -9.5675 & 20.1031 & -9.6349 \\ 0 & 0 & 0 \end{bmatrix}$$

SN13829^{RED} calibration matrix

$$[C_{SN13829}]^{RED} = \begin{bmatrix} 0 & 0 & 0 \\ 0 & 0 & 0 \\ -837.3353 & -856.3873 & -844.1284 \\ 17.3321 & 0.2115 & -17.3690 \\ -9.9838 & 20.5128 & -10.0615 \\ 0 & 0 & 0 \end{bmatrix}$$

SN15029^{RED} calibration matrix

$$[C_{SN15029}]^{RED} = \begin{bmatrix} 0 & 0 & 0 \\ 0 & 0 & 0 \\ -853.4989 & -864.7975 & -859.9961 \\ 17.1533 & -0.1775 & -17.7158 \\ -9.8293 & 21.1324 & -9.8508 \\ 0 & 0 & 0 \end{bmatrix}$$

When the physical channels of the load cell are multiplied by the reduced calibration matrix, a 6 columns matrix is obtained: column 3, 4 and 5 contain non-zero values (F_Z, M_X, M_Y) and the other three columns replace missing data of F_X, F_Y, M_Z with zeros. This allows a straightforward compatibility with softwares developed for the full matrix system.

2.3. Acquisition systems

In order to acquire the load cells signals, two acquisition systems were used. These were the *SoMat* and the *DTS Slice Nano*.

The *SoMat* eDAQ lite by HBM (Darmstadt, Germany) consists of one base processor layer and eight optional layers that can be added or removed as needed (*Figure*). Each layer is 17.3 cm wide and 11.7 cm deep and could collect up to four channels with simultaneously data sampling. Moreover, these layers have specialized hardware for strain gages signal conditioning (ELBRG) or general purpose analog data collection (ELHLS). The base layer is 7,3 cm tall while the additional layers are 1,7 cm tall. It can acquire data with a sample rate from 0.1 Hz to 100 kHz.

Figure 2.8. SoMat acquisition system with all the eight layers

DTS Slice Nano is a much newer and compact acquisition system, ideal for in field use (***Errore. L'origine riferimento non è stata trovata.***). As the SoMat its modular and user-configurable with its base module being 26 mm wide 31. mm deep and 8 mm tall. Each module collects up to three channels such as half and full Wheatstone bridges or analog input (up to 5 V). Each unit could acquire up to 24 channels at a sample rate

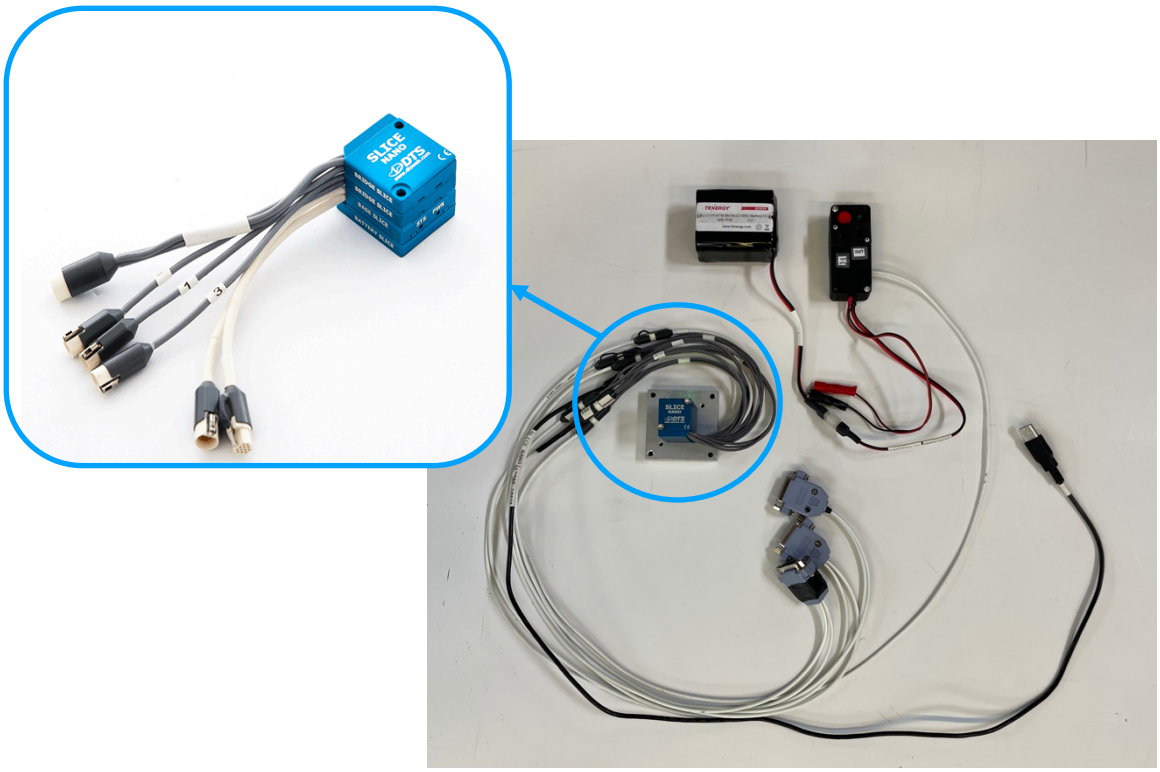

Figure 2.9. DTS Slice Nano acquisiton system in the configuration used in the outdoor tests

variable from 10 Hz to 500 kHz.

With the modules currently available at the University of Padova it is possible to acquire up to 18 channels.

Both acquisition systems can be used with a power cord attached to the electric outlet or with an external 12 V battery.

2.4. Ski preparation

The *Blizzard Firebird GS* 188 cm and the *Nordica Dobermann SLWC* 165 skis were equipped with the loadcells.

For both the *Blizzard* and the *Nordica*, on one of the skis, two load cells were installed between the ski plate and each front and rear binding. The two load cells were secured to custom made aluminum 7075 alloy plates to interface with the ski and the bindings (*Figure 2.10*). Lower plates connect the load cells to the interface plate, while upper plates connect loadcells to the ski bindings. On the other ski, two dummy load cells were installed in the same position to match the bindings height (*Figure 2.11*) and load cell weight. On both the *Nordica* and the *Blizzard* the SN13828 cell was mounted under the front binding and the SN13829 cell under the rear binding.

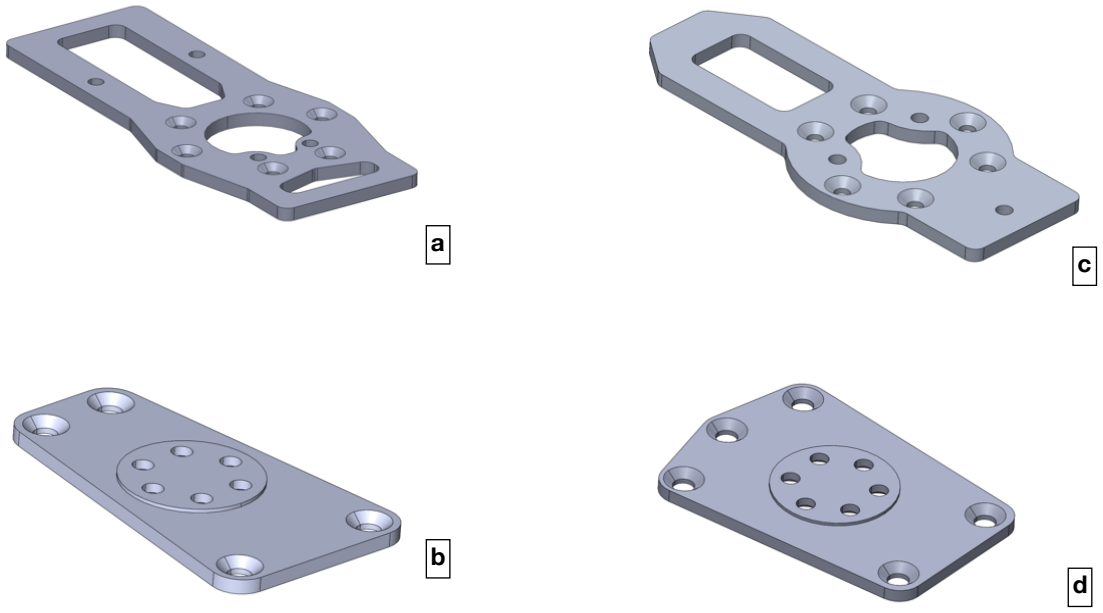

Figure 2.10. Rear top (a) and bottom (b) plates and front top (c) and bottom (d) plates

Figure 2.11. *Instrumented slalom Nordica Dobermann SLWC 165 cm skis with Marker WC PC interface plate and Marker* Comp *20.0 EPS bindings (a and b). Close up of the bindings on the instrumented ski (c) and the normal ski with the shims (d).*

The reference system of the ski was located on the ski center which is given by the constructor. The X axis follows the ski length pointing forward, the Z axis is normal to the ski plane pointing upwards and the Y axis points left completing the Cartesian coordinate system. The loadcells were mounted so that their reference system was aligned to the reference system of the ski (*Figure 2.12*). In this configuration the loads measured by the load cells are the ground reaction forces and ground reaction moments that the snow applies to the front and rear bindings. They are centered on the center of the load cells and are oriented as the global reference system of *Figure 2.12*.

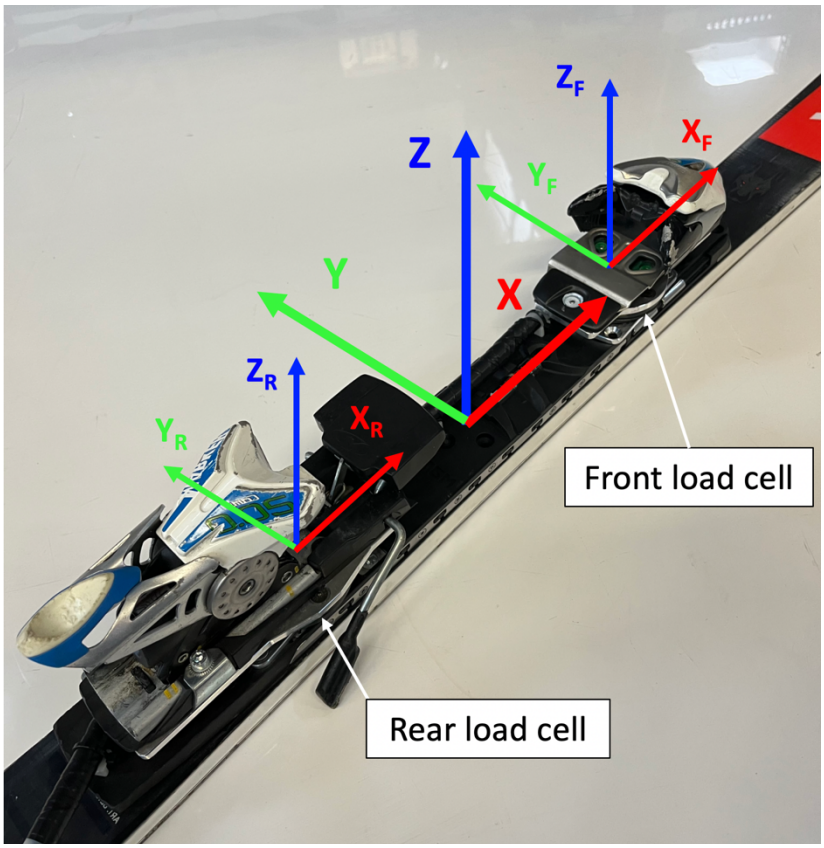

Figure 2.12. Ski and cells reference system

As a result, 2 sets of 6 forces and moments are acquired, one of the load cell under the front binding:

- column 1 for F_{XF};
- column 2 for F_{YF};
- column 3 for F_{ZF};
- column 4 for M_{XF};
- column 5 for M_{YF};
- column 6 for M_{ZF};

and one of the cell under the rear binding:

- column 1 for F_{XR};
- column 2 for F_{YR};
- column 3 for F_{ZR};
- column 4 for M_{XR};
- column 5 for M_{YR};
- column 6 for M_{ZR}.

Another setup used with the *Nordica SLWC* skis is with both skis equipped with load cells. In this setup the dummy load cells of the second ski were replaced with SN13827 cell on the front and SN15029 on the rear (*Figure 2.13*).

Figure 2.13. Instrumented Nordica Dobermann SLWC 165 cm skis

In this configuration, potentially, all the 24 load components (six for each binding) could be determined. However, using the lightweight system (DTS Slice Nano) this was not possible. Luckily, to determine the global GRF under each ski for the highest magnitude components (F_Z, M_X, M_Y), collecting only the three channels responsible for these load components for each load cell is still a viable option which introduces acceptable errors. This trick made possible to collect only 12 channels to determine the GRF under the two skis.

2.5. System validation

Before doing the field tests with athletes, some bench tests were carried out to verify the accuracy of the loadcells and of the whole assembled system.

Loadcell validation

The transducers accuracy was verified mounting each load cell on a structure through which it was possible to apply the load components independently (*Figure 2.14*). On the bottom, the loadcell was fixed to the structure, while on the top of the loadcell a vertical pole was mounted. The F_Z load was applied by stacking round calibrated weights with a center hole on the pole over the loadcell. The X and Y forces and moments were applied through a rope and pulley system. F_X and M_Y were applied by tying one side of the rope

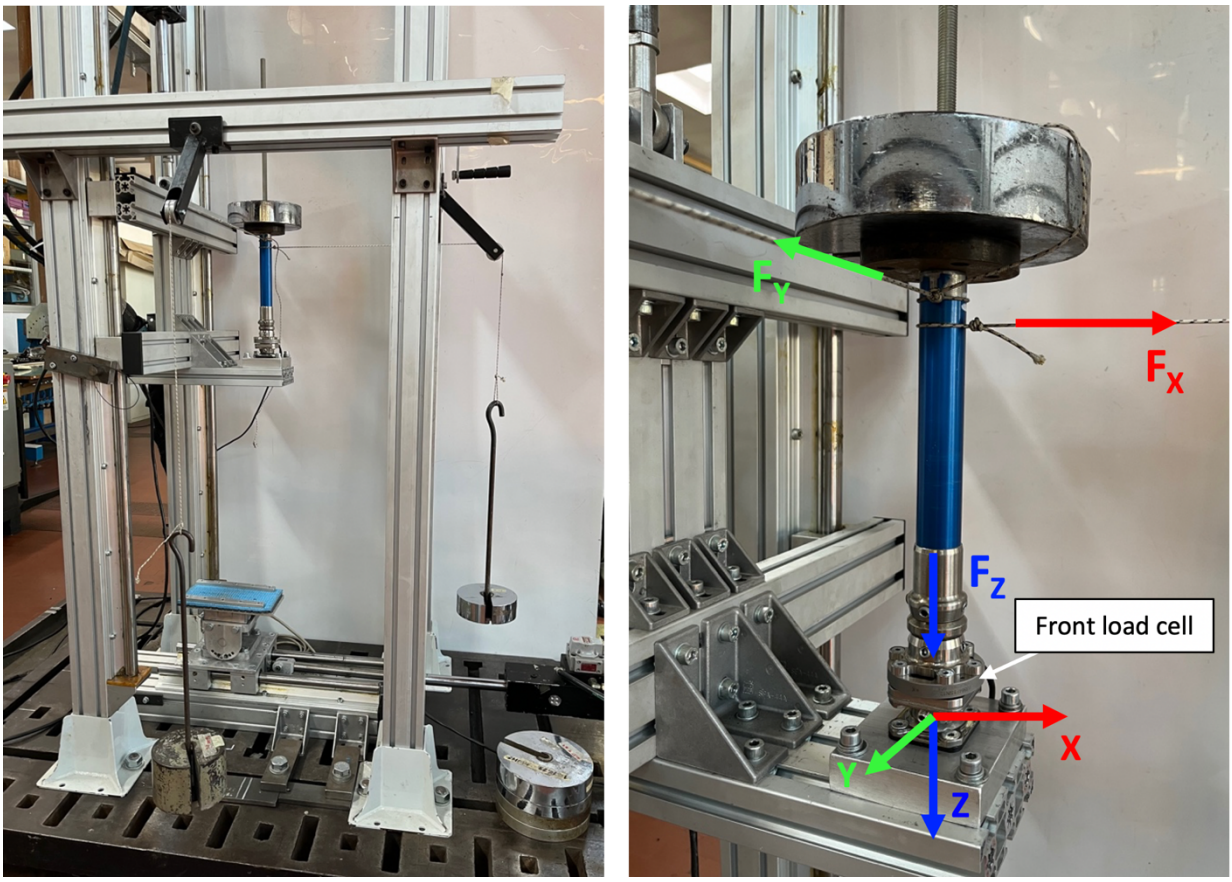

Figure 2.14. Load cell validation setup

around the pole so that when tensioned it was aligned with the X axis of the cell. The distance between this rope and the X axis of the cell was 23.8 cm. The rope was then tensioned through the pulley and another set of calibrated weights was suspended on its other end. This setup applied a F_X force which introduced also a M_Y moment given its 23.8 cm lever arm with respect to the load cell origin. The same thing was done for F_Y and M_X tying the rope so that when in tension it was aligned with the Y axis of the cell. The distance between this second rope and the Y axis of the cell was 22.3 cm. This applied simultaneously a F_Y force and a M_X moment with a lever arm of 22.3 cm. M_Z was not applied as it has a minor role in the study when compared to other load components.

The weight mass applied in the different directions are reported in *Table 2.2*:

	F_Z *[kg]*	*F_X and M_Y* *[kg]*	*F_Y and M_X* *[kg]*
1	13.40	10.23	6.28
2	9.20	9.18	10.25
3	13.85	9.20	6.18
4	10.25		6.17
5	11.20		6.17
6	10.25		
7	11.20		
tot	79.35	28.61	35.05

Table 2.2. Applied weights in the different directions

The numbers identify the order in which the weights were applied one above the other for each direction. Weights were then removed following the opposite order until the load in that direction returned to zero.

The sequence in which the directions were loaded was chosen to cover all the possible scenarios that occur while skiing (*Table 2.3*; *Figure 2.15*):

0. System unloaded;
1. F_Z load was applied;

2. F_X (M_Y) load was added to F_Z;
3. F_Y (M_X) load was added to F_Z and F_X (M_Y);
4. F_X (M_Y) load was removed;
5. F_Y (M_X) load was removed;
6. F_Z load was removed.

	0	*1*	*2*	*3*	*4*	*5*	*6*
F_Z		X	X	X	X	X	
F_X *and* M_Y			X	X			
F_Y *and* M_X				X	X		

Table 2.3. Loading sequence

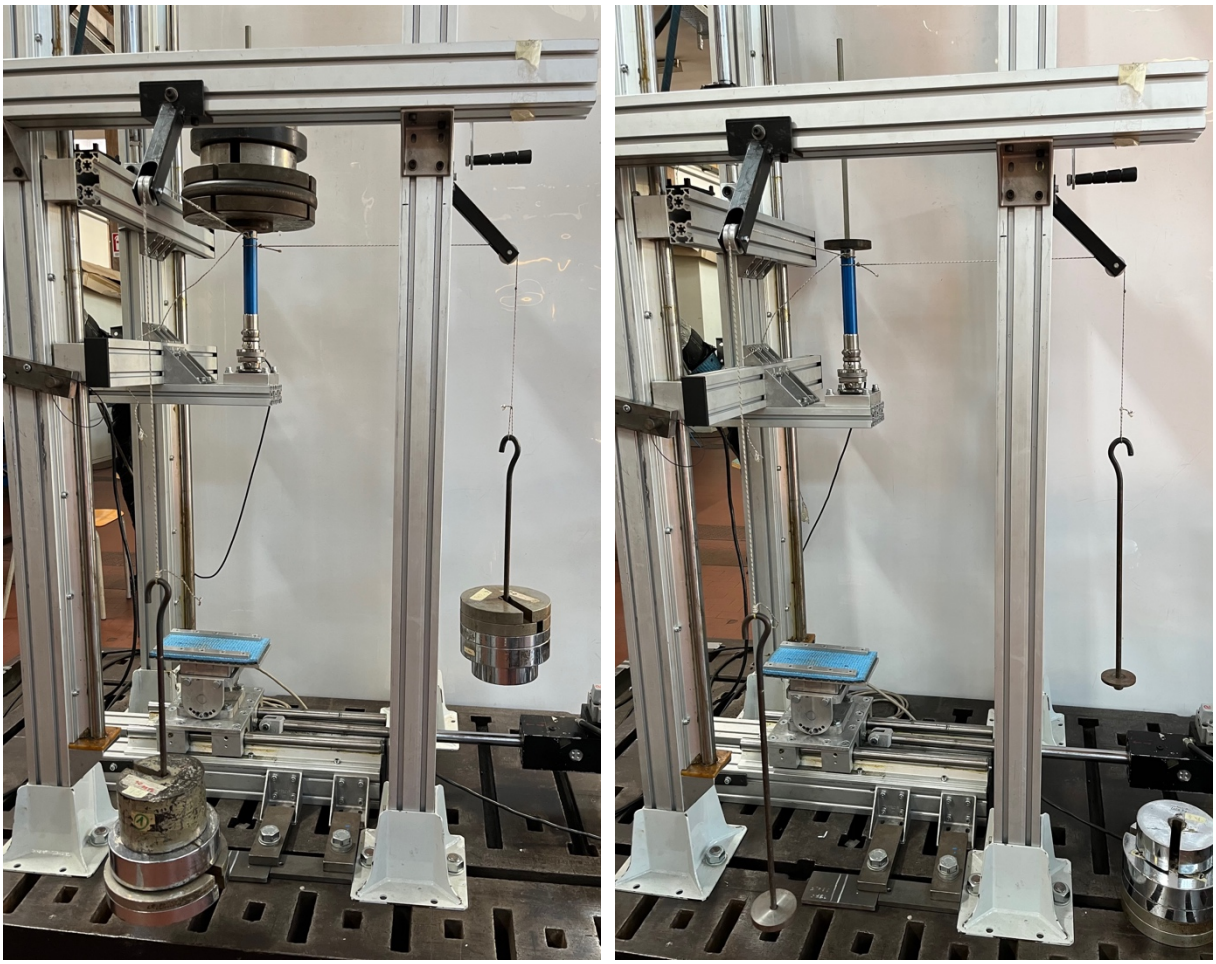

Figure 2.15. Validation of the loadcells. System unloaded on the left (0) and fully loaded on the right (3)

This loading sequence allowed to evaluate the output of the channels when all the main load components are applied independently. F_Y (M_X) and F_X (M_Y) were not evaluated alone because F_Z load component is always present while skiing.

Load cell data was acquired with *DTS Slice Nano* acquisition system. The results of the test are shown below (*Figure 2.16*; *Figure 2.17*; *Figure 2.18*; *Figure 2.19*). SN13828 graph is referred to the load cell after repair.

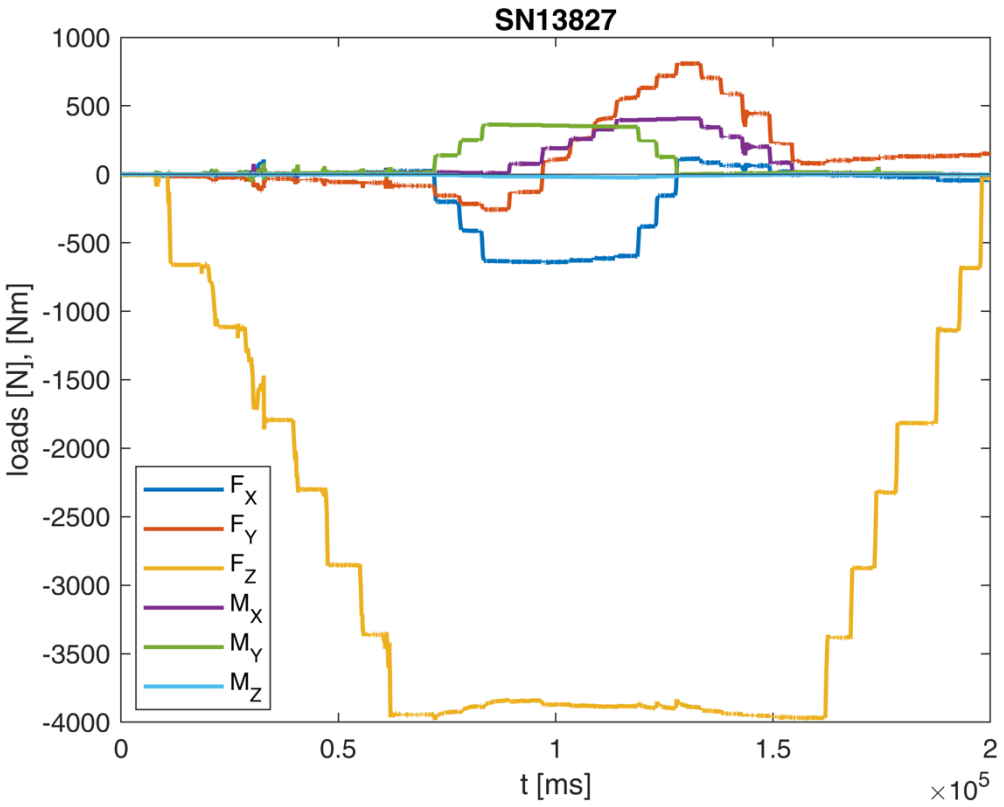

Figure 2.16. SN13827 Validation

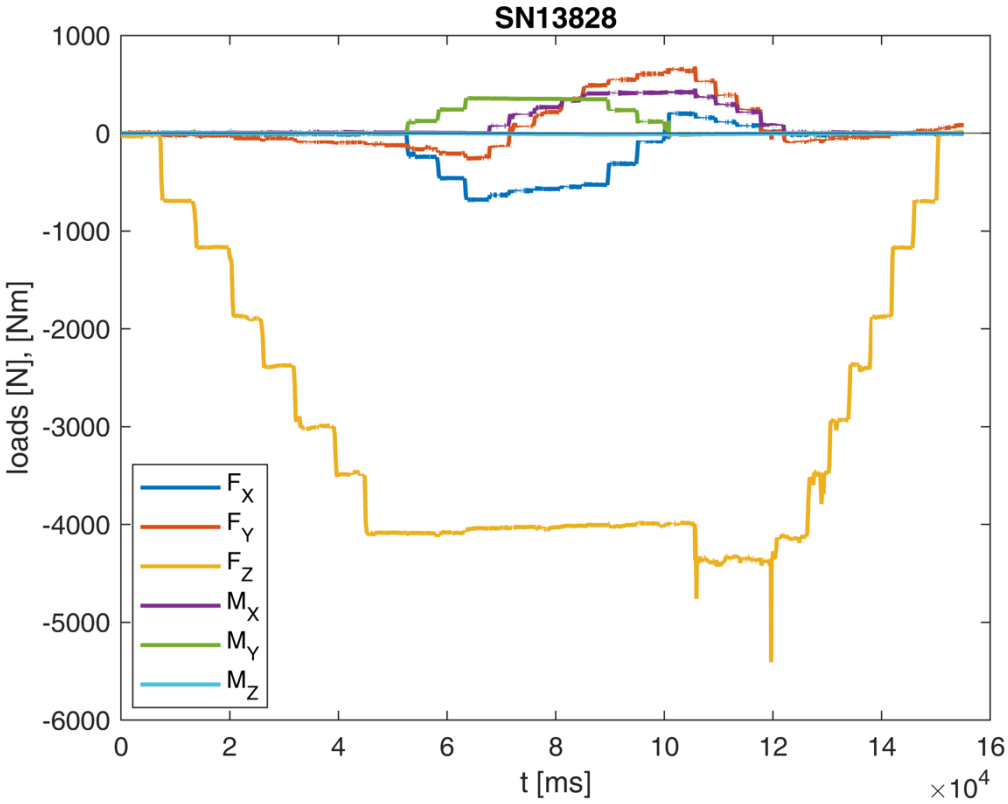

Figure 2.17. SN13828 Validation after repair

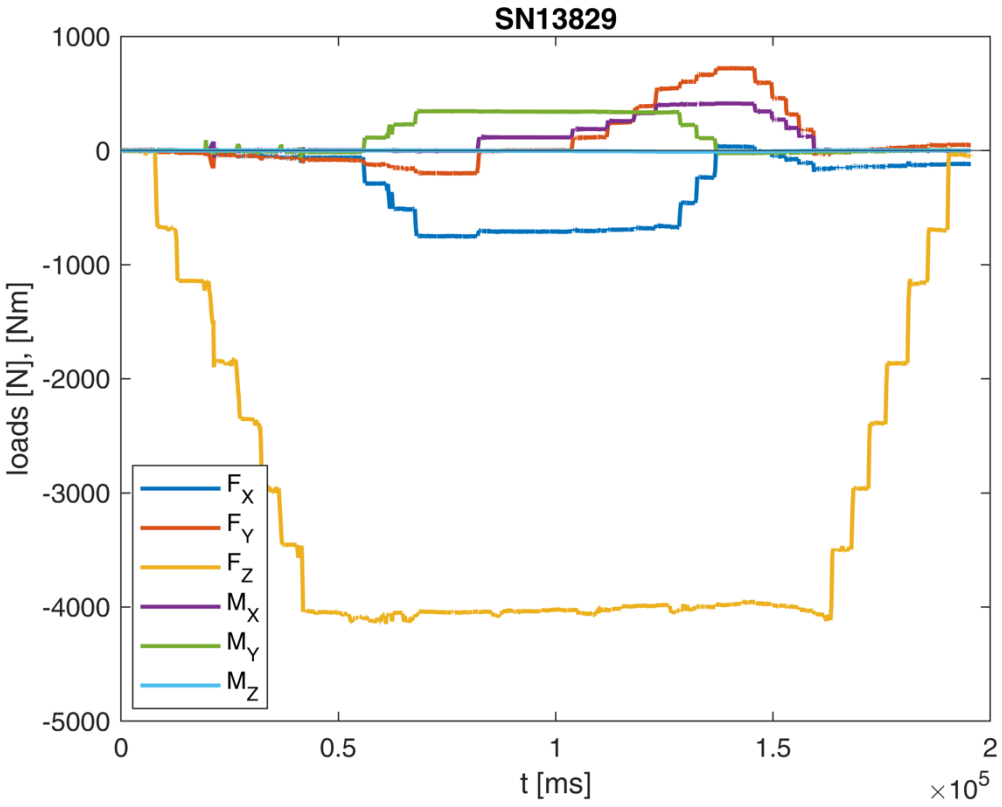

Figure 2.18. SN13829 Validation

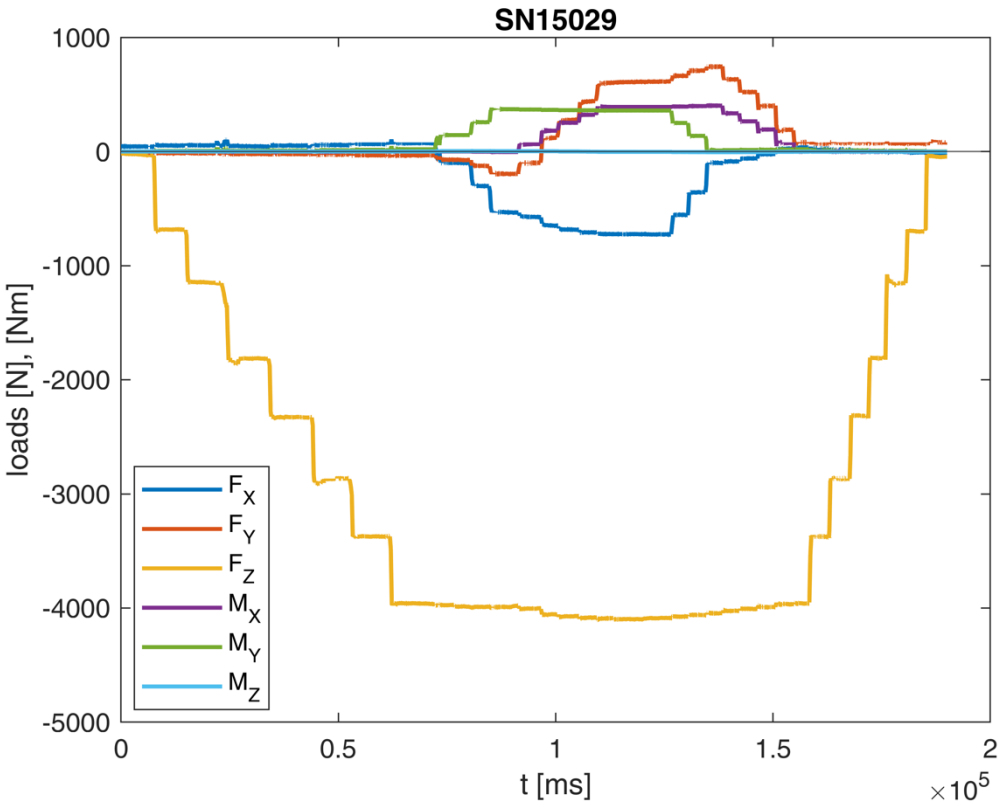

Figure 2.19. SN13827 Validation

The test results show a noticeable cross talk on the load components in all four loadcells. When F_X (M_Y) and F_Y M_X) are applied, a drop of F_Z is measured even though the load in that direction doesn't change. This also happens on all the other load components, and it inevitably affects the accuracy of data acquired. Although, for the purpose of this study this phenomenon wasn't considered, it is important to be aware of its existence.

Full GRF system validation

The assembled ski in its 12 channels configuration was validated mounting the instrumented ski on a dynamometric platform and comparing data collected by the two. The force platform (P-6000, BTS, Italy) was considered more accurate than the cells so it was used as a reference for the validation.

The instrumented ski was fixed over the platform so that the two origins had the same X and Y coordinates. A person wearing a ski boot fastened it to the ski bindings and applied typical skiing loads, alternating lateral, longitudinal and cross loads (*Figure 2.20*).

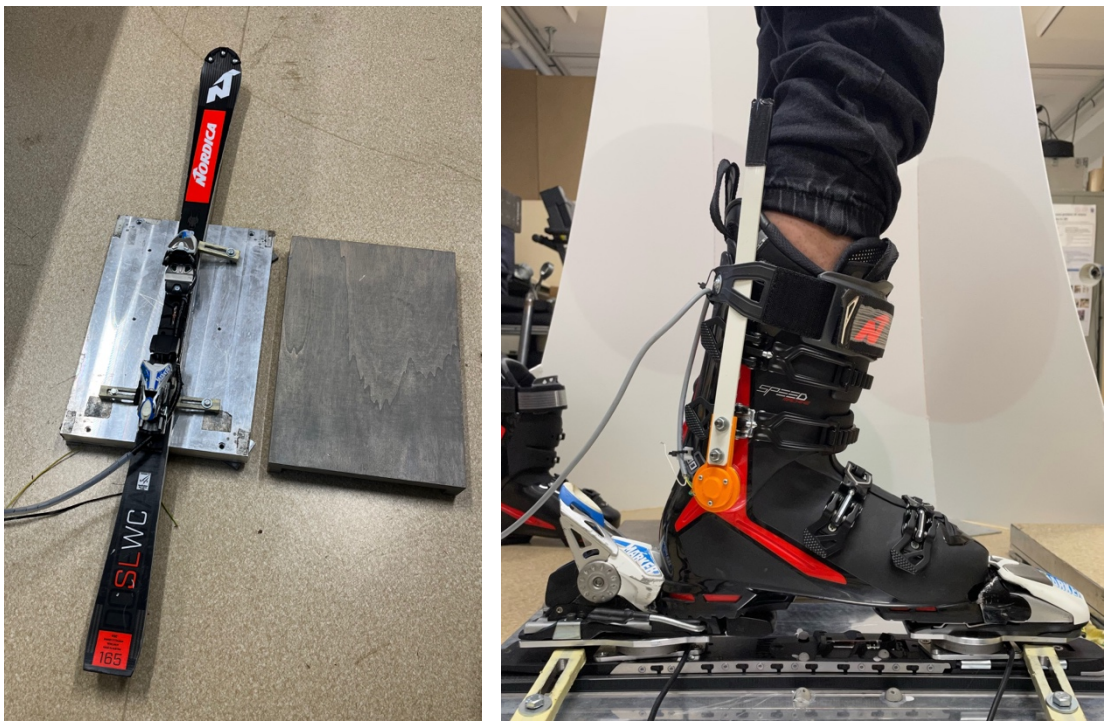

Figure 2.20. 6 channels system validation Set up

Data collected by the *BTS* platform and by the instrumented ski was multiplied by the calibration matrix. The ski global GRFs were determined and were compared to the ones detected by the force platform. The results are shown below in the time domain (*Figure 2.21*) and based on the movement performed by the person wearing the ski on the *BTS* force platform (*Figure 2.22*).

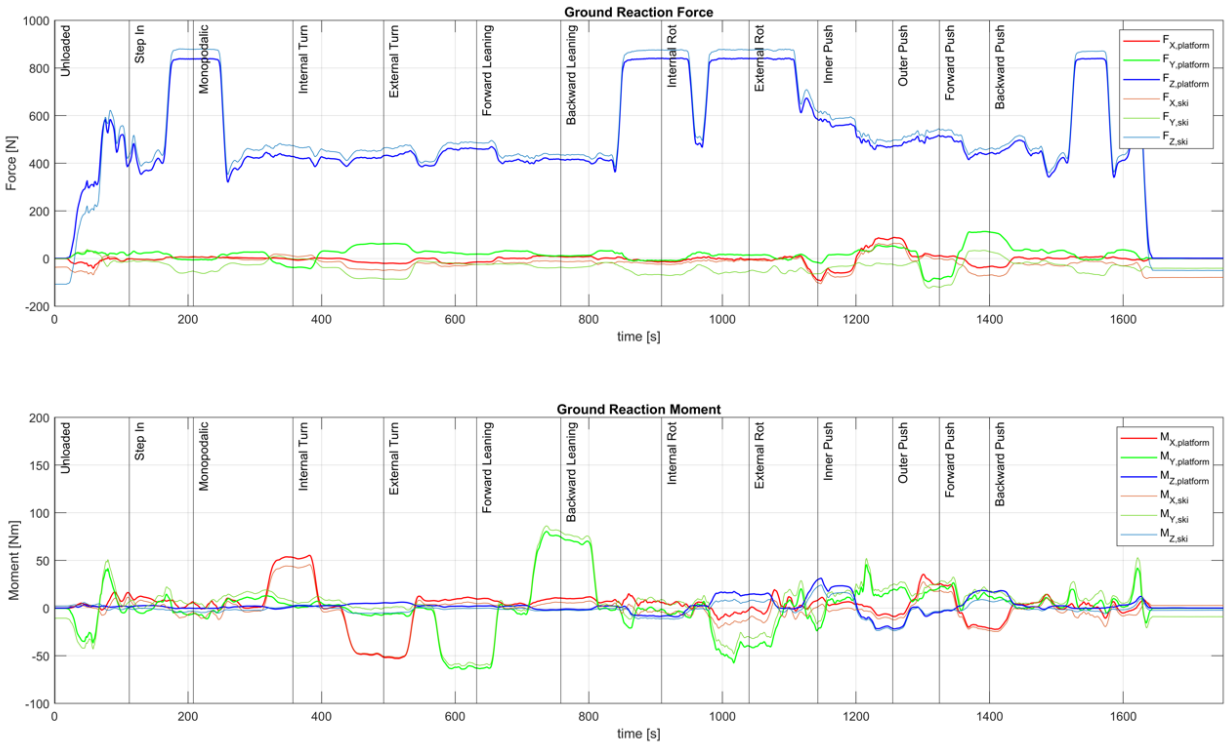

Figure 2.21. BTS platform and 6 channels instrumented ski comparison in the time domain

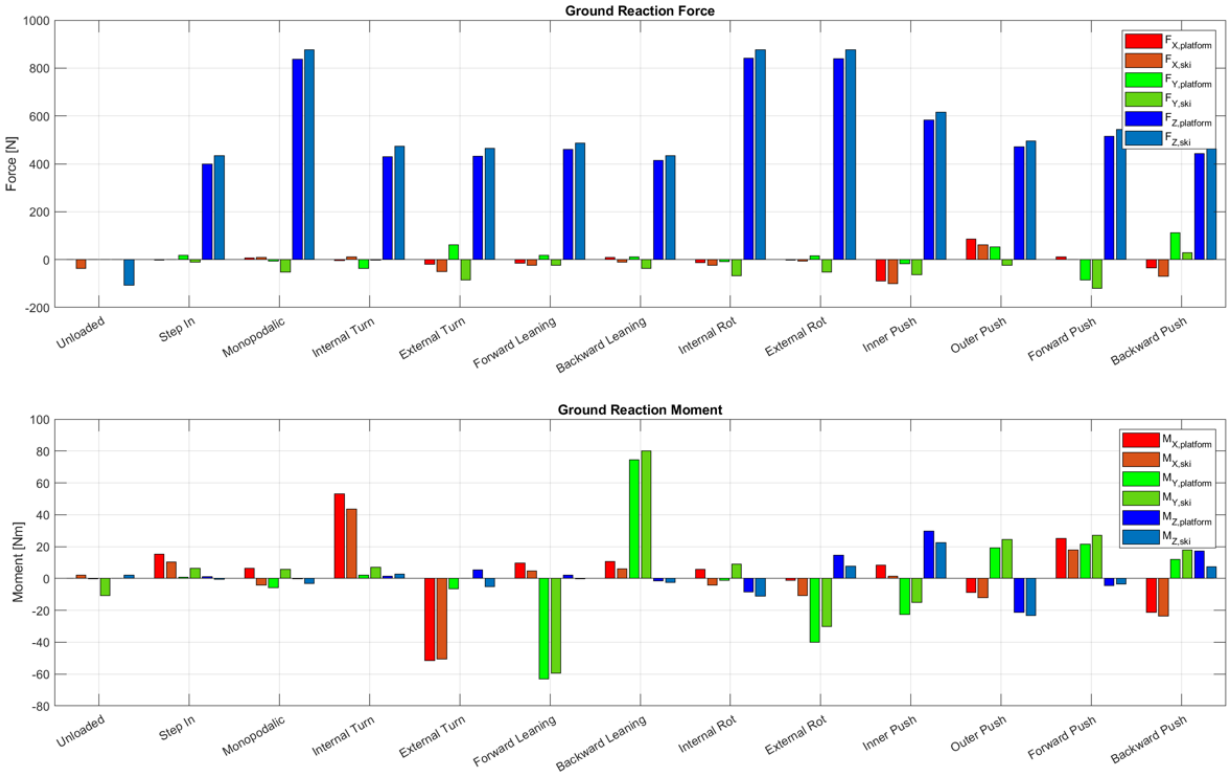

Figure 2.22. BTS platform and 6 channels instrumented ski comparison based on the movement performed

The RMSE between the ski and the platform curves of *Figure 2.21* was determined for each load component:

- RMSE F_X = 28.0415 N
- RMSE F_Y = 61.2842 N
- RMSE F_Z = 37.5354 N
- RMSE M_X = 6.1700 Nm
- RMSE M_Y = 7.1766 Nm
- RMSE M_Z = 4.4893 Nm

From the comparison shown above, load cell data maintains the same pattern of force platform data but is homothetically shifted. This discrepancy is even more highlighted when combined loads are applied. Most critical component appears to be F_Y which changes sign (with respect to force platform) when an M_X is applied. This phenomenon will not be considered in the following analysis, but it is important to acknowledge it. Finally, it was observed that best behavior is obtained when the ski is zeroed after stepping in the boot on the bindings with no external loads. Therefore, during field test the procedure started by acquiring few seconds of the skier locked into the bindings and with the ski lifted from the ground.

Reduced GRF system validation

The validation of the 6 channel system was done on the already collected data. Indeed, the same data acquired for the full GRF system were used ignoring contribution from channels 2, 4 and 6 and pre multiplying by the reduced matrixes. The results of this operation are shown in *Figure 2.23* and *Figure 2.24*. In *Figure 2.23* the curves relative to the platform are all load sensitive, while for the ski only F_Z, M_X and M_Y curves are evaluating to meaningful data.

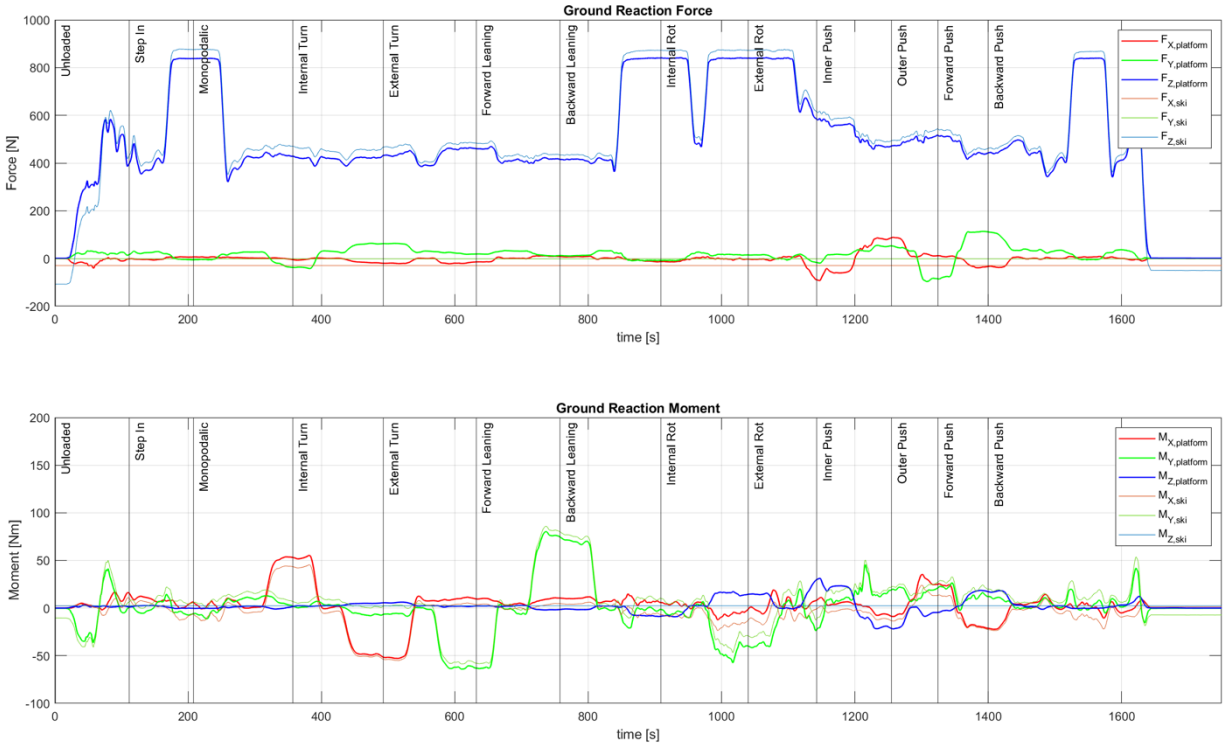

Figure 2.23. BTS platform and 3 channels instrumented ski comparison in the time domain

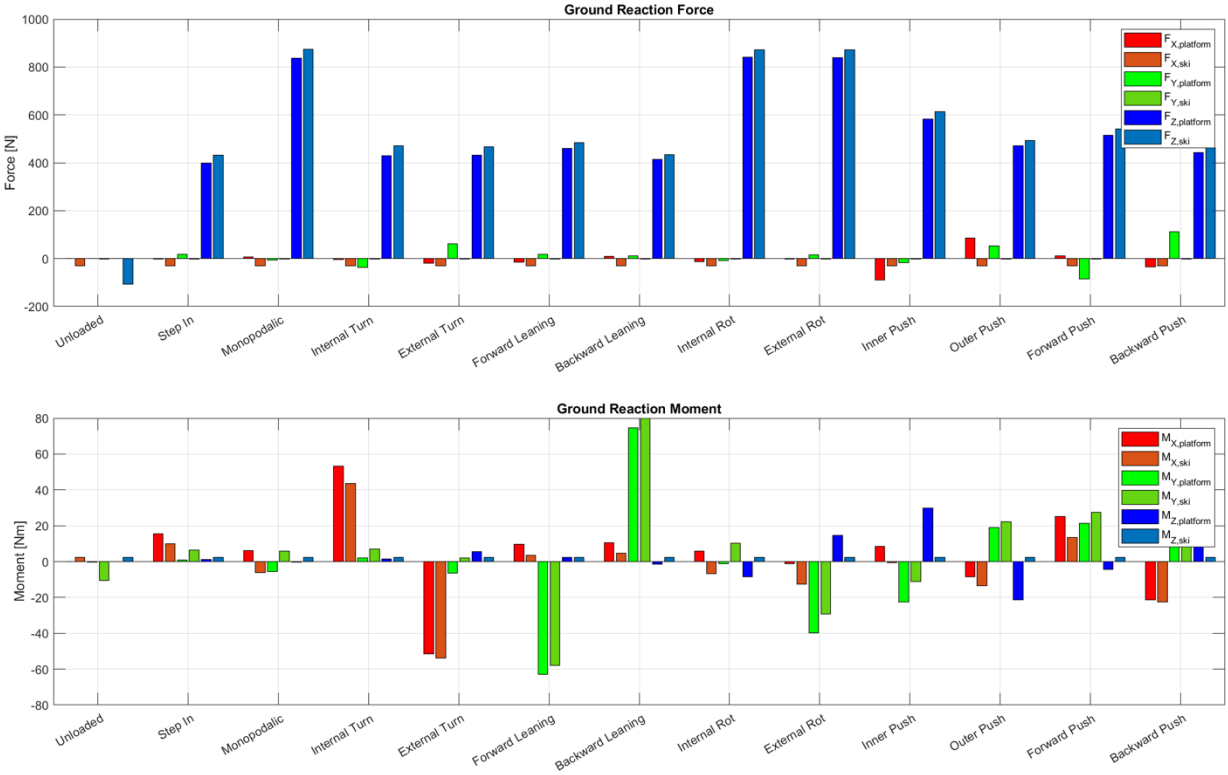

Figure 2.24. BTS platform and 3 channels instrumented ski comparison based on the movement performed

The RMSE between the ski and the platform curves of each load component, in this case are:

- RMSE F_X = 34.9933 N
- RMSE F_Y = 36.1200 N
- RMSE F_Z = 36.4509 N
- RMSE M_X = 7.4938 Nm
- RMSE M_Y = 7.6913 Nm
- RMSE M_Z = 7.7469 Nm

The RMSEs didn't show many differences between the results obtained with the full system and the ones obtained considering channels 1, 3 and 5. F_Z, M_X and M_Y show a very similar RMSE in the two cases. This is what it was expected for how the reduced calibration matrixes were obtained.

From what was seen so far, in the laboratory, on the picked signals, considering 3 channels seem entirely comparable to consider all the 6 channels of the full system. But does this also happen in field? To answer this question, previously acquired data was used. This data was acquired during a in vivo outdoor GS test session on the 11th of March 2022, with ex World Cup athlete Stefano Baruffaldi (GS1).

F_Z, M_X and M_Y were determined in the two cases for both front and rear cells. For the full system, data from all the 6 channels of each load cell was multiplied by the correspondent full calibration matrix. From the same raw data of the two cells, channel 2, 4 and 6 were removed and everything was multiplied by the correspondent reduced calibration matrix. The resultant values of F_Z, M_X and M_Y were then normalized by the athlete's bodyweight BW, which besides his unclothed weight includes: the acquisition system, the battery, the suit, the helmet, the poles and the boots. The total athlete bodyweight amount to about 95 kg which equals to 931,95 N. The results of this comparison are represented in *Figure 2.25*.

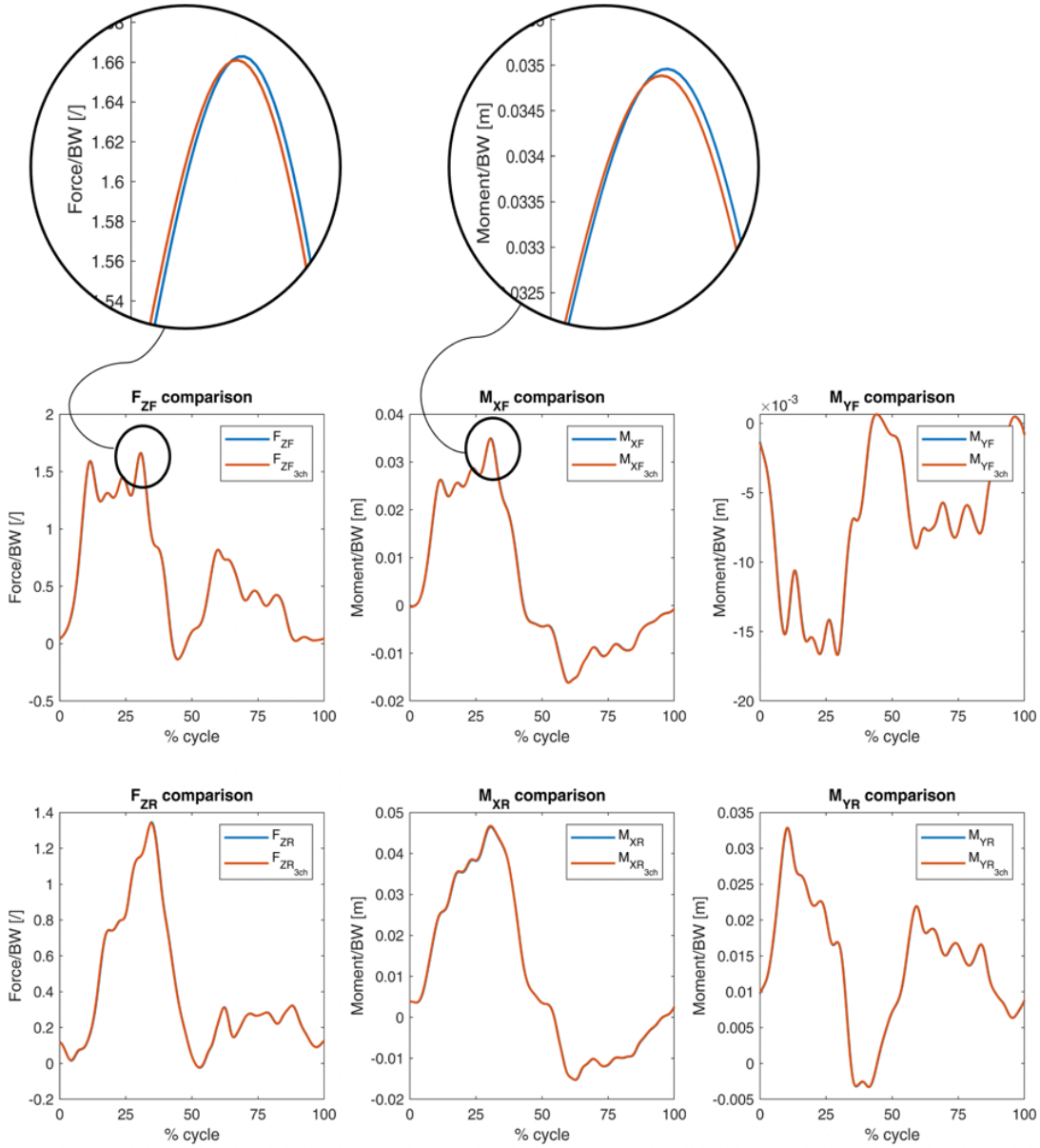

Figure 2.25. Comparison between load values measured by the 6 channels system and the 3 channels system

The RMSE was determined for each couple of loads:

- RMSE F_{ZF} = 0.0079 N/BW
- RMSE M_{XF} = $1.4978 \cdot 10^{-4}$ Nm/BW
- RMSE M_{YF} = $8.6910 \cdot 10^{-5}$ Nm/BW
- RMSE F_{ZR} = 0.0044 N/BW
- RMSE M_{XR} = $1.6482 \cdot 10^{-4}$ Nm/BW
- RMSE M_{YR} = $1.2260 \cdot 10^{-4}$ Nm/BW

The results of this comparison are encouraging. The curves almost overlay and the RMSE are very low considering that the forces are in the range of 1500 N and the moments of 50 Nm. This shows that considering only 3 of the 6 channels doesn't compromise the calculated values of F_Z, M_X and M_Y of the GRF of the ski.

Finally, to have the complete validation of the reduced system, the instrumented ski in the 3 channels set up was mounted on the BTS dynamometric platform. An in vivo indoor comparison was carried out with the same procedure of the one previously done with the 6 channels system. The resultant RMSEs are the following:

- RMSE F_X = 35.4734 N
- RMSE F_Y = 37.2034 N
- RMSE F_Z = 36.5593 N
- RMSE M_X = 7.2356 Nm
- RMSE M_Y = 7.8934 Nm
- RMSE M_Z = 8.2374 Nm

The RMSEs obtained with the 3 channels reduced system are totally comparable to the ones obtained from the full system considering channels 1, 3 and 5.

All this suggests that a reduced system is completely feasible, with a negligible error which does not compromise the results of data analysis.

3. Indoor Edge Load Profile tests

3.1. Edge Load Profile test bench

Edge Load Profile test bench is a lab equipment by Slytech for testing the ski edge load profile at different static loads and inclinations. It's made of 21 uniaxial planar load cells fixed to a rigid frame and a linear actuator with 3 degrees of freedom for allowing the positioning of the ski (*Figure 3.1*). An aluminum dummy boot sole connects the ski to the actuator (*Figure 3.2*). This dummy boot has 5 positions of application of the load spaced 50 mm from each other.

The actuator can slide vertically and horizontally and can be inclined from 0 to 70 degrees. When activated, it pushes the ski to the array of load cells. An additional load cell is installed on the actuator. This load cell measures the applied force and regulates the actuator linear movement to match the set load. All the load cells are connected to a data acquisition system that communicates with a PC from which the operator can set the force that the actuator has to apply and can read the measured loads.

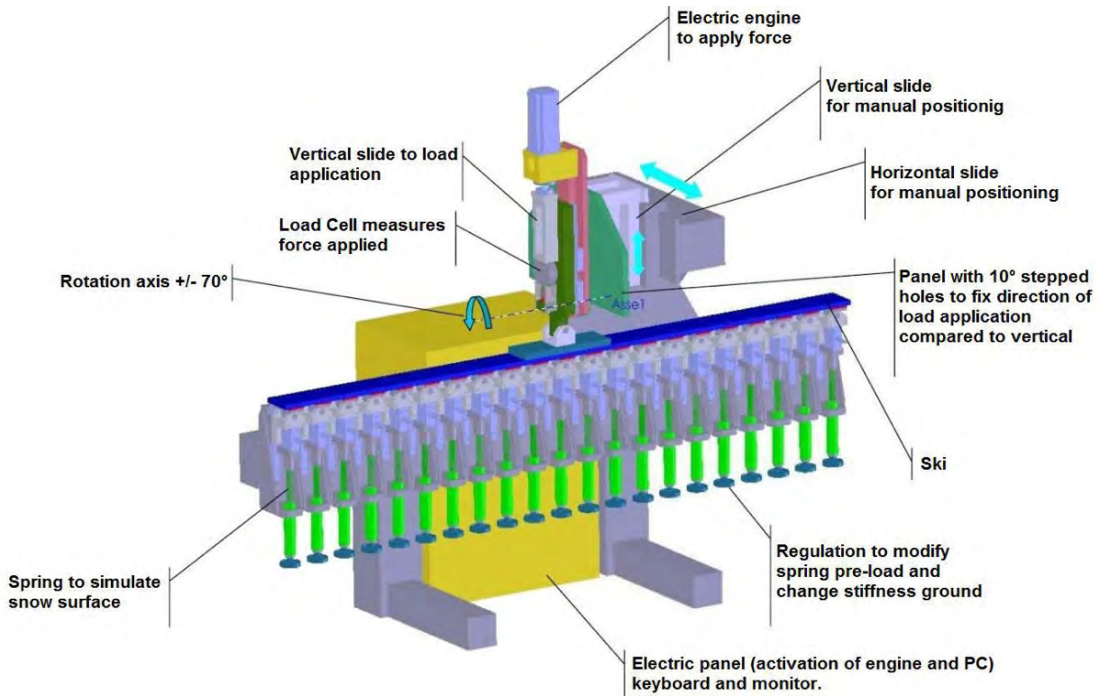

Figure 3.1. 3D model of Slytech testbench

Figure 3.2. Dummy boot sole

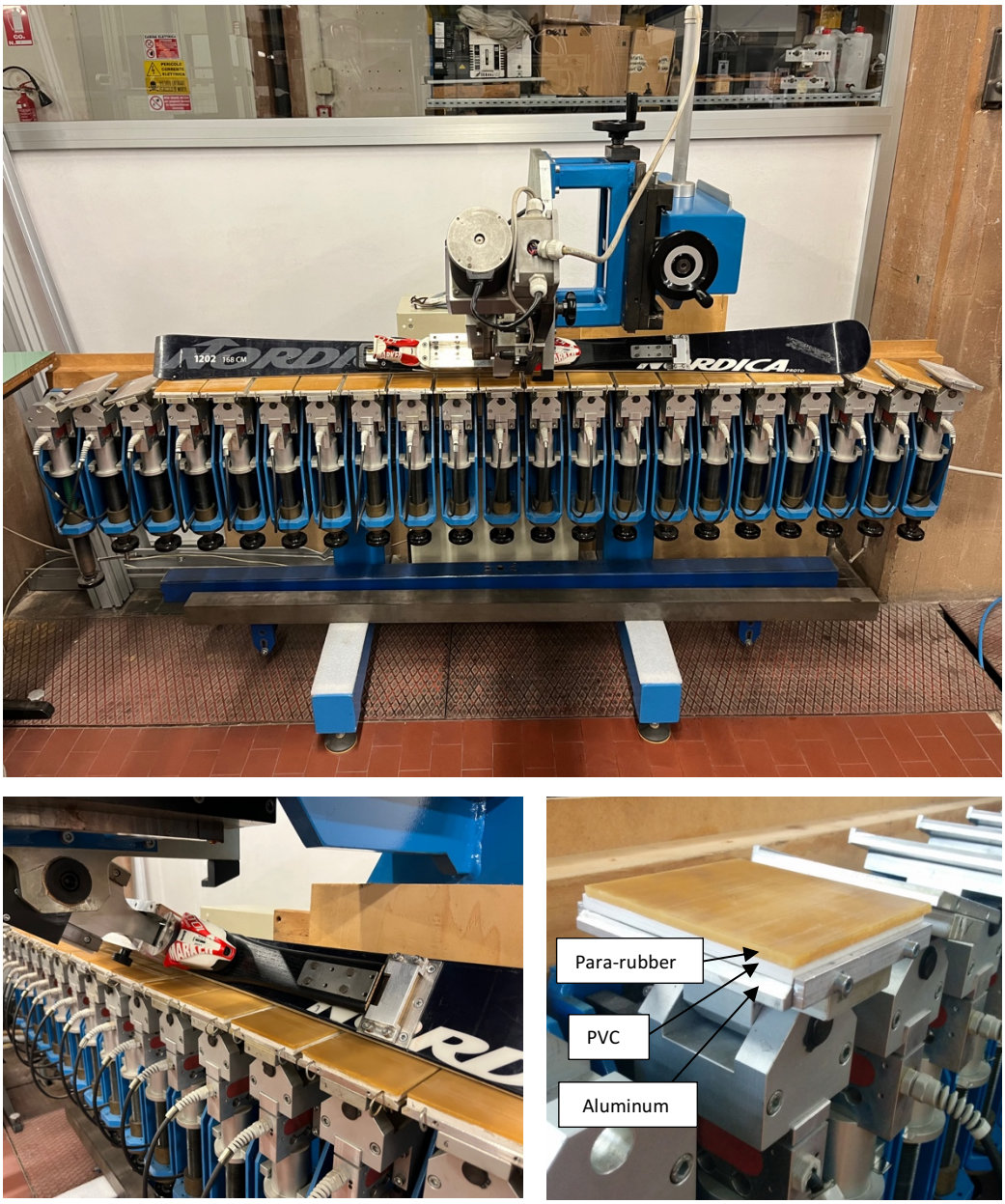

Figure 1.3. Slytech testbench in use (up and down left) and close up of the plate layers

Each of the 21 load cells is connected to the frame through a spring with variable stiffness and it contacts the ski through a hinged aluminum plate of 110 x 100 x 8 mm.

On one hand the springs allow to simulate different snow conditions. Their pre load can be changed by rotating the screw that's positioned under each cell, from being completely screwed in (simulating hard snow), to being fully unscrewed (simulating soft snow). On the other hand, the aluminum plates can rotate on an axis which is orthogonal to the length of the ski. The hinge allows the plates to follow the ski flexion, making it adhere to the plate for all its length. On the surface of each aluminum plate is placed a polyvinylchloride (PVC) plate, on which a layer of Para-rubber is glued. This very layer contacts the ski and grips to its steel edge, deforming it and simulating a curved turn (*Figure 3.4*).

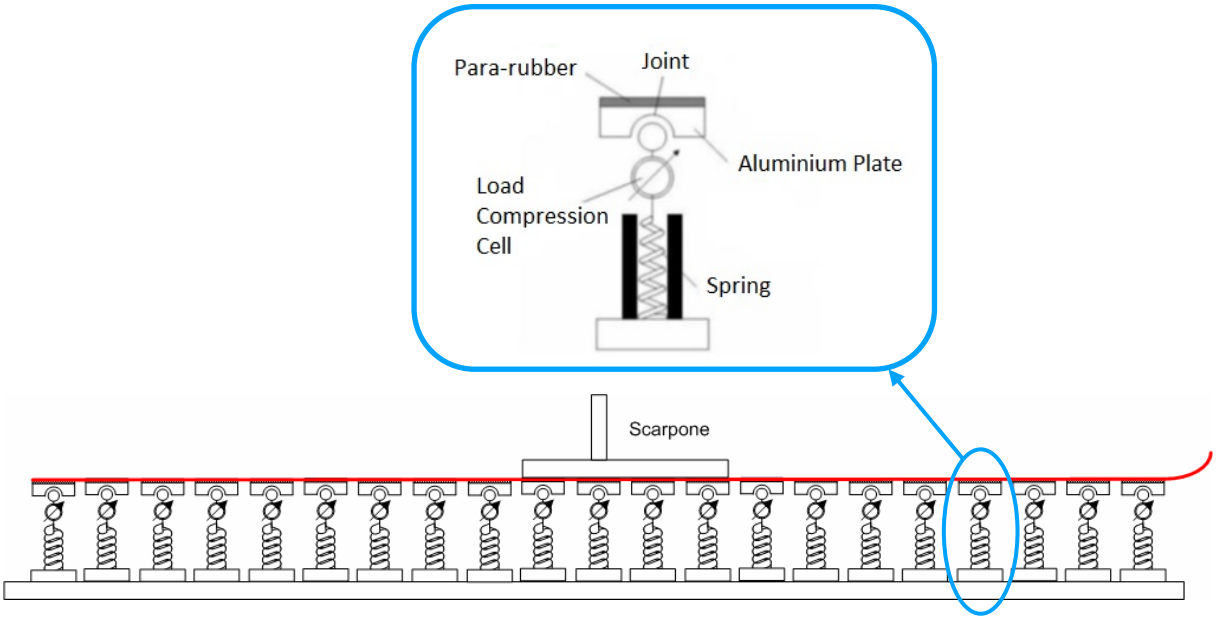

Figure 3.2. Frontal view of the load cell array

When the actuator is set vertically and pushes the ski, the force that it applies on the layer of Para-rubber is vertical. When it's set on an inclination angle that is different from 0, the force that it applies is inclined with respect to the vertical direction of the same angle. The force set by the operator will be the vectorial sum of a specific percentage of the skier bodyweight (vertical component) and the centrifugal force (horizontal component). Each load cell will just measure the vertical force component (the bodyweight one), transferred from the ski edge to the plate (*Figure 3.5*).

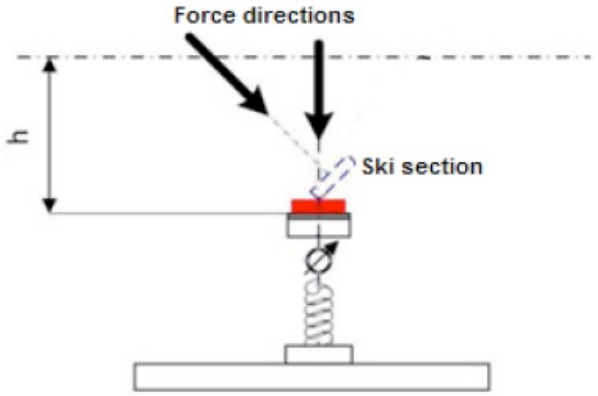

Figure 3.3. Side view of one load cell with forces

The output data of the Slytech testbench and its acquisition system is elaborated and displayed by a dedicated software installed on the PC and based on *LabView*. The loads measured by each cell are plotted in kilograms along the ski length, in order to obtain the Edge Load Profiles (ELP). A *.txt* file with the load value expressed in kilograms measured by each cell, can be saved for further data elaboration.

This testbench allows to compare different skis under the same conditions and to evaluate the effect of different geometries, constructions, and materials on the Edge Load Profile.

3.2. Test methods

Before performing the tests, the Edge Load Profile testbench was calibrated. A rigid straight steel bar was laid on the testbench and metal shims of different thicknesses were put under each aluminum plate so that the cells gave the same load measurement (*Figure 3.6*).

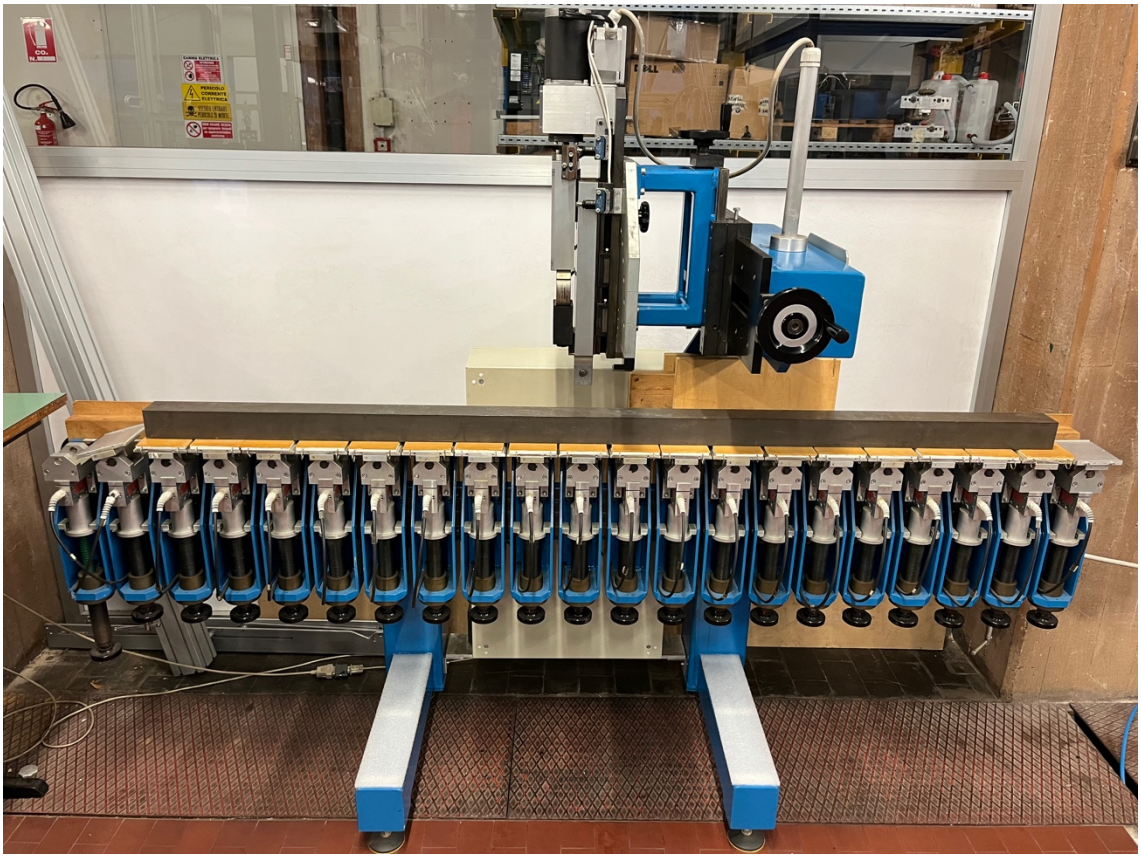

Figure 3.6. Edge Load Profile testbench during calibration

A table with the metal shims placed under each aluminum plate is reported below (*Table 3.1.*).

Cell	1	2	3	4	5	6	7	8	9	10	11	12	13	14	15	16	17	18	19	20	21
Thickness [mm]	0	0.15	0	0.7	0.3	0.1	0.1	0.1	0.1	0.22	0.1	0.1	0.12	0.1	0.4	0.1	0.2	0.1	0.12	0	0

Table 3.1. Shims thickness under each aluminum plate

Two different pair of skis were tested on the Slytech testbench: the Nordica Prototype (standard and modified) and the instrumented Nordica SLWC (6 ch/loadcell and 3 ch/loadcell).

The edge load test consists in: mounting the ski on the testbench, setting the edge angle, and applying a constant load. At each angle corresponds a precise load value reported on *Table 3.2*:

Angle [°]	Load [kgf]
10	60
20	70
30	85
40	100
50	120
60	140

Table 3.2. Ski inclination angles and corresponding loads to apply

These values of force come from the vectorial sum of the skier bodyweight percentage that the leg can transfer to the ground (vertical component) and the centrifugal force calculated for speeds and turn radiuses compatible with the corresponding inclination (horizontal component).

Every ski was tested 3 times on the same angle and load. After every change of variables, the testbench cell offset was resetted. For each load cell, the average value of the 3 measures was considered. The average values were then plotted along the ski edge profile on a *Cell - Force* graph. This graph has the testbench cells on its X axis, and the measured force values at that cell are read on the Y axis. The forces values were finally interpolated with a polynomial curve to obtain the Edge Load Profile curve of the ski at that inclination.

3.3. Test results

Nordica Prototype

Presented below are the results of the Edge Load Profile tests on *Nordica_Proto_Standard* ski and on *Nordica_Proto_VQ* ski. These two skis have the same length, sidecut, construction and materials but on one of them is applied a wood superstructure designed by Professor Quaggiotti presented in chapter 2.

10° inclination angle and 60 kg load ELP test on hard snow

NORDICA_PROTO_STANDARD

NORDICA_PROTO_VQ

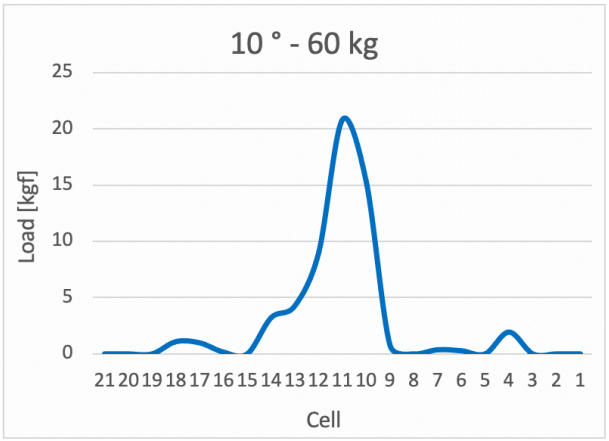

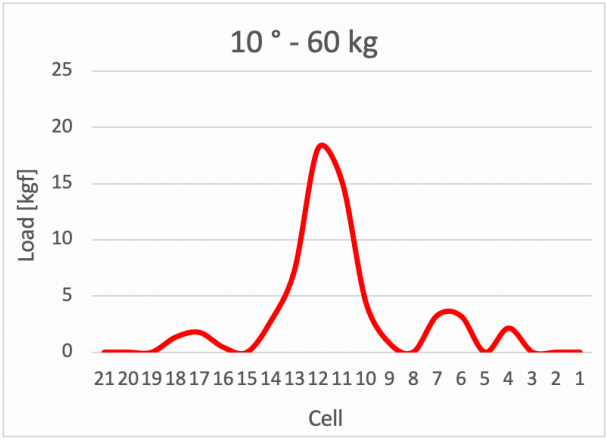

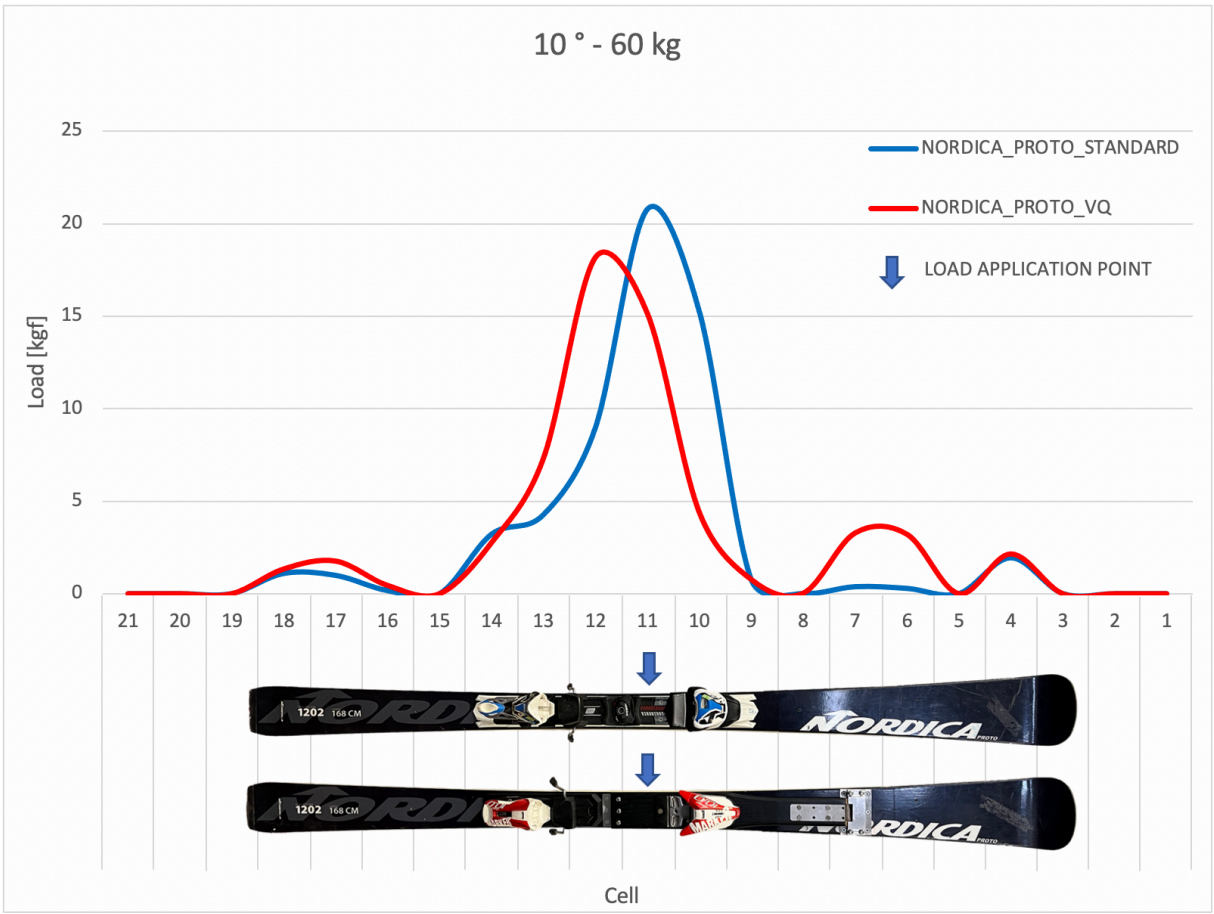

20° inclination angle and 70 kg load ELP test on hard snow

NORDICA_PROTO_STANDARD

NORDICA_PROTO_VQ

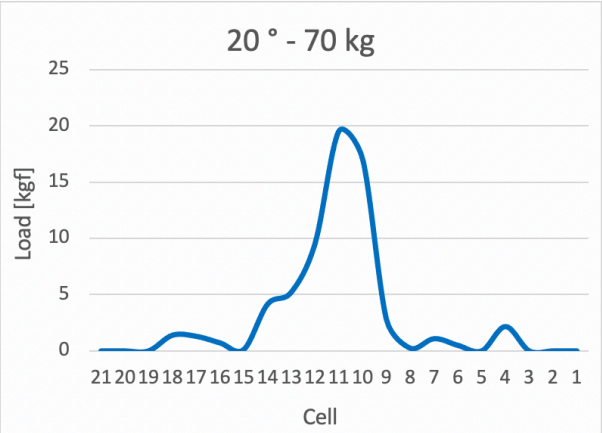

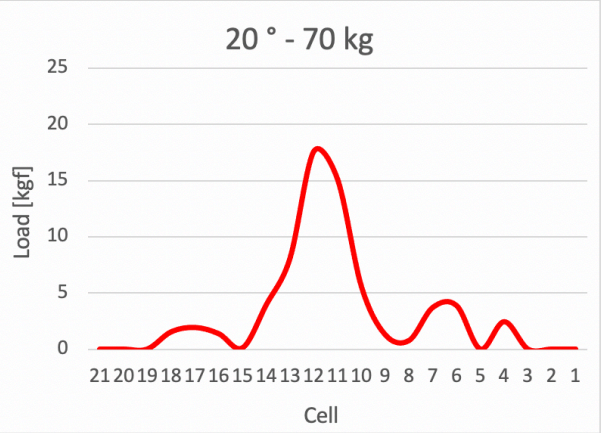

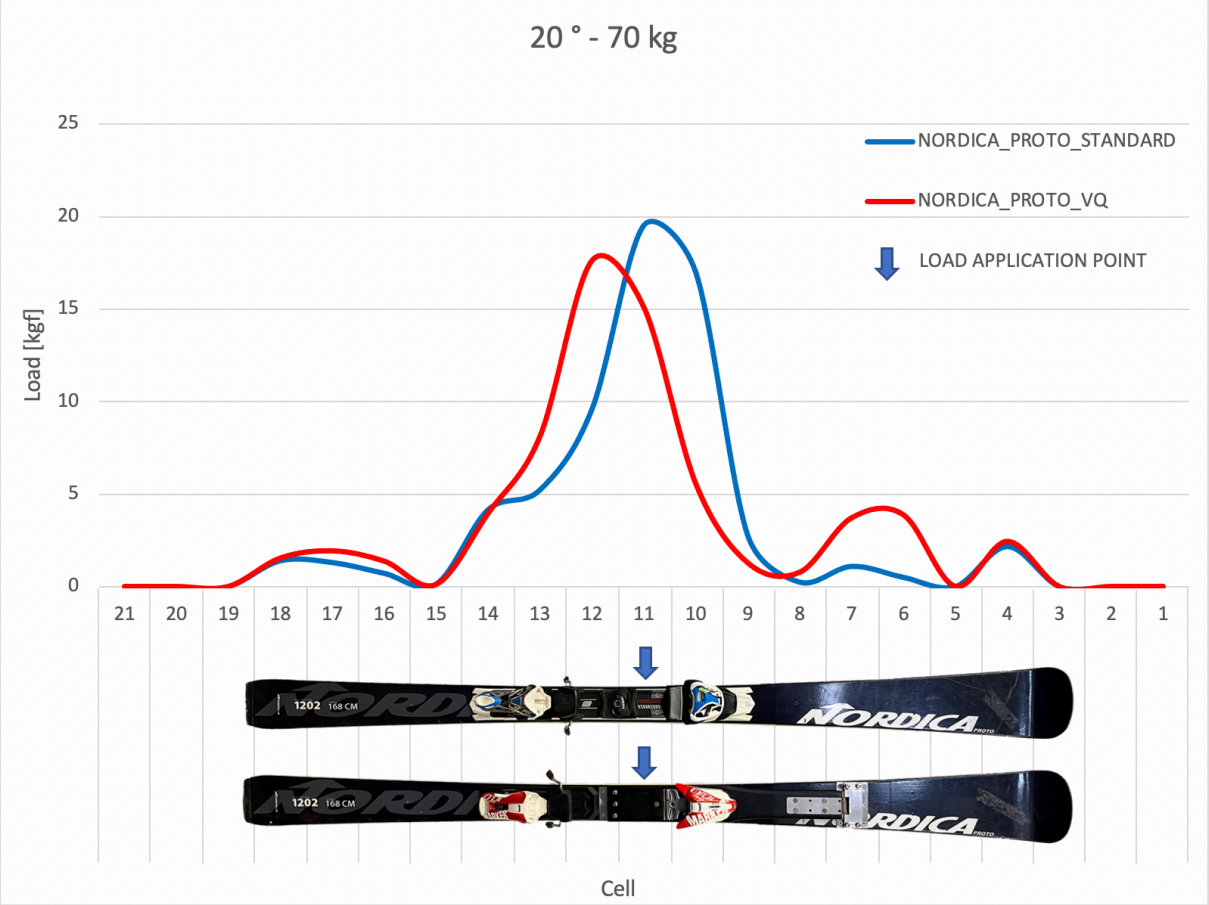

30° inclination angle and 85 kg load ELP test on hard snow

NORDICA_PROTO_STANDARD

NORDICA_PROTO_VQ

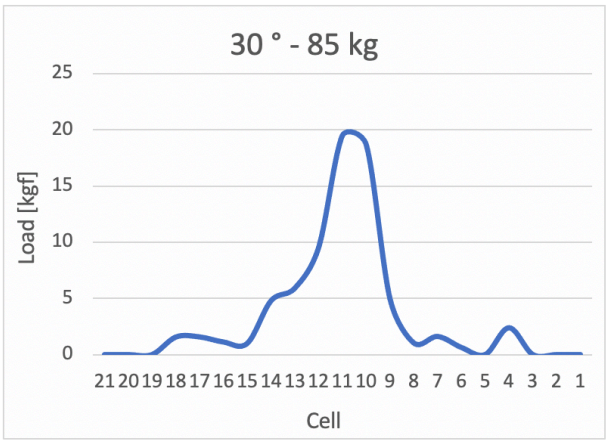

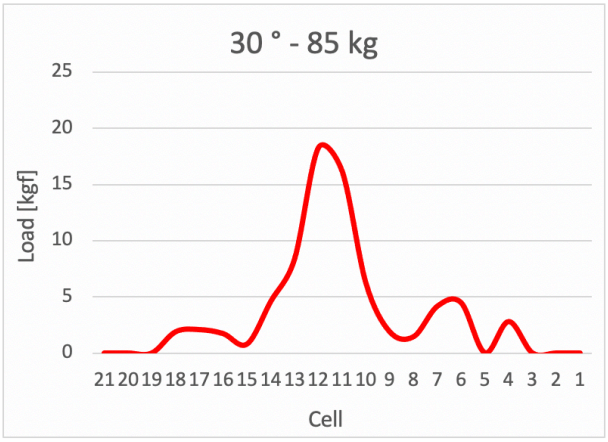

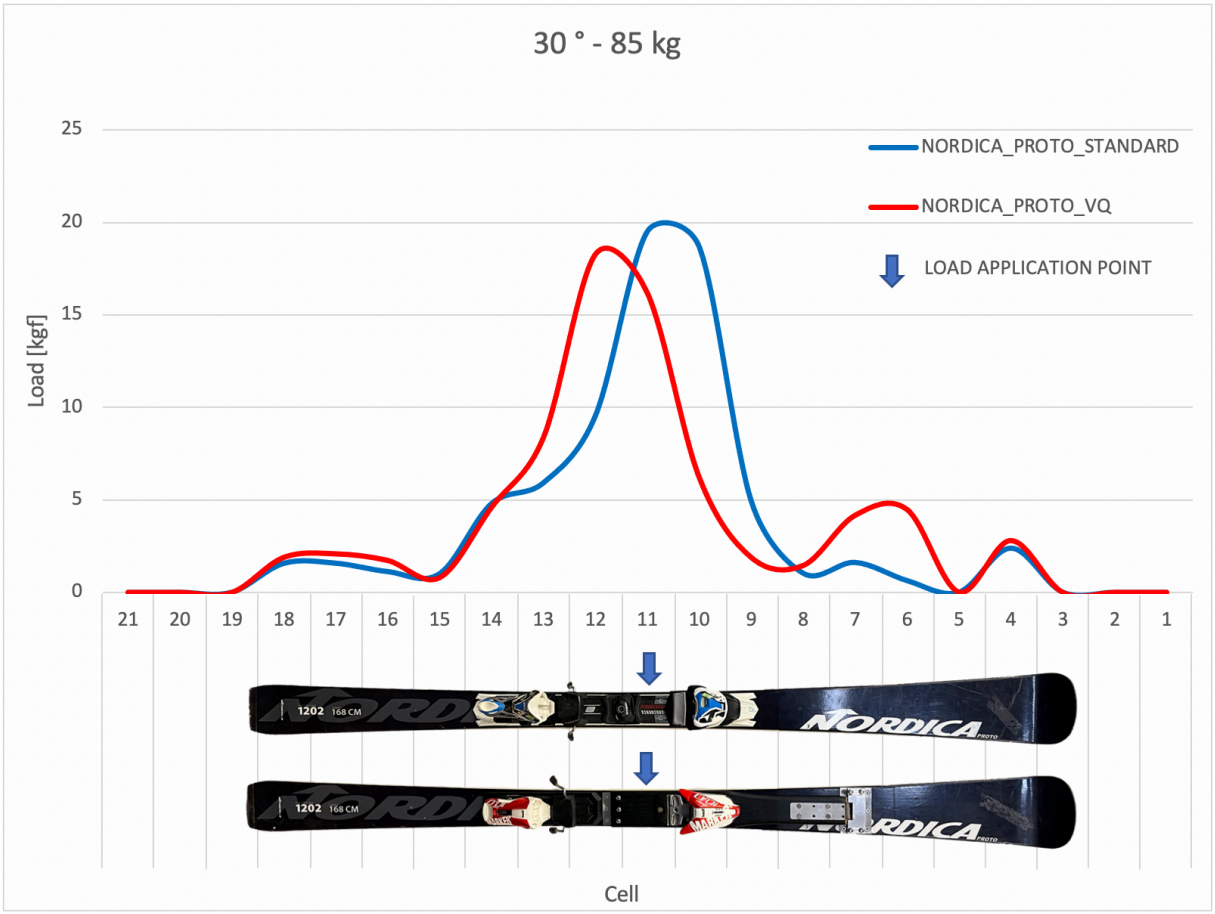

40° inclination angle and 100 kg load ELP test on hard snow

NORDICA_PROTO_STANDARD

NORDICA_PROTO_VQ

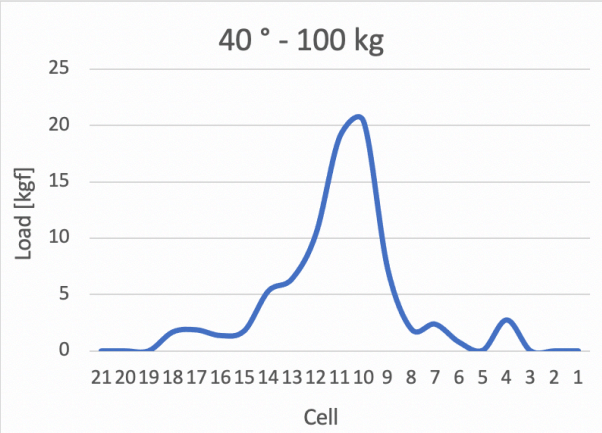

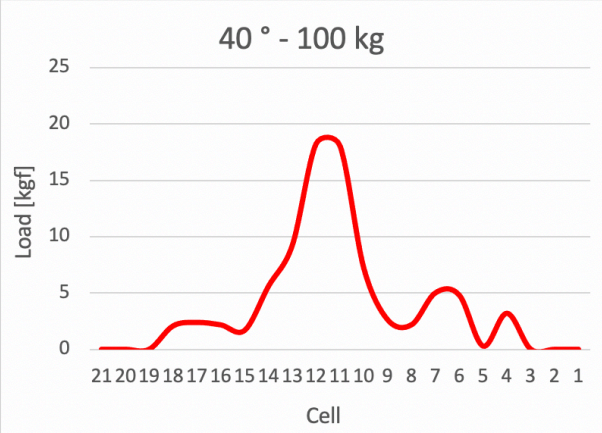

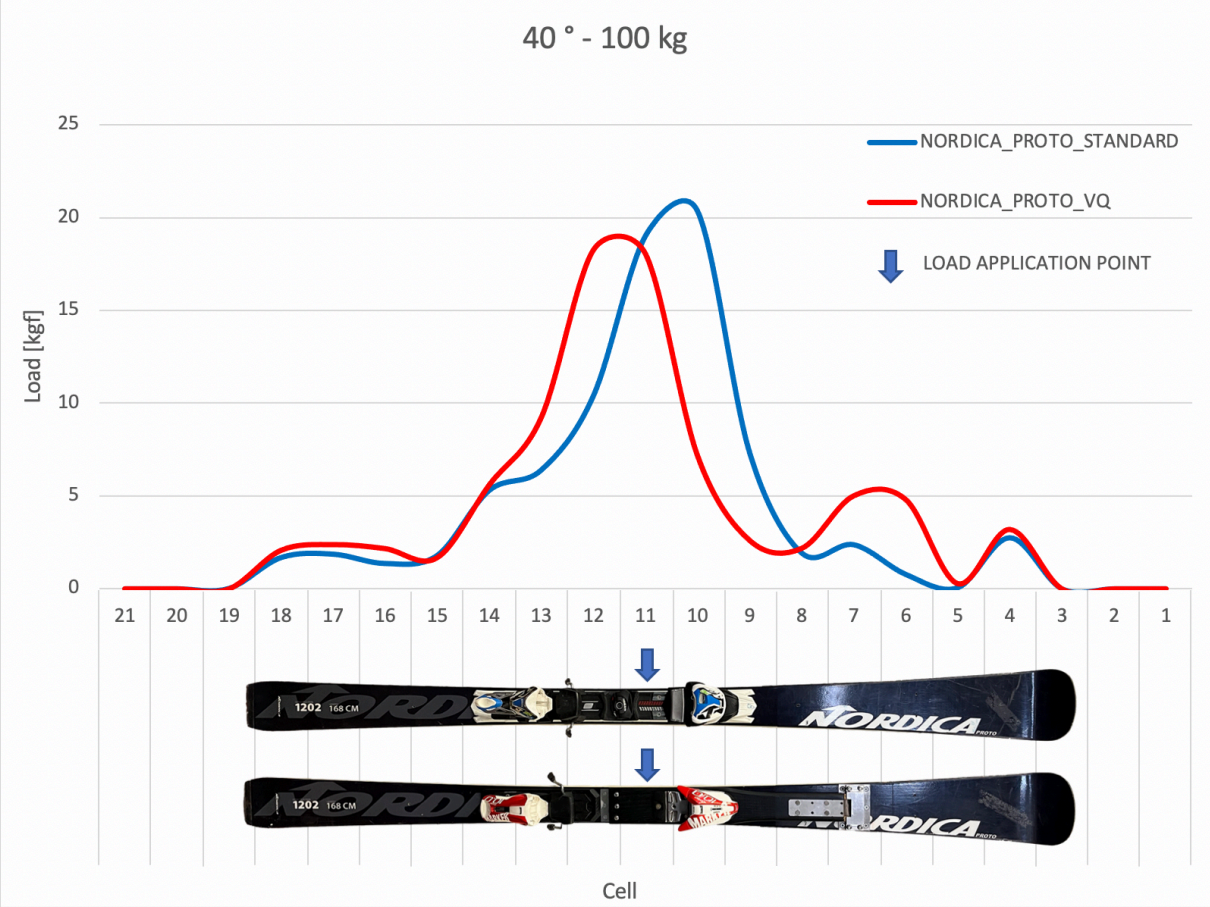

50° inclination angle and 120 kg load ELP test on hard snow

NORDICA_PROTO_STANDARD

NORDICA_PROTO_VQ

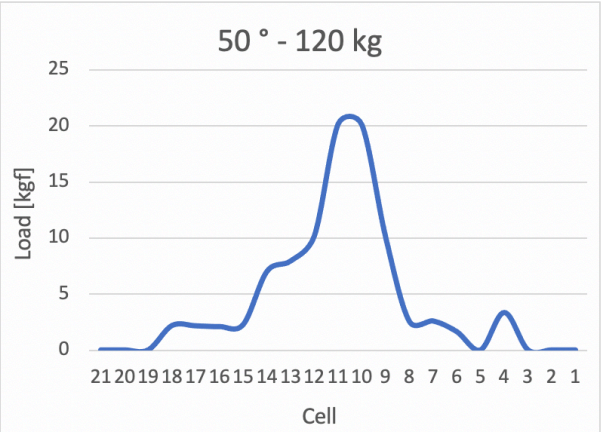

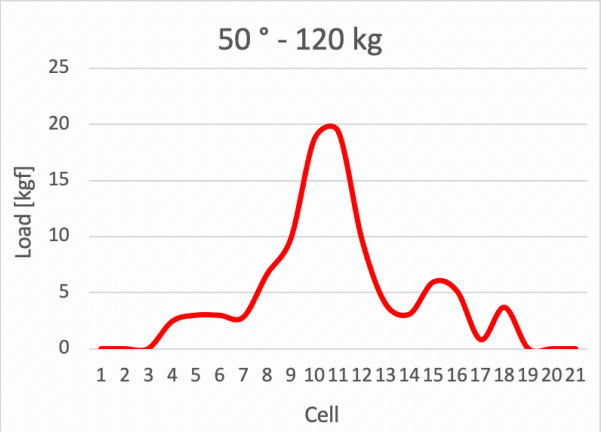

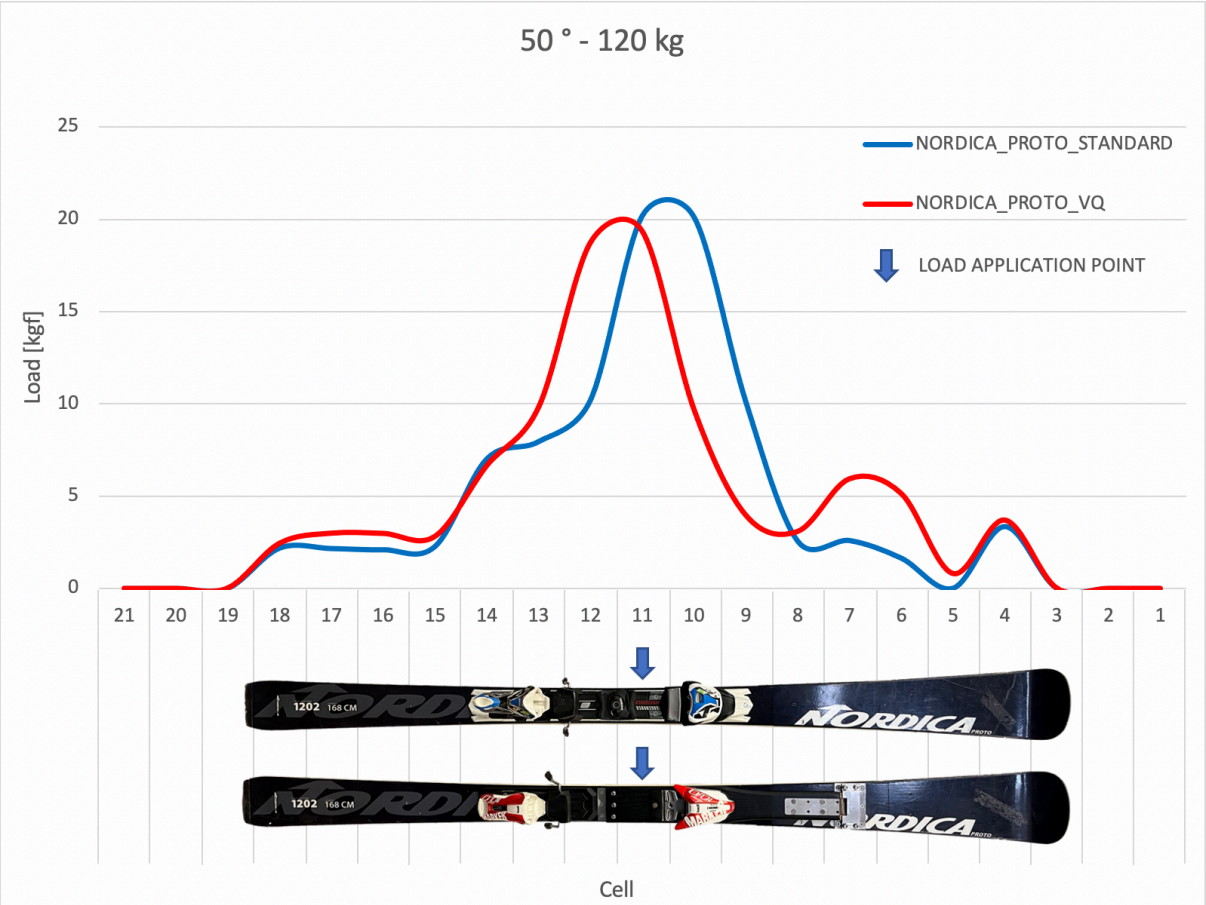

60° inclination angle and 140 kg load test on hard snow

NORDICA_PROTO_STANDARD

NORDICA_PROTO_VQ

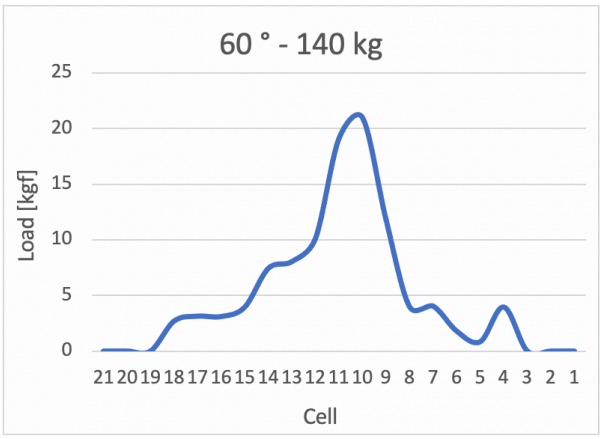

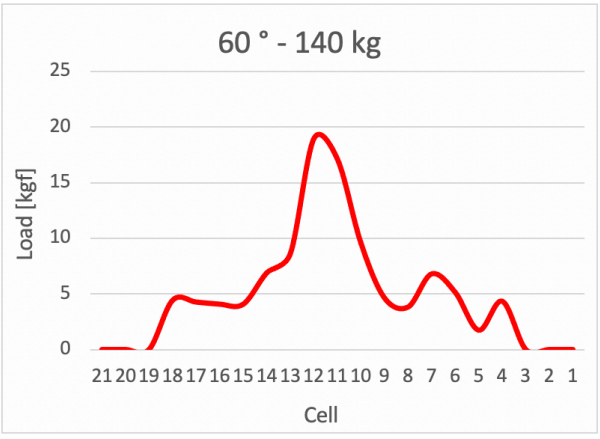

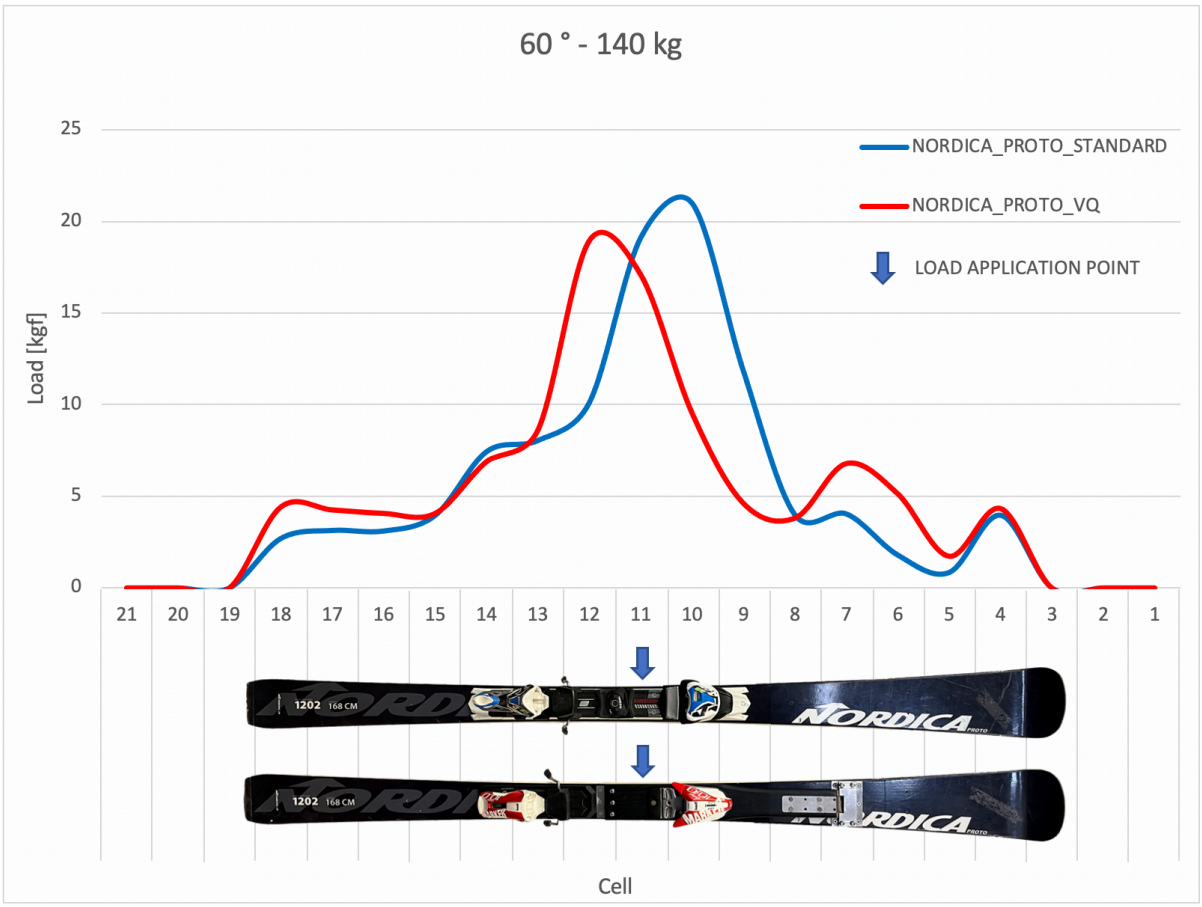

The test output show that the superstructure applied on Nordica_Proto_VQ has an appreciable effect on the ski Edge Load Profile.

The very tip (cell 4) and the tail (cells 15, 16, 17, 18) of both the skis have a similar trend of Edge Load Profile in all conditions. They respectively show a minor peak and a plateau of the load. Also, the main peaks have a similar trend at every inclination and load. They are all close to where the force is applied (blue arrow, above cell 11), but on the standard version of the ski the peak is higher and ahead of the force application point while on Professor Quaggiotti's prototype it's lower and behind the application point.

The main difference is found above cells 5, 6 and 7. The standard version of the ski have a sudden drop of the Edge Load Profile for all the inclinations and loads. The ski transfers no load at all to the snow on cell 5 and a very small percentage of the load on cells 6 and 7. This means that that ski part doesn't support the skier during turns. For this reason, this ski section is called by the Italian professional skiers "buco" ("hole" in Italian). Professor Quaggiotti's prototype have the same sudden drop of the Edge Load Profile on cell 5, but on the following cells 6 and 7 the ski turns out to be loaded a lot more than the standard version for all the inclinations and loads. This results in a better distribution of the force on the snow and better support of the skier during turns.

To highlight what is the effect of the inclination angle on the Edge Load Profile, the results of the tests are plotted on the same graph for each ski (*Figure 3.7* and *Figure 3.8).*

The two graphs shows that the main peak decreases and slightly slides towards the tail of the ski with greater inclination angles, while the rest of the profile increases. The 60° Edge Load Profile curve in both cases results to be the one with the greatest underlaying area even though most of the applied force is parallel to the cell and therefore shouldn't appear in the measurement. They also show that similar results are obtained for 10° and 20° and for 30° and 40°.

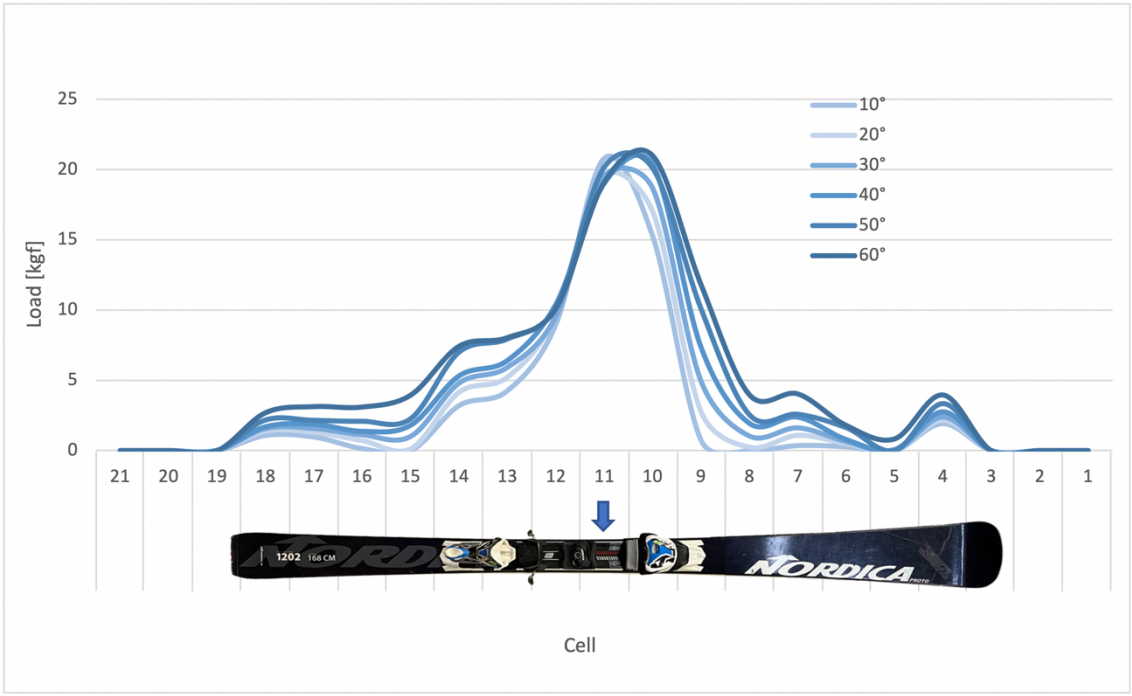

Figure 3.7. *Nordica_Proto_Standard Edge Load Profile at different inclination angles*

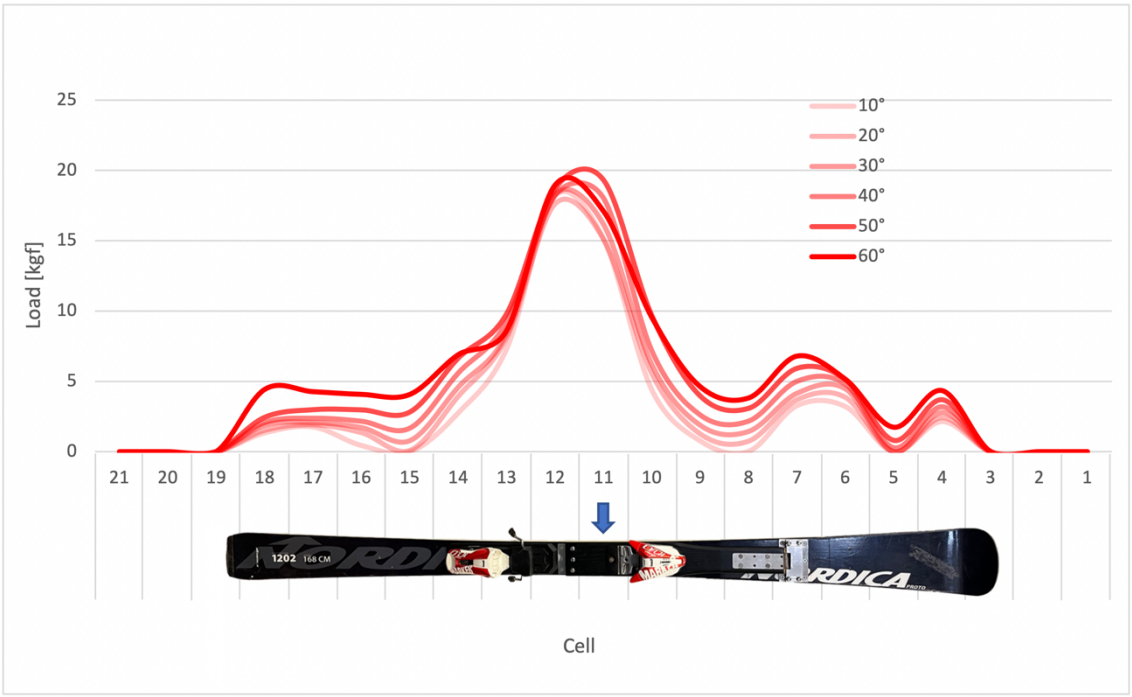

Figure 3.8. *Nordica_Proto_VQ Edge Load Profile at different inclination angles*

Nordica SLWC 165 cm

The same tests were done with the instrumented *Nordica SLWC* skis. The ski was mounted on the testbench and during the tests also the load measured by the cells on the ski were collected. The acquisition system used was the *DTS Slice Nano*. The aim of this test, other than determine the Edge Load Profile of the ski, was to see if the vertical component of the applied force is equal to the vertical component of the global GRF determined with the cells on the ski. This was verified with the skis in both 6 and 3 channels configurations. For the 6 channels configuration the vertical component of the applied load should be equal to the vertical component of F_Z and F_Y:

$$F \cdot \cos\alpha = F_Z \cdot \cos\alpha + F_Y \cdot \sin\alpha$$

with α the inclination angle of the ski (*Figure 3.9.a*).

For the 3 channels configuration, as F_Y isn't determined, the relation becomes:

$$F \cdot \cos\alpha \simeq F_Z \cdot \cos\alpha$$

This last relation is an approximation because the F_Y vertical component, even if small compared to the F_Z one, still contributes to balance the applied force (*Figure 3.9.b*).

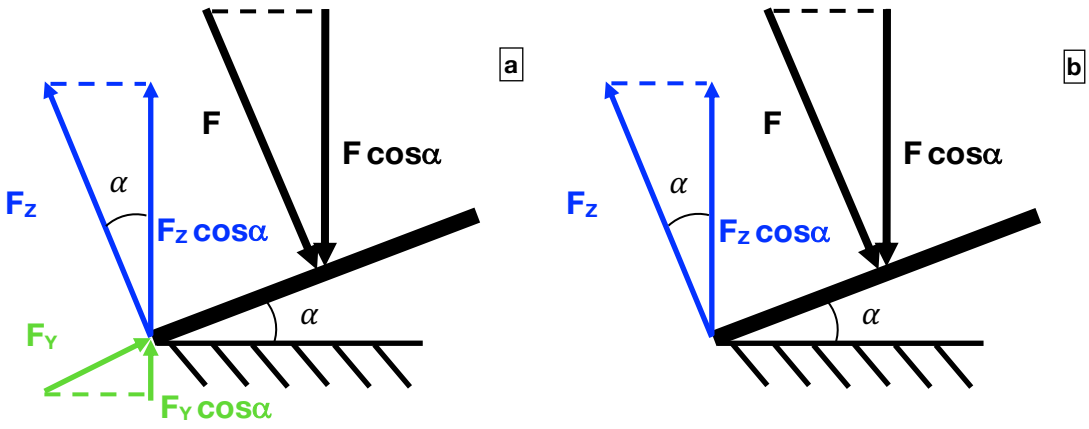

Figure 3.9. (a) loads on the 6 channels configuration; (b) loads on the 3 channels configuration

10° inclination angle and 60 kg load ELP test on hard snow

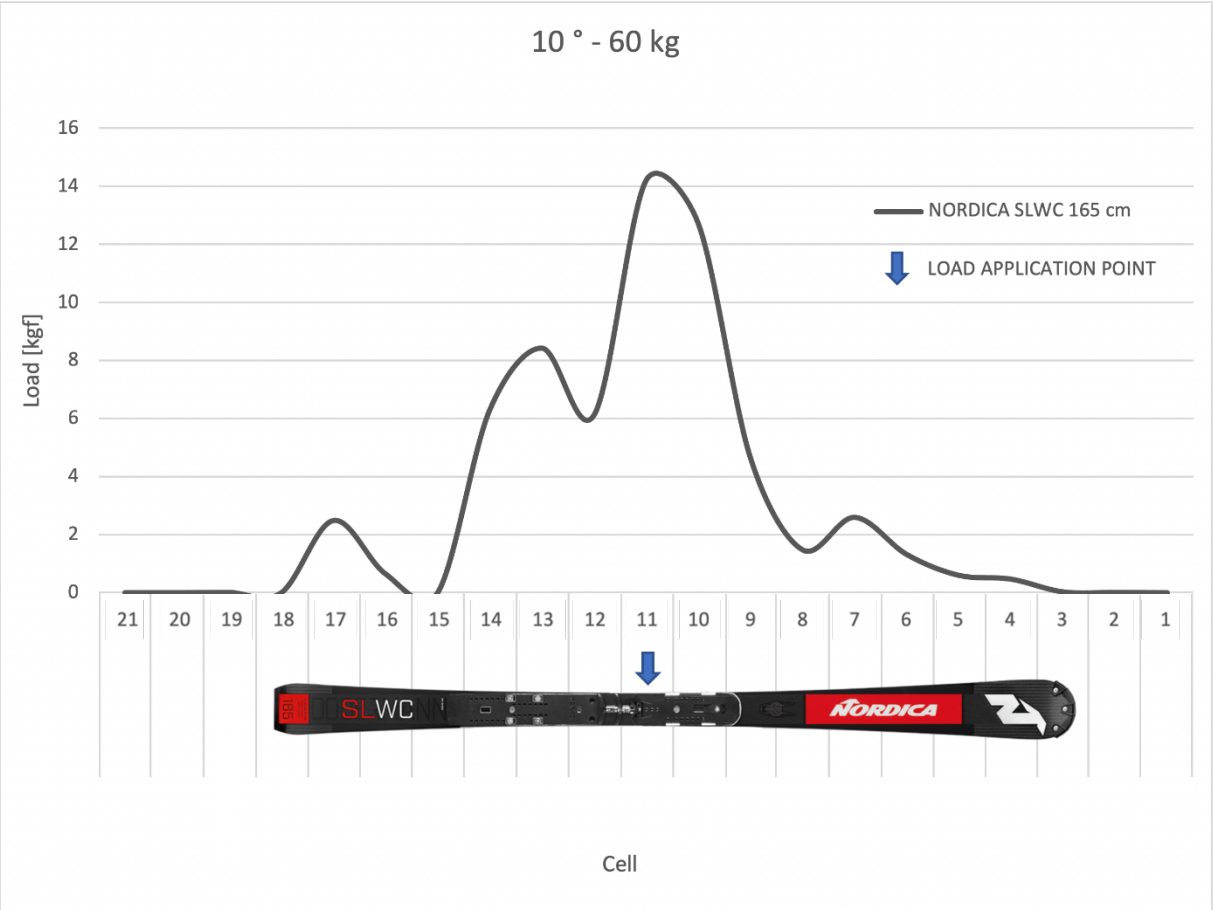

$$F \cdot \cos\alpha = 60 \cdot 9.81 \cdot \cos 10\,° = 579.66\ N$$

$$F_Z \cdot \cos\alpha + F_Y \cdot \sin\alpha = 574.73\ N$$

$$F_Z \cdot \cos\alpha = 569.32\ N$$

20° inclination angle and 70 kg load ELP test on hard snow

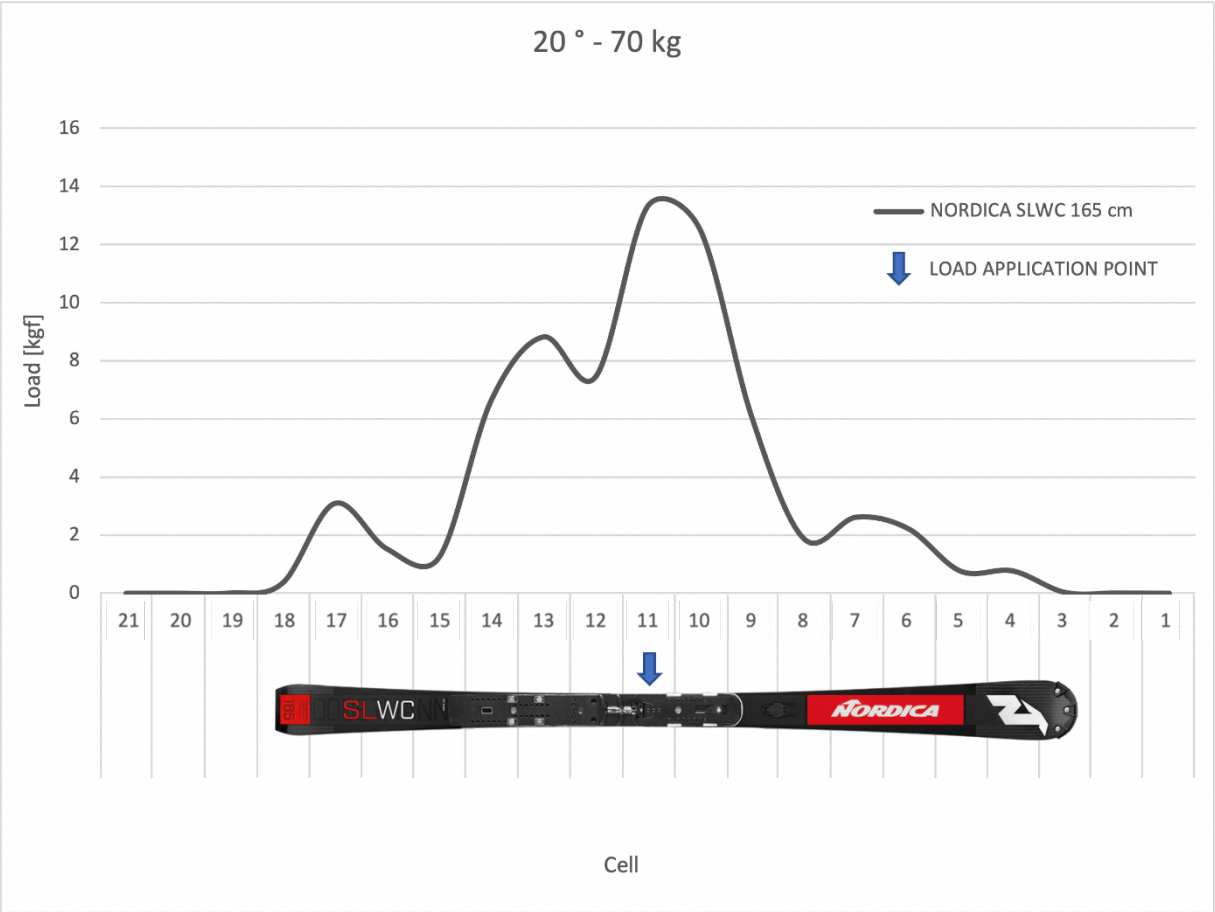

$$F \cdot \cos\alpha = 70 \cdot 9.81 \cdot \cos 20\,° = 645.29\ N$$

$$F_Z \cdot \cos\alpha + F_Y \cdot \sin\alpha = 640.43\ N$$

$$F_Z \cdot \cos\alpha = 634.25\ N$$

30° inclination angle and 85 kg load ELP test on hard snow

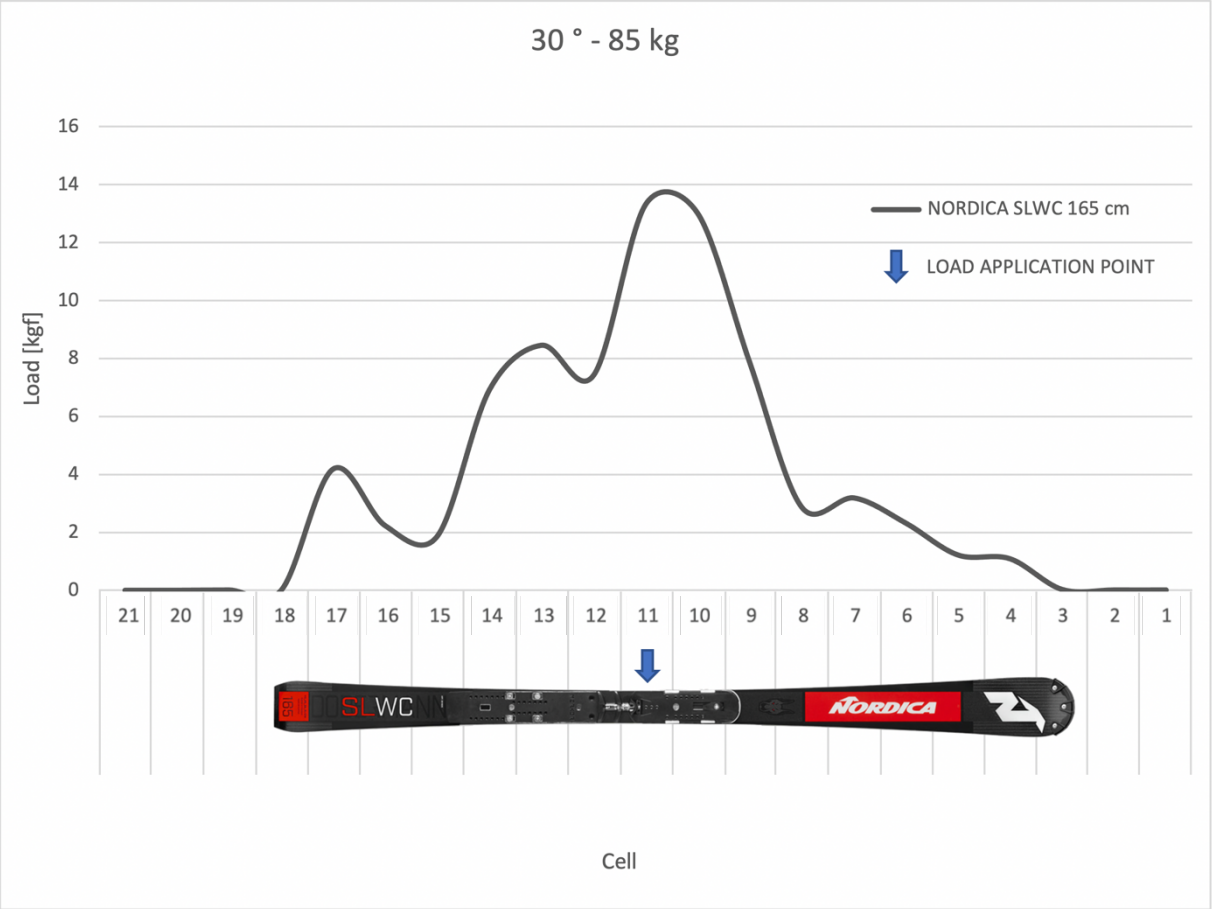

$$F \cdot \cos\alpha = 85 \cdot 9.81 \cdot \cos 30\,° = 722.14\ N$$

$$F_Z \cdot \cos\alpha + F_Y \cdot \sin\alpha = 715.57\ N$$

$$F_Z \cdot \cos\alpha = 708.32\ N$$

40° inclination angle and 100 kg load ELP test on hard snow

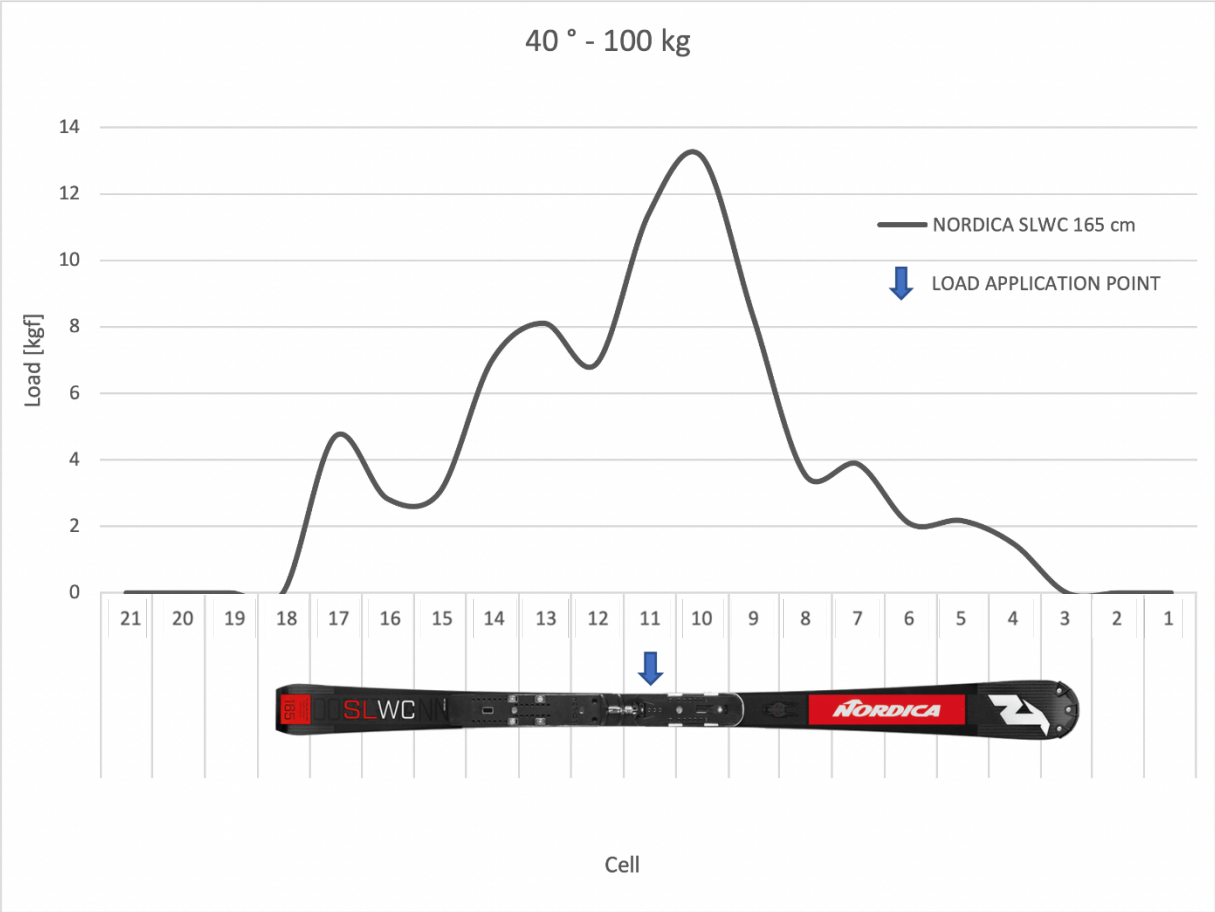

$$F \cdot \cos\alpha = 100\ 9.81 \cos 40\,° = 751.49\ N$$

$$F_Z \cdot \cos\alpha + F_Y \cdot \sin\alpha = 740.55\ N$$

$$F_Z \cdot \cos\alpha = 729.83\ N$$

50° inclination angle and 120 kg load ELP test on hard snow

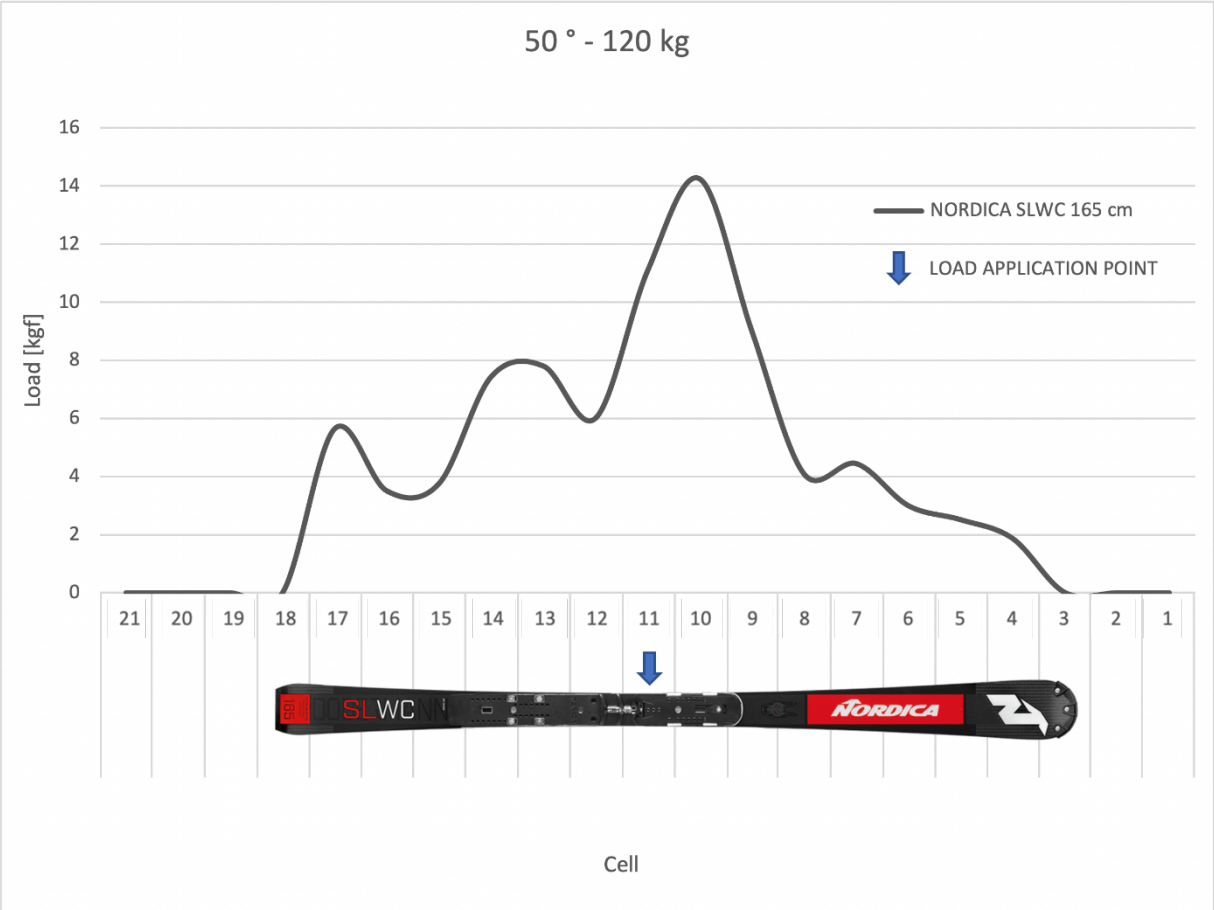

$$F \cdot \cos\alpha = 120\ 9.81 \cos 50\,° = 756.69\ N$$

$$F_Z \cdot \cos\alpha + F_Y \cdot \sin\alpha = 742.28\ N$$

$$F_Z \cdot \cos\alpha = 726.17\ N$$

60° inclination angle and 140 kg load ELP test on hard snow

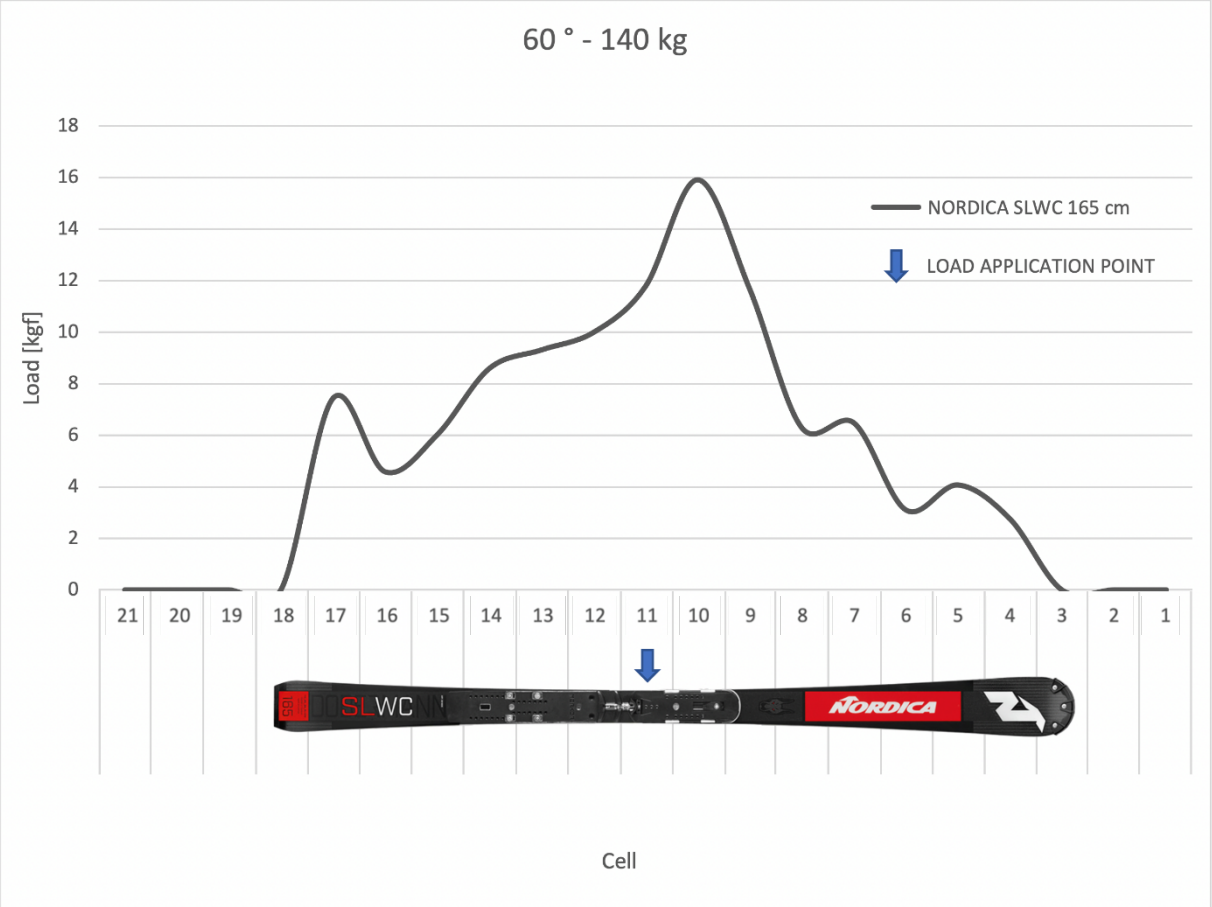

$$F \cdot \cos\alpha = 140\ 9.81 \cos 60\,° = 686.70\ N$$

$$F_Z \cdot \cos\alpha + F_Y \cdot \sin\alpha = 669.54\ N$$

$$F_Z \cdot \cos\alpha = 654.95\ N$$

As before the tests results show that the Edge Load Profile rises with the increase of the inclination angle and of the applied load (*Figure 3.10*). The main peak decreases going from 10° to 40° and increases from 40° to 60°. It also slightly slides towards the tip of the ski with greater inclination angles.

The 60° Edge Load Profile curve once again has the greatest underlying area, even though the majority of the force is parallel to the ground.

Also the difference between the theoretical force and the measured one increases with greater inclination angles and applied loads.

On the *Nordica SLWC* skis the "hole" is not as evident as in the Nordica Prototype. A slight drop in Edge Load Profile curve in correspondence of cell 5 and 6 can be seen at 20°, 30° and 40°, while a considerable drop is visible at 60°. This may be due to the sidecut of the Slalom skis that, as seen in chapter 2 (*table 2.1*), has two Turn Radiuses: a smaller on the front of the ski and a wider one on the back. This should make the ski adhere better to the snow along all his length, explaining the absence of the "hole".

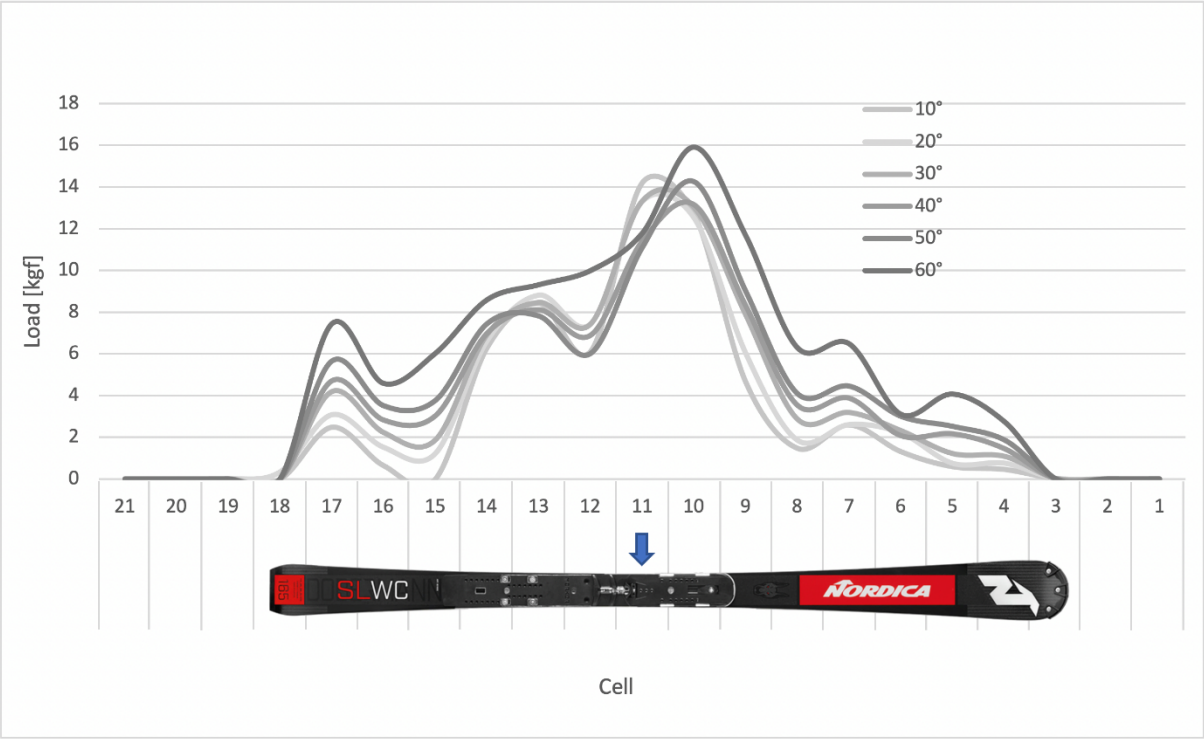

Figure 3.10. *Nordica SLWC 165 cm Edge Load Profile at different inclination angles*

4. In vivo outdoor test sessions

The instrumentation presented in the previous chapters was used on in-vivo outdoor tests. Data collected in these tests will be then elaborated and analyzed in detail along this chapter.

4.1. Analysis methods

Between March 2022 and March 2023, three different in-vivo outdoor test sessions were performed. Two former Ski World Cup athletes skied on 3 different Slalom and Giant Slalom courses. An overview of the test sessions with the Set up used and the details of the track and the skier is reported below (*Table 4.1.*; *Table 4.2.* ; *Table 4.3.)*.

	Date	*Location*	*Discipline*	*Gates*	*Snow conditions*	*Average Gradient*	*Maximum Gradient*
GS1	11/03/22	Alloch	Giant Slalom	*15*	n. d.	27%	49%
SS2	16/12/22	Col Gallina	Slalom	*19*	*Fresh snows, soft*	*23.6%*	*34.5%*
SS3	16/03/23	Lavarone	Slalom	*10 + 22*	*Artificial snow, hard and grippy*	*n. d.*	*n. d.*

Table 4.1. Overview of slope characteristics

	Skis	*Acquisition system*	*Instrumented skis*	*Cells (lower S N° on front)*
GS1	*Blizzard Firebird GS*	*SoMat (1000Hz)*	1/2 on right leg 6 channels system	SN13828 SN13829
SS2	*Nordica Dobermann SLWC*	*DTS (1000Hz)*	1/2 on right leg 6 channels system	SN13828 after repair SN13829
SS3	*Marker WC PC*	*DTS (1000Hz)*	2/2 On both legs 3 channels system	SN13828 after repair } right SN13829 SN13827 } left SN15029

Table 4.2. Overview of Set up used

	Athlete	*Height [cm]*	*BW [kg]*	*Valid Runs*	*Notes*
GS1	Stefano Baruffaldi	173	104	GS1.1 GS1.2 GS1.3 GS1.4	/
SS2	Stefano Baruffaldi	173	101	SS2.3 SS2.4	Broken cables Run 3: anterior cell Run 4: posterior cell
SS3	Davide Da Villa	188	106	SS3.1 SS3.2 SS3.3 SS3.4 SS3.5	Run 4: powerful Run 5: carving

Table 4.3. Overview of Athlete and performed runs

Even though every test session had a different athlete, location and set up, a general method was used. This method standardizes the acquisition process and gives a general approach for the data analysis. It can then be modified and adapted at each case because the method is not specific to Giant Slalom or Special Slalom but it's applicable to every alpine skiing discipline dividable in cycles that repeat themselves.

Starting with the acquisition, all data was acquired at a sample rate of 1000 Hz. In order to have a sync reference and a zero-offset value for signal adjustment, at the beginning and end of every run a specific procedure was followed in all the test sessions:

1. Each run started with the ski boot detached from the ski bindings.
2. The athlete attached the ski boots.
3. The athlete rose his right leg, lifting the instrumented ski from the snow for 3 seconds
4. The athlete lowers the instrumented ski
5. Right before starting the slalom the athlete hits 3 times the snow with the instrumented ski.

At the end of the slalom the skier followed the same procedure backwards before the run was stopped.

Moving on to data analysis, the method consists of the following steps:

1. All load cell physical channels are loaded in mV/V, eventually dividing mV data by 5 V (i.e., nominal supply voltage of the load cell)
2. A Butterworth lowpass zero-phase filter (4^{th} order, cut-off: 5 Hz) is applied to smooth data from high frequency ski vibrations and electrical noise.
3. Data in mV/V is pre multiplied by the calibration matrixes to obtain values in N and Nm and by the rotation matrix to align load cell to ski reference system with the following formula:

$$[F_X \quad F_Y \quad F_Z \quad M_X \quad M_Y \quad M_Z] = ([R]([C] \cdot [ch_1 \quad ch_2 \quad ch_3 \quad ch_4 \quad ch_5 \quad ch_6]^T))^T.$$

At the end of these operations the forces F_X, F_Y, F_Z [N] and moments M_X, M_Y, M_Z [Nm] are obtained. Both forces and moments are expressed in the reference system of the ski.

4. In order to simultaneously analyze data of different turns, the whole acquisition is divided in cycles. M_X is used to segment data because its sign is positive when the skier is turning left and negative when he is turning right. This change of sign allows to divide the slalom performance into multiple cycles, one every negative to positive zero-crossing of M_X. In each cycle the skier performs a left turn around one gate and a right turn around the following gate.
5. Of these cycles, a few consecutive ones are selected (3 for the Giant slalom and 5 for the slalom) to consider only the "stationary" phase and neglect starting and finishing transients.
6. All the channels are in the time domain and the duration of each cycle is never equal due to differences in the gradient of the slope, in the position of the gates but also to the intrinsic human factor involved in the sport performance. In order to overlap and operate with forces and moments, all data of each of the cycles is normalized to 1001 samples. The progression of the samples from 1 to 1001 is also a measure of the cycle advancement from 0% to 100% of the cycle duration.
7. From the normalized data, the average curves of all load components in the normalized cycles are determined for both front and rear cells.
8. The mean forces and mean moments are then combined with the position of the front and rear cell to calculate the GRF and GRM under the ski.
9. In order to compare the performance of different athletes with different weights the GRFs and GRMs are normalized by the bodyweight BW which includes the weight of the athlete, of the acquisition system and of the ski equipment.
10. The center of pressure position during the average cycle is determined.

This General method will be applied as it is in the GS1 test session and will be modified for SS2 and SS3 test sessions.

4.2. GS1

The GS tests were performed in Aloch Ski Stadium, Pozza di Fassa (TN), on March 11th 2022 by the former World Cup skier Stefano Baruffaldi (weight 85 kg, height 173 cm).

The skis used were the *Blizzard Firebird GS* 188 cm in the 6 channels configuration. The one with the load cells was attached to the athlete's right foot. The SoMat and its battery were placed in a backpack. The load cell signal cables ran from the transducers to the acquisition system along the athlete right leg (*Figure 4.1*). The total mass of the athlete dressed and equipped with the backpack was 104 kg.

Figure 4.1. GS1 Setup

Aloch slope has an average gradient of 27% and a maximum gradient of 49%. 15 gates were planted, the first being on the left.

A total of 4 runs were performed: GS1.1, GS1.2, GS1.3, GS1.4. GS1.1 was the first to be studied.

GS1.1

In order to simultaneously analyze data of different turns, the whole acquisition was divided in cycles using M_{XF} (*Figure 4.2*)

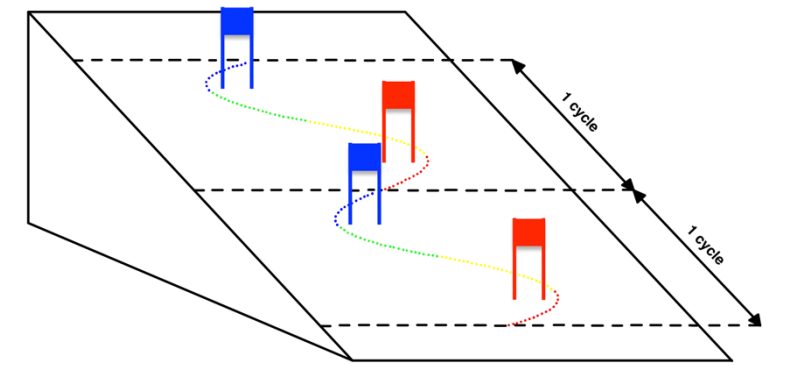

Figure 4.2. *Segmentation of the GS in cycles*

Of these cycles, three were selected specifically the consecutive with the most resembling plot of M_{XF} (*Figure 4.3*).

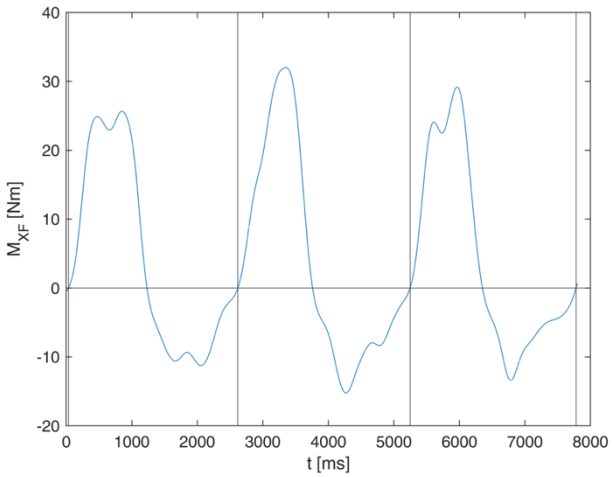

Figure 4.3. *Segmentation of GS using M_{XF} sign*

The load components of these three cycles was normalized to 1001 samples.

The mean curve of all channels in these three normalized cycles was determined for both front and rear cells. The results are represented separately in *Figure 4.4* and with their standard deviation over the three cycles in *Figure 4.5*.

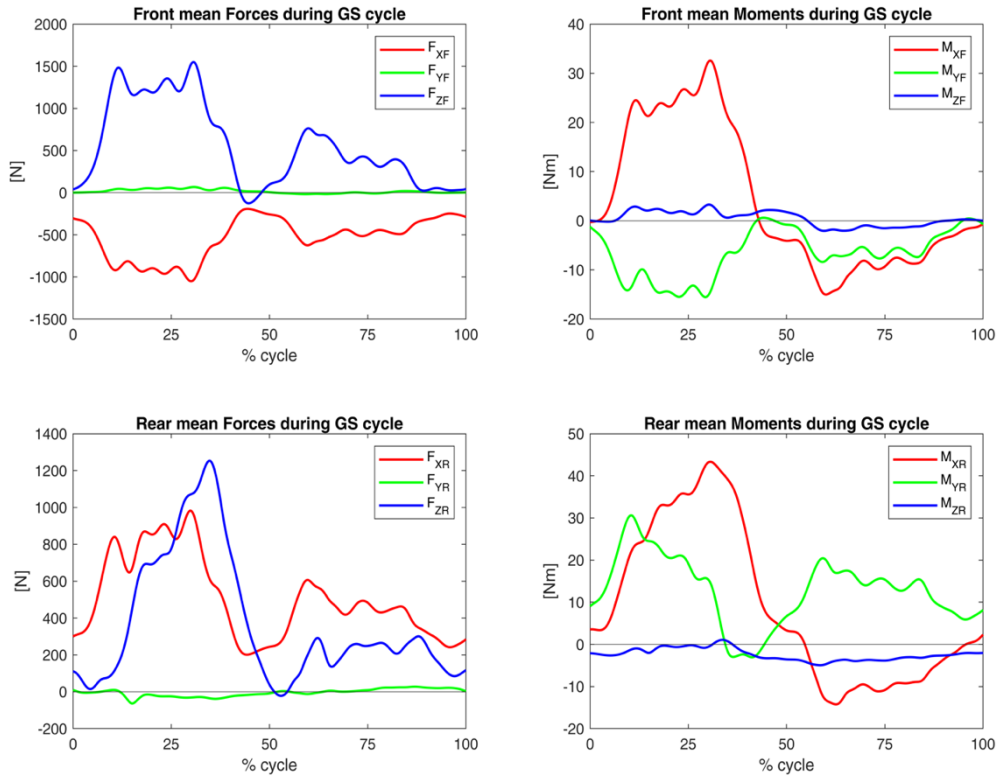

Figure 4.4. Mean Forces (left) and Mean Moments (right) acquired by the front cell (top graphs) and by the rear cell (bottom graphs) during a full GS cycle. GS1.1

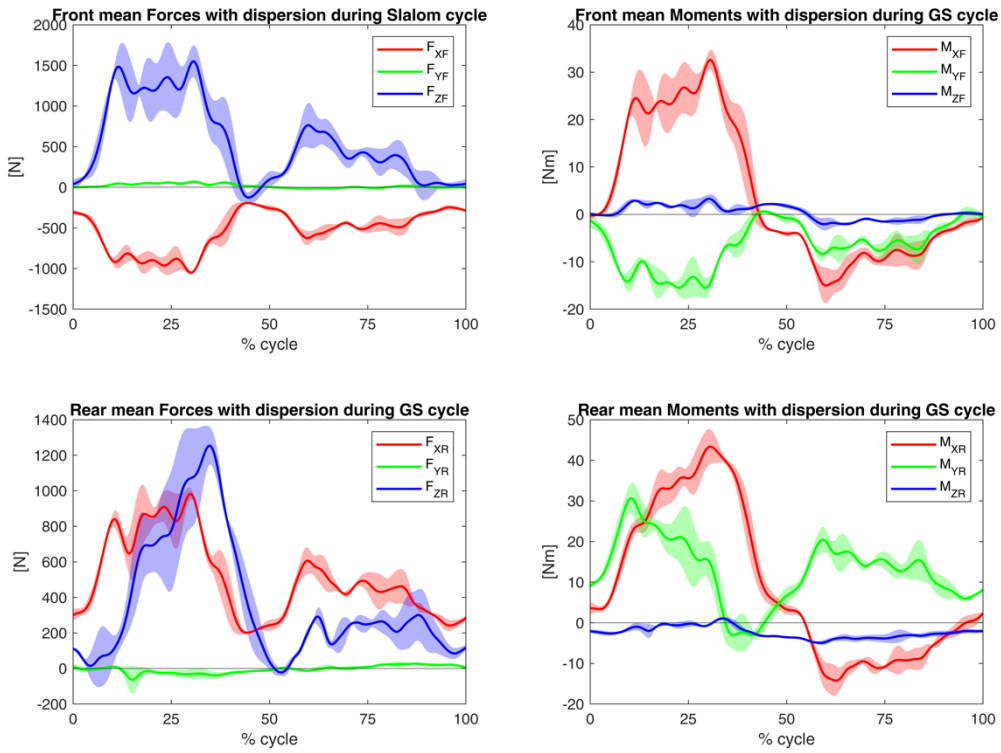

Figure 4.5. Mean Forces (left) and Mean Moments (right) acquired by the front cell (top graphs) and by the rear cell (bottom graphs) with dispersion during a full GS cycle. GS1.1

The mean forces and mean moments were combined with the position of the front and rear cell to calculate the GRF. In order to compare the performance of different athletes with different weights the GRFs and GRMs were normalized by the bodyweight BW which includes the weight of the athlete, of the acquisition system and of the ski equipment (*Figure 4.6*).

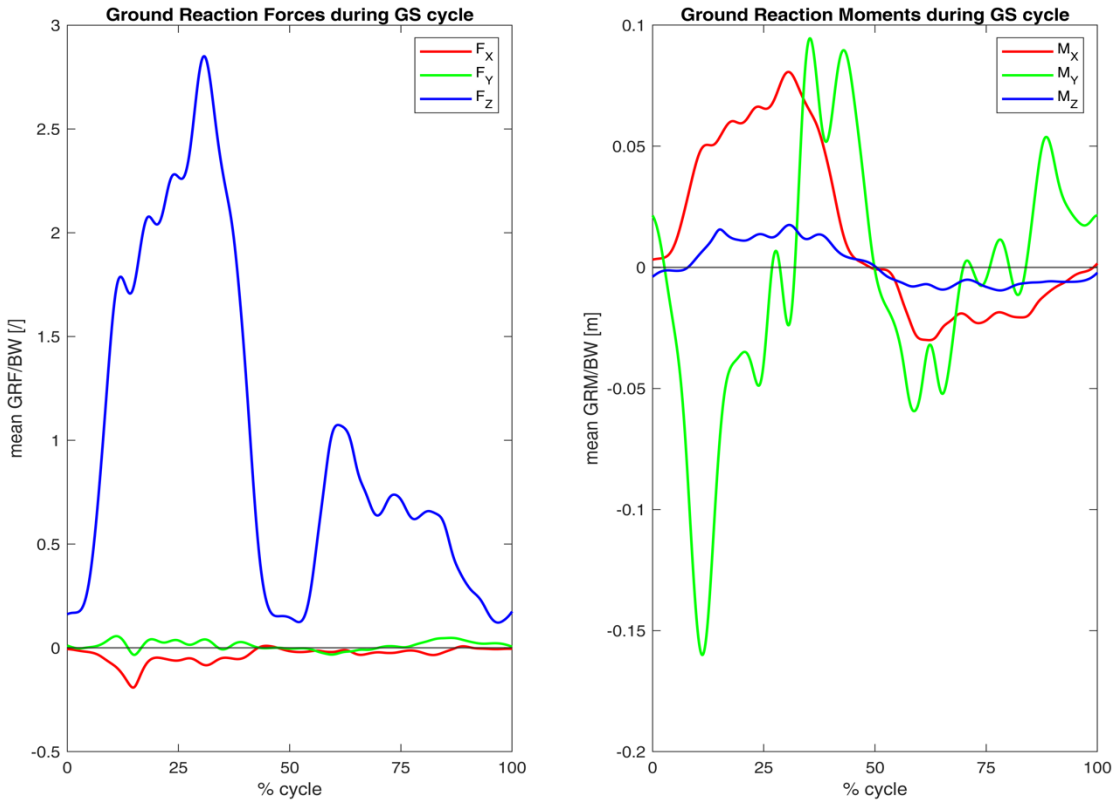

Figure 4.6. Ground reaction forces on the left and ground reaction moments on the right, normalized by bodyweight, during the GS cycle. GS1.1

The GRFs were also determined for each of the three normalized cycles in order to evaluate the Standard deviation (*Figure 4.7*). *Figure 4.7* shows a small dispersion of the GRFs in the three cycles which is a good sign as it means that the three selected cycles were similar in terms of forces and moments applied.

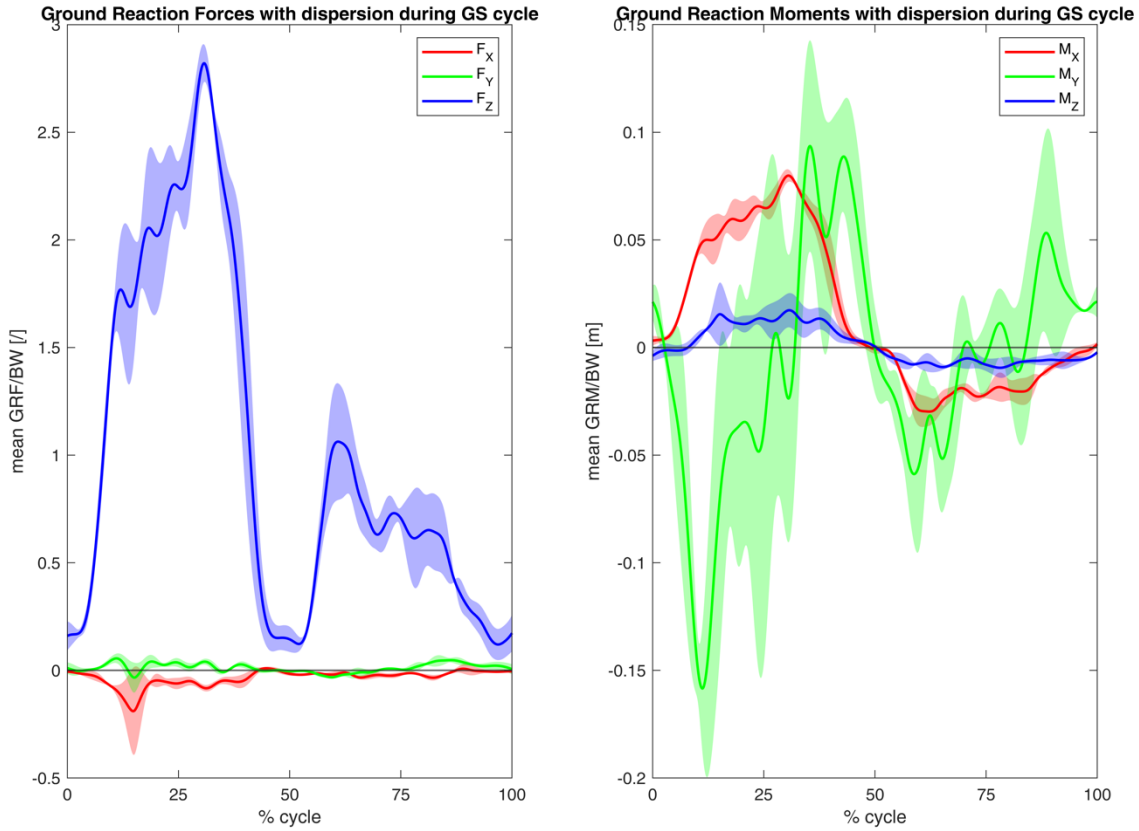

Figure 4.7. *Ground reaction forces on the left and ground reaction moments on the right, normalized by bodyweight, during the GS cycle. GS1.1*

Finally the center of pressure position during the mean cycle was determined. It's coordinates are illustrated in function of the cycle advancement percentage in *Figure 4.8*. To get a better vision of the movement of the COP during one slalom cycle, in *Figure 4.9* its represented in the ski XY plane.

Figure 4.8. *COP coordinates during the GS cycle*

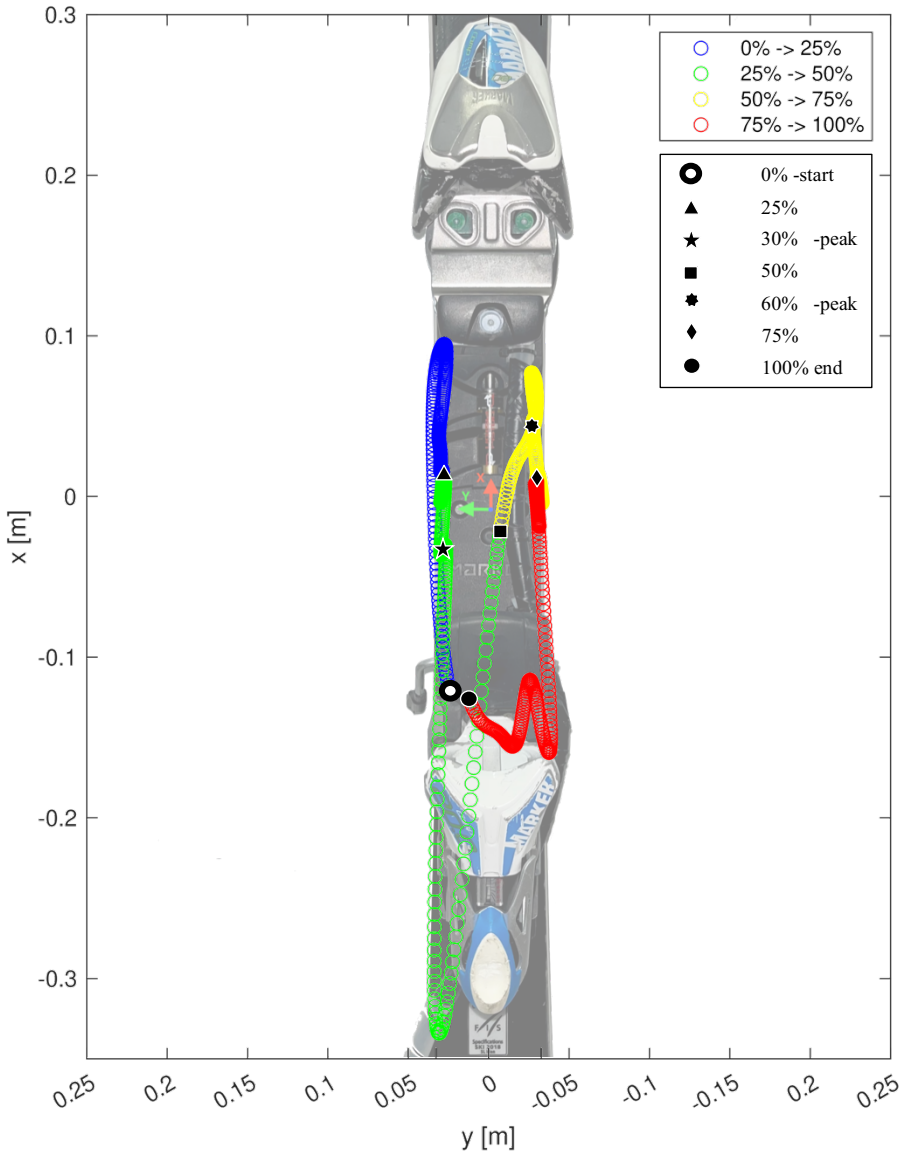

Figure 4.9. *COP movement on the ski during GS cycle. GS1.1*

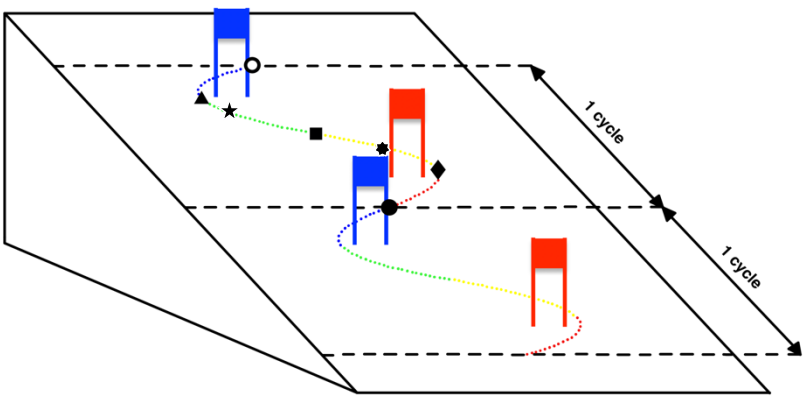

Figure 4.10. *Space representation with markers*

The different symbols and colors used in *Figure 4.9* represent the advancement of the cycle as shown in *Figure 4.10*.The empty circle represents the beginning of the cycle (0%). In this instant the skier has just transferred its weight from the right edge to the left one preparing for a left turn. All the ground reaction forces and moments are almost null. During this turn the instrumented ski is in the outer leg which usually is the most loaded.

The blue color represents the advancement of the cycle from 0% (empty circle) to 25% (triangle). The skier is in left turn entry phase and the loads begin to rise. The locus of points of the COP moves forward along the ski edge and then comes back. At the end of this phase the skier is fully committed to the turn, in an inclined body position pushing the ski edges deep into the snow.

The phase from 25% (triangle) to 50% (square) of the GS cycle is represented by the green color. During this period, around 30% of the cycle (star), F_Z and M_X GRFs reach their absolute peak to then come back to zero while concluding the left turn. Given that at 30% of the cycle the skier is in full left lean, and recalling that the instrumented ski is in his right leg, the calculated GRFs seem coherent to reality. In this instant the COP briefly stabilizes at 8 mm from the ski edge, on the inner side of the ski. This behavior is probably due to the increase of the forces, especially F_Z, that make the ski sink deeper into the snow, increasing the contact surface and moving the COP inwards. Advancing with the cycle the COP keeps going backwards, precisely following the ski edge with an offset of 3 mm for then going upward and inward when the skier starts to change edge. At 50% (square) the ground reaction forces and moments go back to zero. The skier is transferring again its weight from the left edge to the right edge and the right turn begins. At this change of edge corresponds a rapid movement of the COP to the other side of the ski. While turning right, the instrumented ski is on the inner leg which usually transfers less weight to the ground.

The phase from 50% (square) to 75% (rhombus) of the GS cycle is represented in yellow. Now the skier is in right turn entry and the absolute value of F_Z, M_X and M_Y begin to rise until reaching the relative peak around 60% of the cycle (7 points star). As expected, the maximum absolute values of F_Z, M_X and M_Y in the inner leg are significantly lower than the ones in the outer leg. In particular F_Z and M_X peak values of the outer leg are about a third of the one in the inner leg. Indeed, in this phase of the

cycle the skier is leaning right transferring most of the load through his outer leg and a minor part of the load through the instrumented inner leg This is also seen on the COP that, at 60% of the cycle, is at 5 mm from the edge on the inner side instead of the 8 mm at 30%. The lower loads make the ski sink less into the snow on the right edge then on the left edge. This phase continues until 75% of the cycle where the skier is fully leaned to the right, committed to the turn.

The last phase in red goes from 75% (rhombus) to the end of the cycle marked with a filled circle. The COP locus of points results sharp and defined also on this side, going down along the shape of the ski edge with an offset of 2 mm. At the end of the cycle the skier changes again edge and gets ready for the new cycle. The GRFs decrease once more to zero and the COP once again goes upward and inward the ski almost closing itself in a loop. Ideally the end of the cycle (filled circle, 100%) should coincide with the start of the cycle (empty circle, 0%), but as each turn depends on the conformation of the slope and as the human factor is involved, each cycle is never perfectly equal to the previous one.

The COP locus of points is represented in isometric view in *Figure 4.11* with the corresponding GRFs.

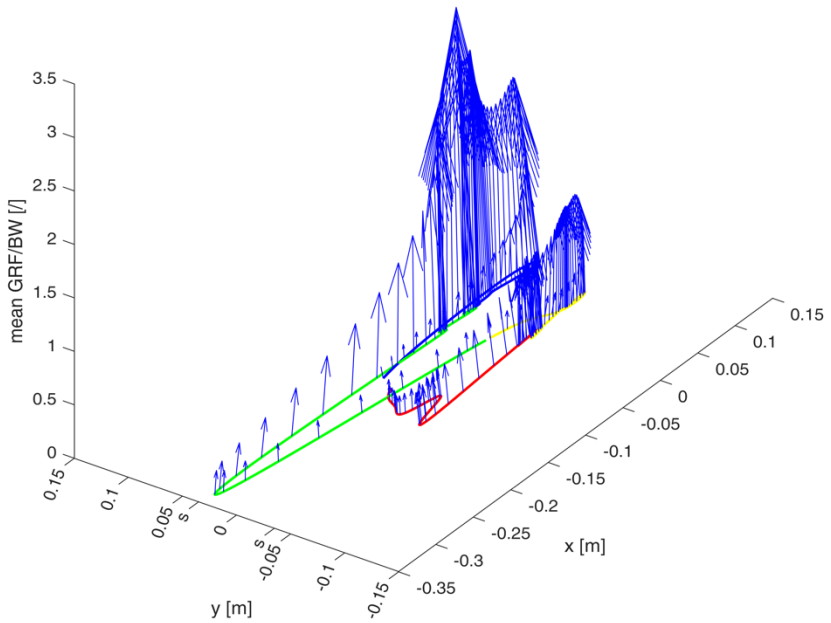

Figure 4.11. 3D plot of the COP with the GRFs. GS1.1

The same analysis was done using data from the other three runs performed. All of them were done using the same three cycles. The results are showed below.

GS1.2

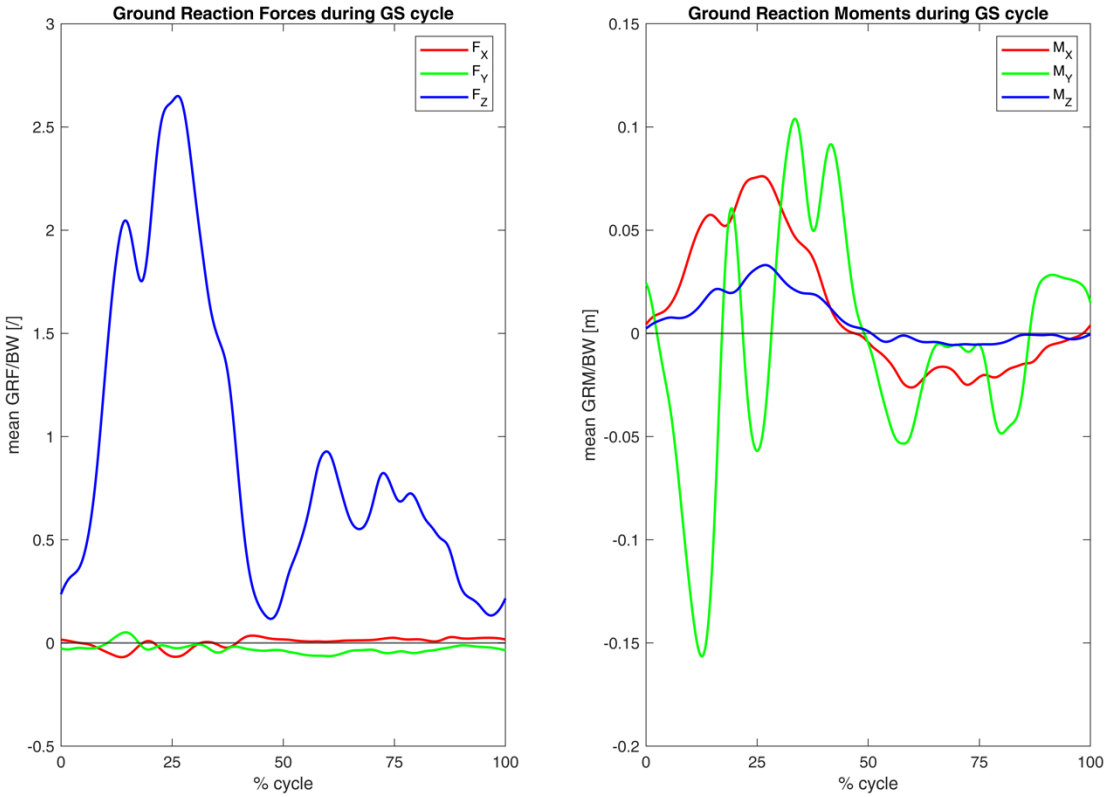

Figure 4.12. Ground reaction forces on the left and ground reaction moments on the right, normalized by bodyweight, during the GS cycle. GS1.2

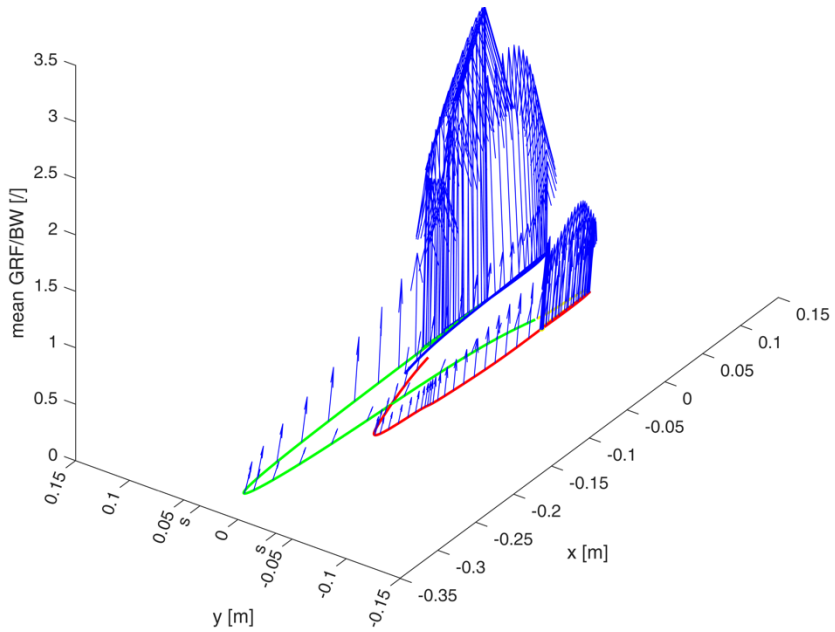

Figure 4.13. 3D plot of the COP with the GRFs. GS1.2

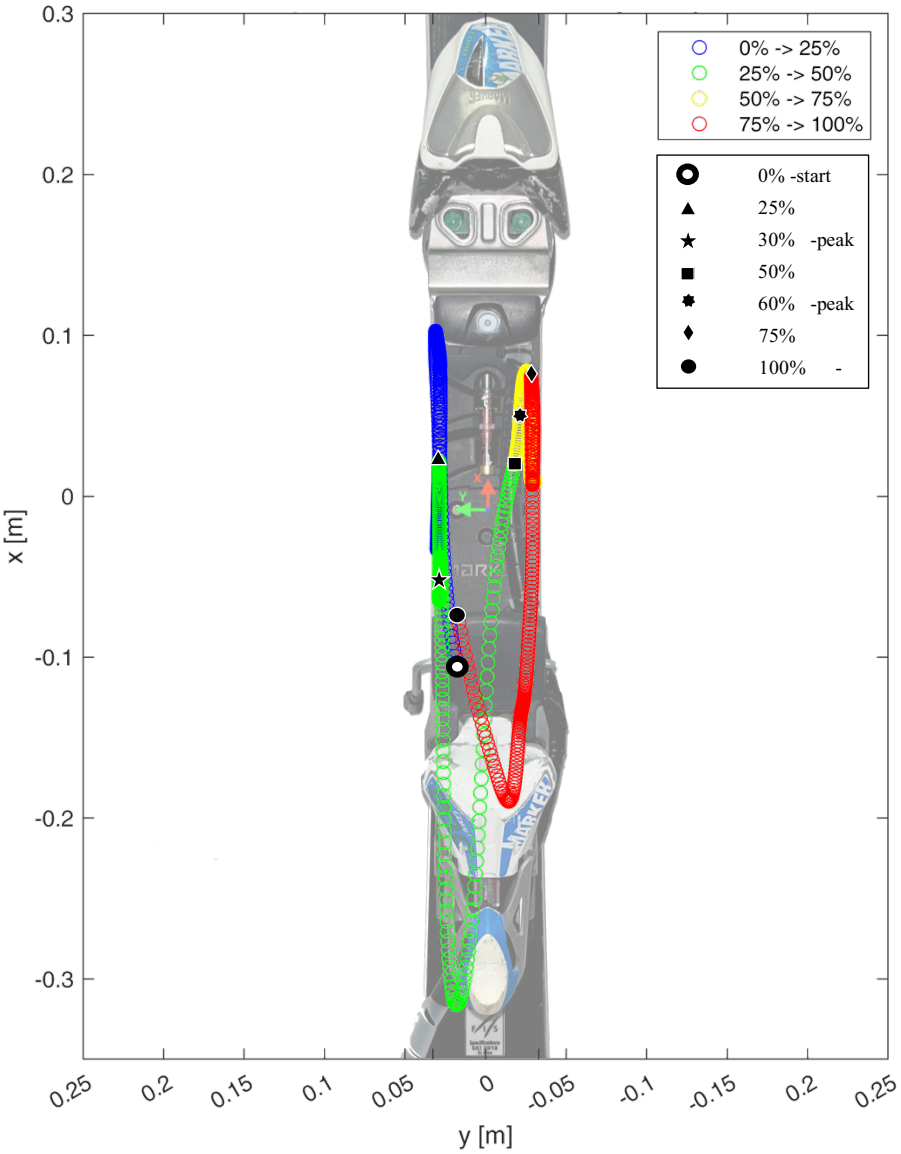

Figure 4.14. *COP movement on the ski during GS cycle. GS1.2*

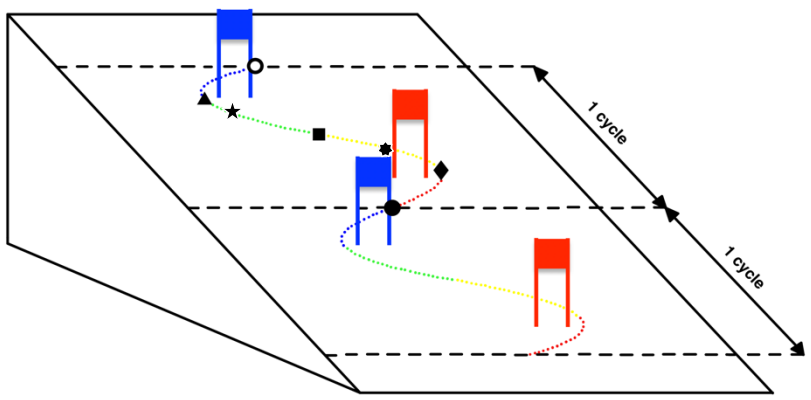

Figure 4.15. *Space representation with markers*

GS1.3

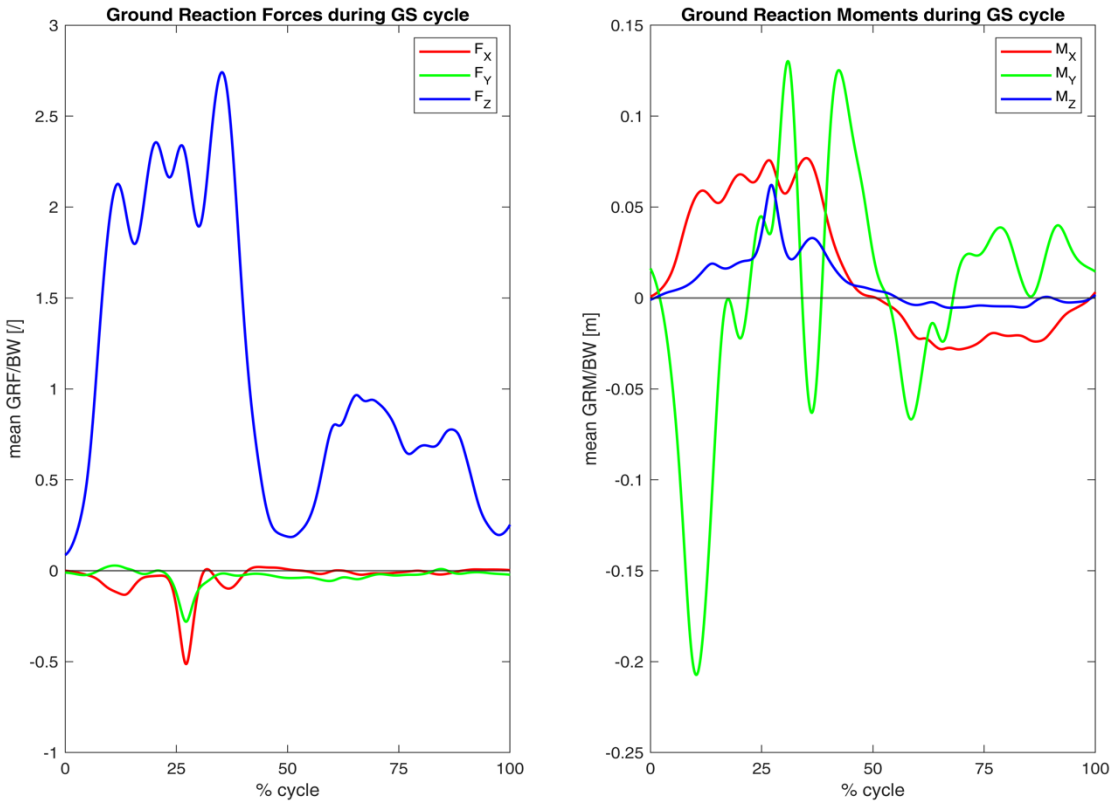

Figure 4.16. Ground reaction forces on the left and ground reaction moments on the right, normalized by bodyweight, during the GS cycle. GS1.3

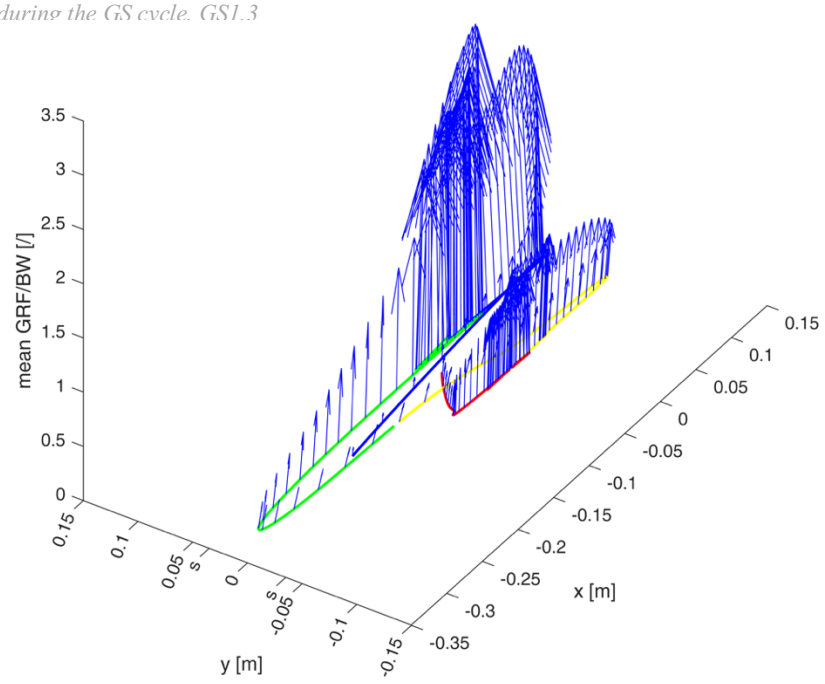

Figure 4.17. 3D plot of the COP with the GRFs. GS1.3

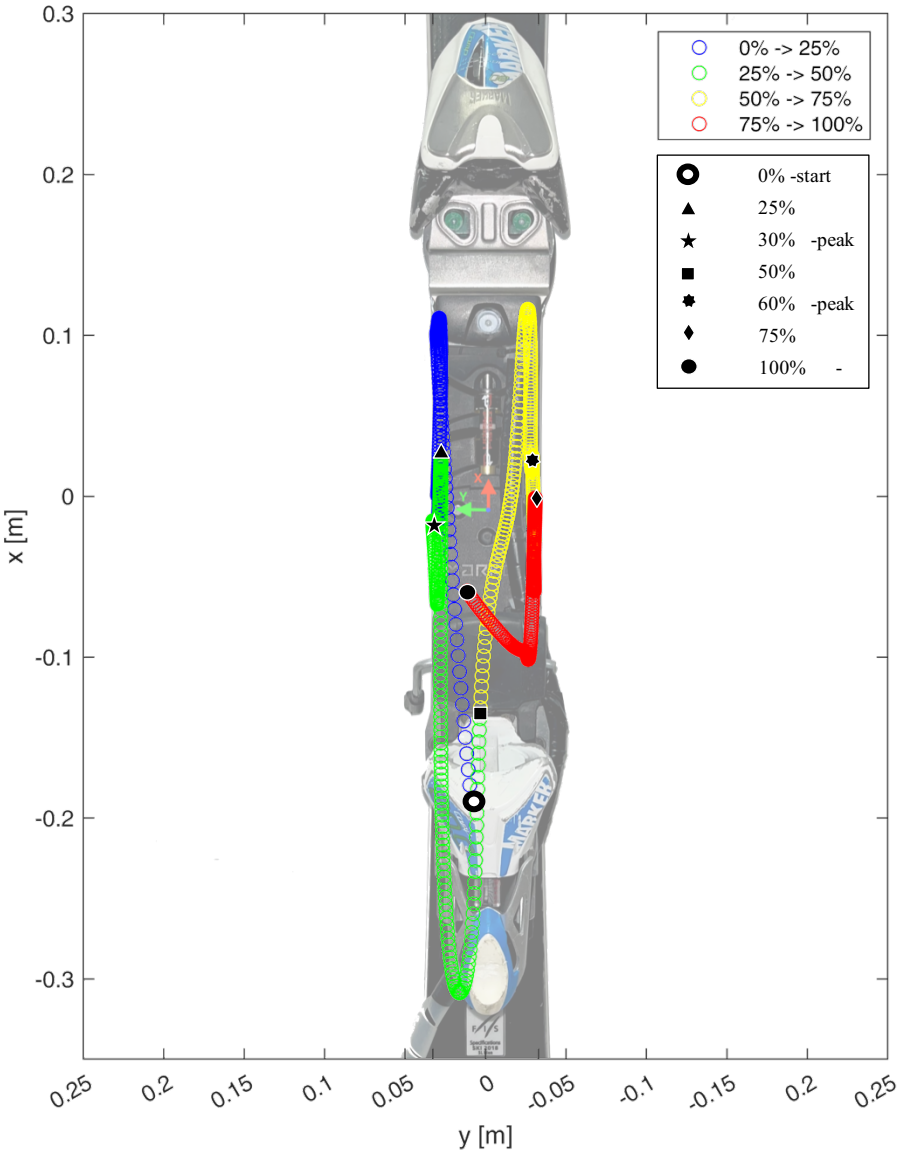

Figure 4.18. COP movement on the ski during GS cycle. GS1.3

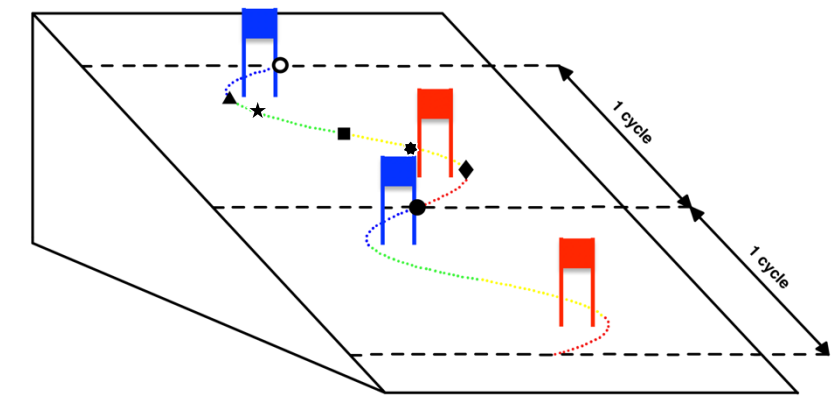

Figure 4.19. Space representation with markers

GS1.4

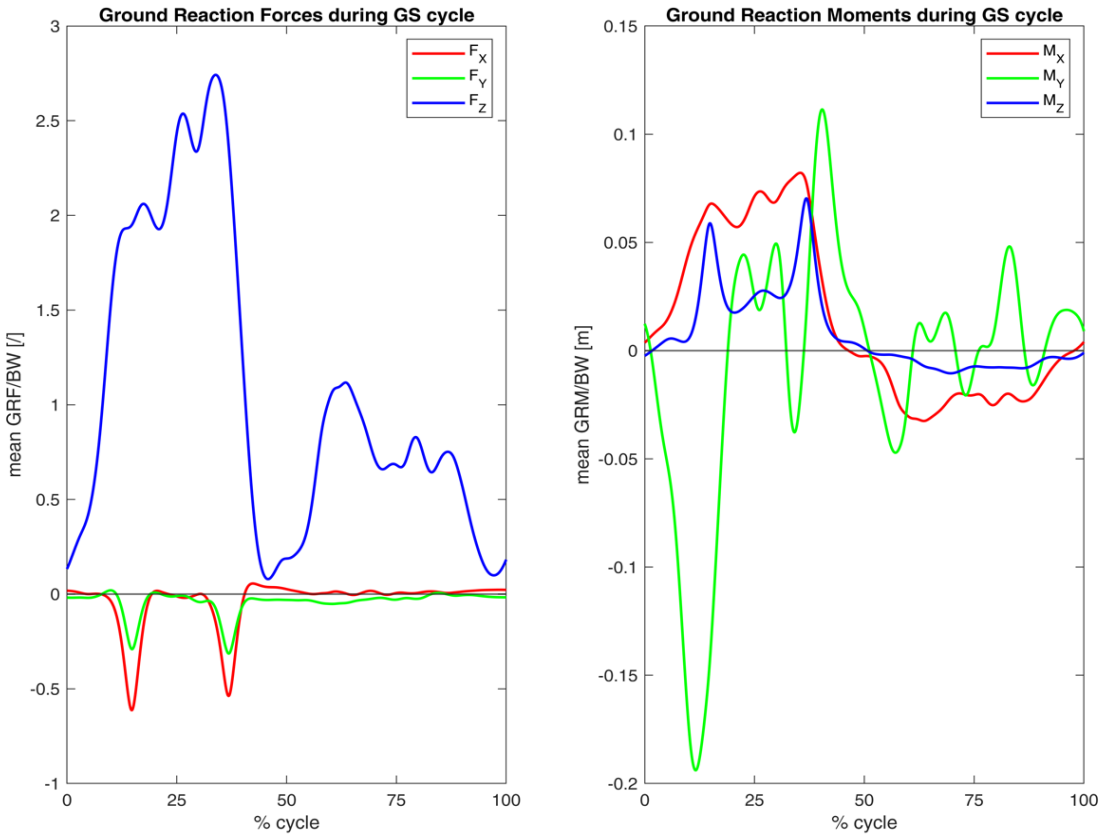

Figure 4.20. Ground reaction forces on the left and ground reaction moments on the right, normalized by bodyweight,during the GS cycle. GS1.4

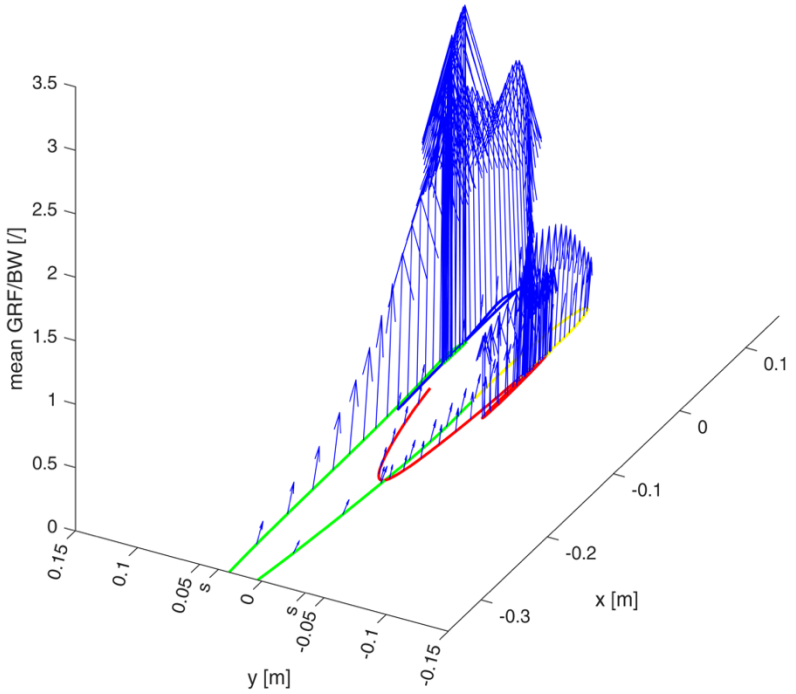

Figure 4.21. 3D plot of the COP with the GRFs. GS1.4

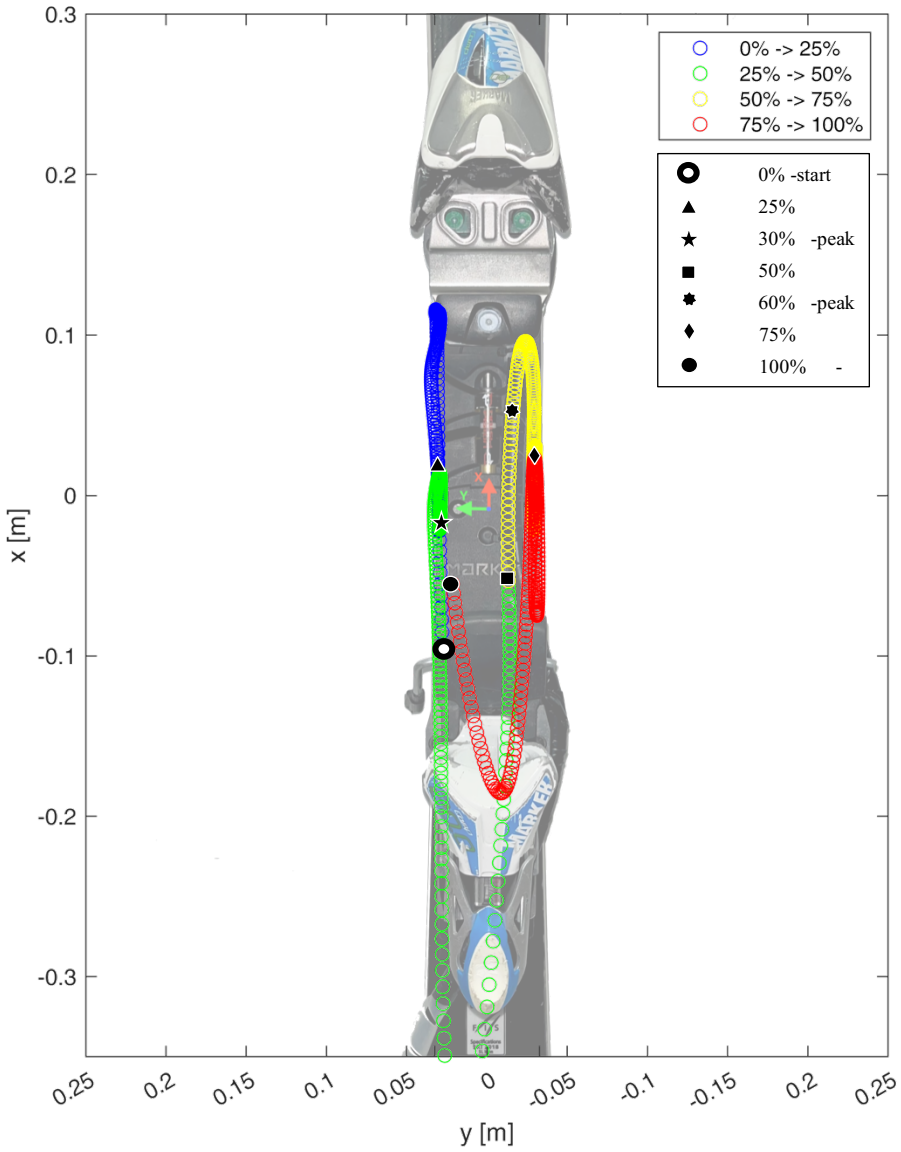

Figure 4.22. *COP movement on the ski during GS cycle. GS1.4*

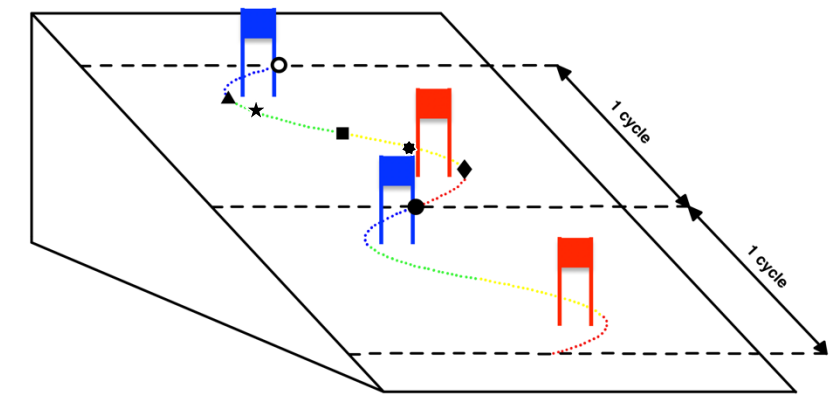

Figure 4.23. *Space representation with markers*

4.3. SS2

A Slalom in vivo outdoor test was performed on December the 16th 2022 in Col Gallina, at Passo Falzarego, Cortina d'Ampezzo (BL). The athlete was the same former World Cup skier Stefano Baruffaldi of the GS tests. (body mass: 80 kg, height: 173 cm).

The ski used were the *Nordica Dobermann SLWC 165 cm* with the same *Marker WC PC* interface plate and same *Marker Comp 16.0 EPS* bindings. The acquisition system used for these tests was the *DTS* that is much lighter and compact then the one used for the GS tests. 6 channels for each cell were acquired.

Col Gallina slope has an average gradient of 23.6% and a maximum gradient of 34.5%. 19 gates were planted, the first being on the left.

During the test session, six runs were performed. Due to technical problems with the acquisition system it was possible to acquire the measurement of only one cell at a time. On the first three runs only the loads measured by the front cell were acquired. On the other three runs only the loads on the rear cell were acquired. Based on the athlete impressions the third (SS2.3) and the fourth run (SS2.4) were the most similar ones in terms of his perceived performances and condition of the slope. Front cell data was taken from SS2.3 and rear cell data was taken from the SS2.4. The two runs were analyzed separately and later combined to calculate the GRFs and the COP.

As for the GS the whole acquisition was divided in cycles composed of a left turn around one gate and a right turn around the following gate (*Figure 4.24*).

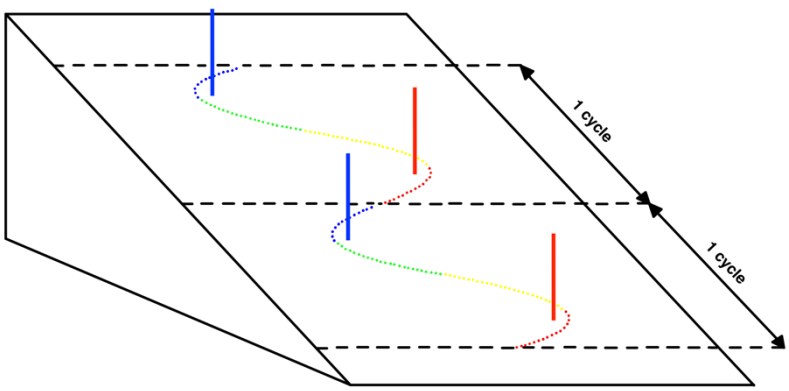

Figure 4.24. Segmentation of the Slalom in cycles

M_{XF} was used to segment data of the front cell, and M_{XR} was used to segment data of the rear cell. As the Slalom has smaller cycles, the same five consecutives were selected for both the front and rear cell instead of the three in the GS analysis (*Figure 4.25*).

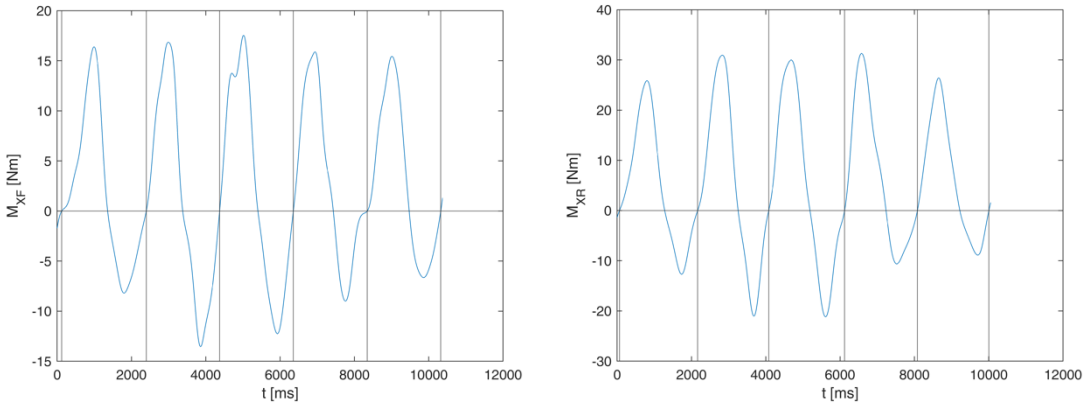

Figure 4.25. Segmentation of SS2.3 and SS2.4 using M_{XF} sign

Each Slalom cycle was normalized in 1001 samples. All the front and rear plots were determined in the normalized cycle and the mean curves were calculated. In *Figure 4.26* the mean forces and the mean moments of the front and rear cell are represented. In *Figure 4.27* the front and rear mean curves are represented with their standard deviation on the corresponding five cycles.

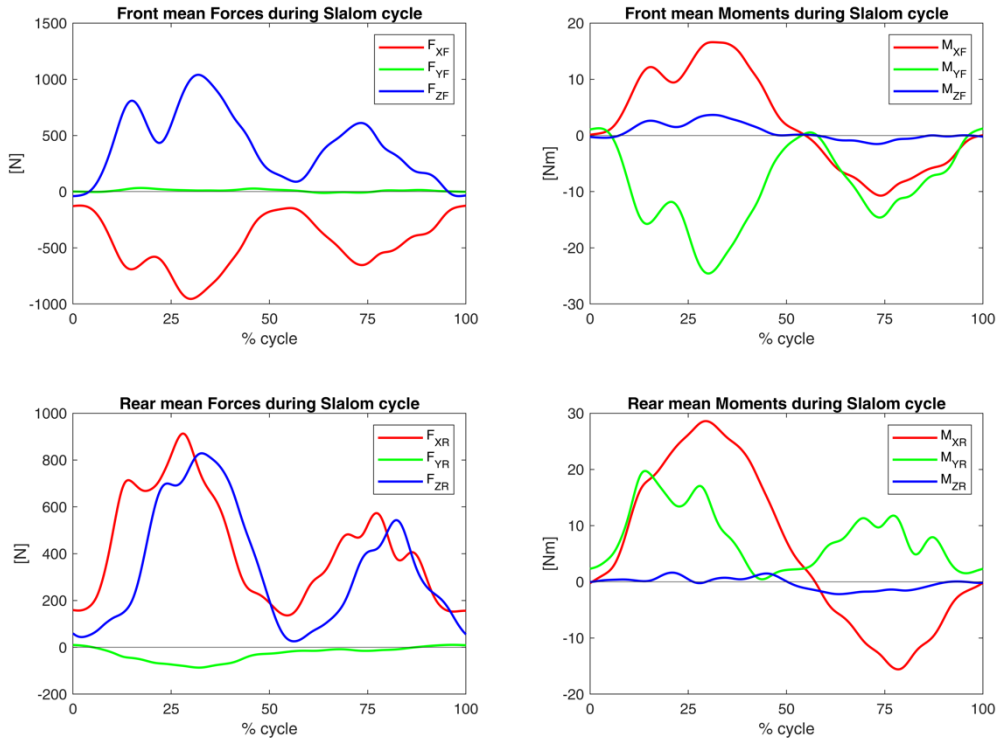

Figure 4.26. *Mean Forces (left) and Mean Moments (right) acquired by the front cell (top graphs) and by the rear cell (bottom graphs) during a full slalom cycle. SS2*

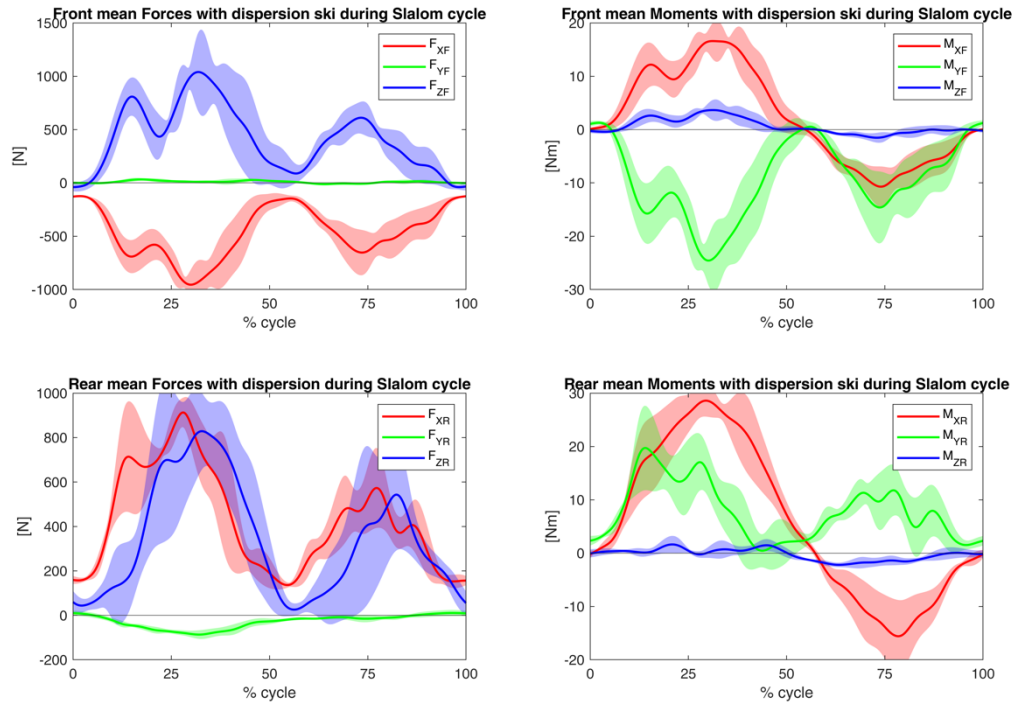

Figure 4.27. *Mean Forces (left) and Mean Moments (right) acquired by the front cell (top graphs) and by the rear cell (bottom graphs) with dispersion during a full slalom cycle. SS2*

All of this being done, the mean forces and mean moments were combined with the position of the front and rear cell, with respect to the reference system of the ski, to calculate the global ground reaction forces and ground reaction moments. The results were then normalized by bodyweight BW which includes the weight of the athlete, of the acquisition system and of the ski equipment (*Figure 4.28*).

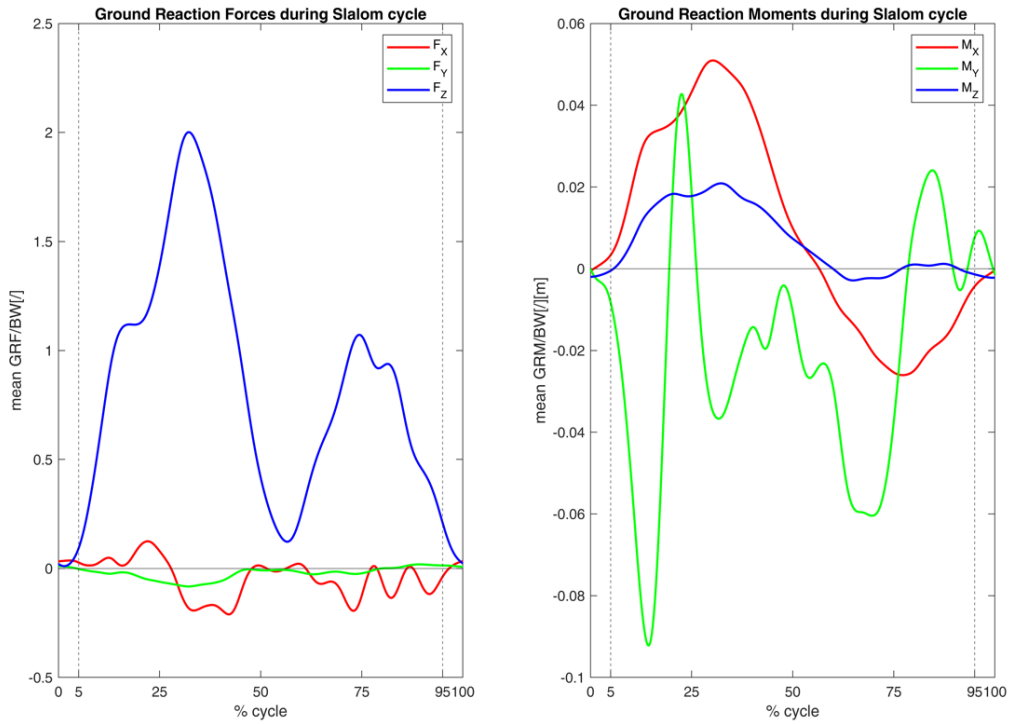

Figure 4.28. Ground reaction forces on the left and ground reaction moments on the right, normalized by bodyweight, during the slalom cycle. SS2

Finally the center of pressure position during the mean cycle was determined. Between 0% and 5% and between 95% and 100%, the COP results very unstable, leaving the ski plane and being far from the shape seen on the previews analysis . This is probably due to the reconstruction of data. In order to save the test session and have a readable COP position, the cycle was reduced from 0% to 100% to 5% to 95%. By eliminating the first and the last 5% of the Slalom cycle the COP coordinates falls all into the ski shape. Ideally in the eliminated part the starting point and the finishing point of the cycle should have the same coordinates closing the COP locus of point in a repeatable loop. In *Figure 4.28* are represented also the vertical lines that delimitates the

reduced cycle from 5% to 95%. In this reduced cycle the COP coordinates are the ones represented in *Figure 4.29.*

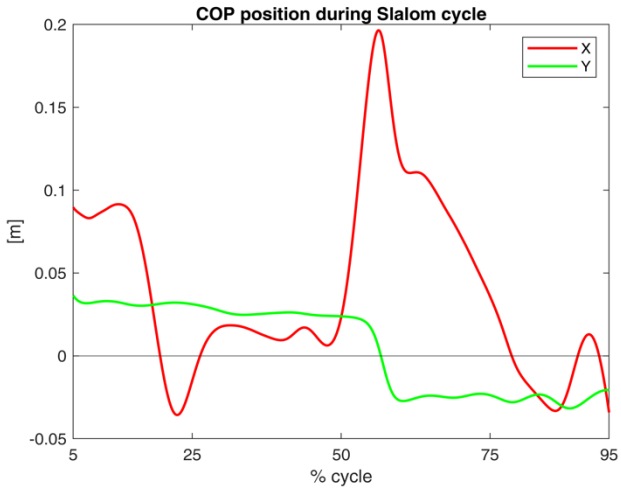

Figure 4.29. COP coordinates during the slalom cycle

To get a better vision of the movement of the COP during one slalom cycle its represented in the ski's XY plane in *Figure 4.30.*

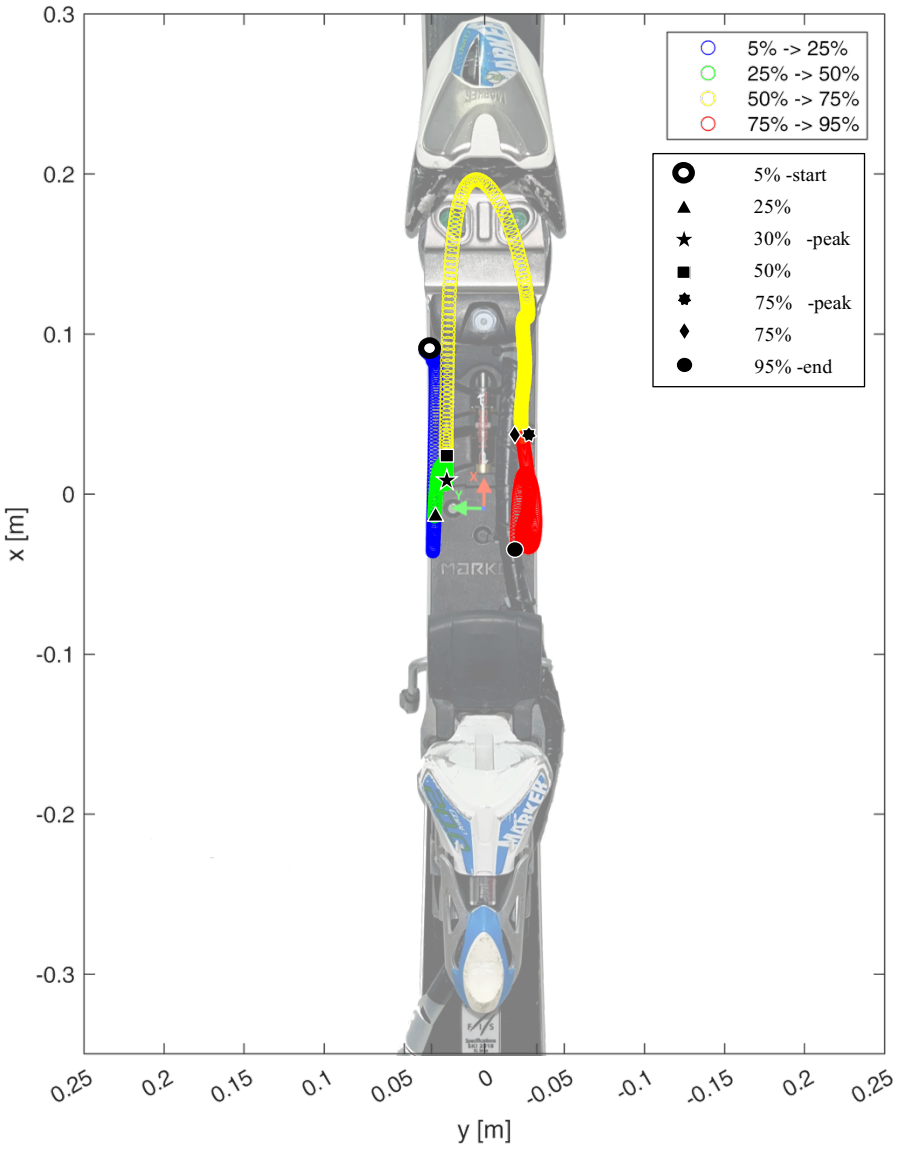

Figure 4.30. *COP movement on the ski during Slalom cycle SS2*

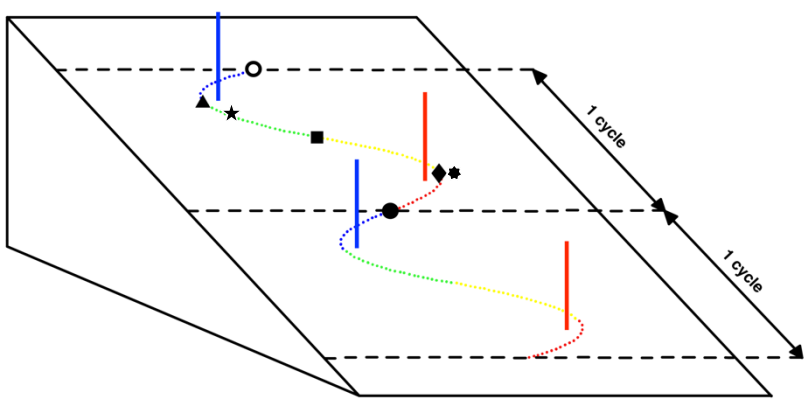

Figure 4.31. *Space representation with markers*

The same symbols and colors used for the GS analysis are used in this instance (*Figure 4.31*). The four colors represent the advancement of the cycle from 5% to 95%.

The first phase in blue is from 5% to 25%. As in the GS, in this phase the COP is very sharp and defined, precisely following the shape of the ski.

The second phase in green is from 25% to 50%. As opposed to the GS where in this phase the COP moved downward over the rear binding, here it slowly moves forward, stabilizing itself at 30 % of the cycle, where F_Z and M_X GRFs reaches their absolute peak.

The skier changes edge and the third phase in yellow begins (50% - 75%). During this phase the COP moves on the right edge. Around 75% the relative peak of Fz and M_X is reached. At the same time the last phase in blue begins (75% - 95%). During this last phase the COP doesn't follow the ski edge like on the other side.

By comparing the locus of points of the COP in the two cases is evident that in the slalom the skier leans more forward than in the GS.

It's also interesting that the peak of the GRFs when the instrumented ski is external remains at 30%, but when the ski is internal it moves from 60% to 75%. This could be due to the Slalom having turns with a minor radius that forces the athlete to load more the skis in order to go around the next gate. However, this could also be caused by the union of the two runs.

Before reaching any other conclusion its necessary to repeat the slalom tests with a fully working setup and the GS tests with the same setup and snow conditions.

4.4. SS3

The last Slalom test session took place in Lavarone (TN) on March 16th, 2023. The athlete was the former World Cup skier Davide da Villa (body mass: 91 kg, height: 188 cm) (*Figure 4.32*).

The skis were the same instrumented *Nordica Dobermann SLWC 165 cm* used in the SS2 tests but this time in their 3 channels configuration seen in chapter 2. In this session, both skis were equipped with two load cells between the ski plate and each front and rear binding, for a total of four load cells. Each pair of load cells were connected using signal cables that ran along the athlete legs to the acquisition system inside a backpack. The acquisition system used was the *DTS Slice Nano*. In order to acquire the channels 1, 3 and 5 of each load cell, two special connectors were made. With this setup 12 channels were acquired. These are the ground reaction force F_z and ground reaction moments M_X and M_Y of every cell. This setup allows to have an overview of the loads acting on the skis and allows for further data analysis. The R or L subscript was added to the previous nomenclature to identify loads on the right and left ski.

The slalom descent consisted of two sectors: a 10 gates first one to worm up followed by the main sector of 22 gates (*Figure 4.33*).

The snow was mostly artificial, and the conditions of the slope were ideal.

It was asked at the athlete to ski uniformly, trying to do left and right turns as similar as possible. A total of 5 Slalom runs were performed: SS3.1, SS3.2, SS3.3, SS3.4, SS3.5. In the first four the athlete skied pushing the skis deeply into the snow and heavily engaging the quadriceps femoris to counterbalance the centrifugal force. SS3.5 was done using less the leg muscles and letting the ski sidecut close the turns. This is a much slower and less intense performance in which the skier is more upright.

SS3.4, according to the athlete, was his best performance, so it was studied first.

Figure 4.32. Athlete ready for the SS3test session

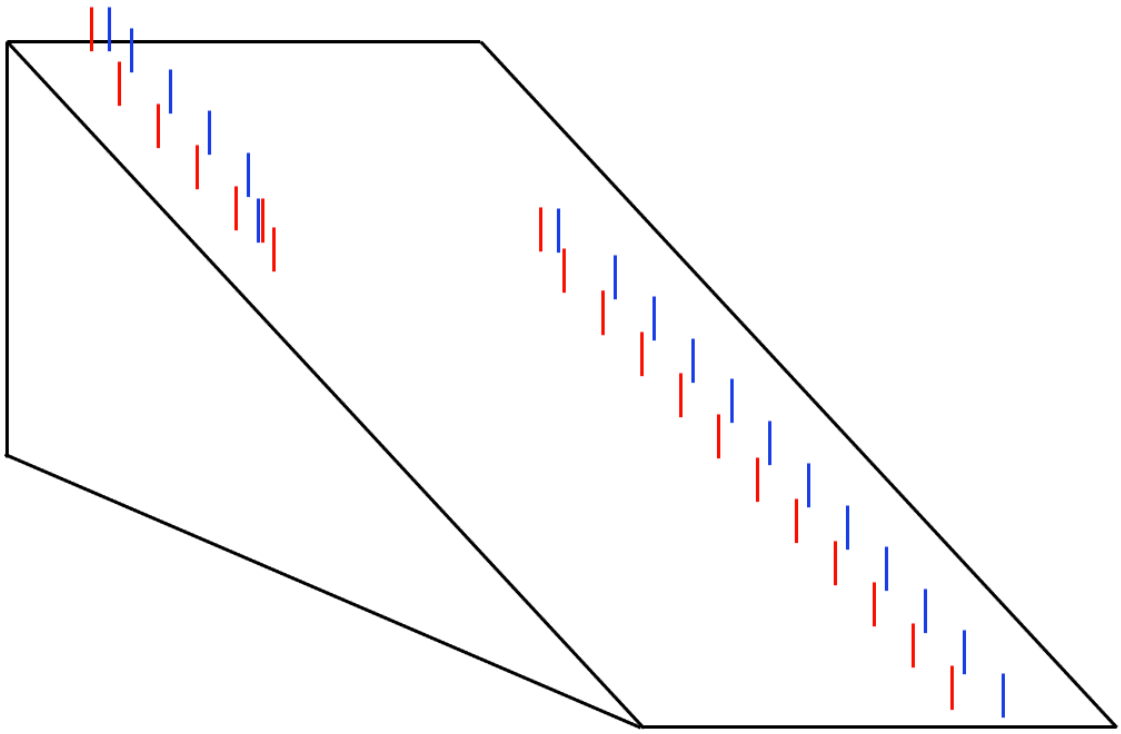

Figure 4.33. Slalom slope scheme

SS3.4

As for the previous Slalom data analysis, 5 turns for each ski were selected among the second sector of 22 gates. The aim of the analysis was to compare the loads acting on the left and right leg when both skis are external and when both skis are internal. The whole acquisition of the right ski was divided into cycles composed of a left turn around one gate and a right turn around the following gate. The acquisition of the left ski was divided in opposite cycles composed of a right turn and then a left turn.

The segmentation of the cycle was done using $M_{XF\ R}$ for the right ski and $M_{XF\ L}$ for the left ski. For the right ski the consecutive five cycles with the most resembling plot of M_{XF} were selected. For the left ski the five cycles starting from the immediately previous gate were chosen (*Figure 4.34*). This choice was done in order to compare the loads acting on the right leg during a right turn with the loads acting on the left leg in the following left turn. This allows to compare the left and right leg in similar conditions of gradient of the slope, snow conditions and athlete fatigue.

Each Slalom cycle was normalized in 1001 samples. The front and rear plots of F_Z, M_X and M_Y were determined in the normalized cycle and the mean curves were calculated for both skis (*Figure 4.35, Figure 4.36*).

All of this being done, the mean forces and mean moments were combined with the position of the front and rear cell, with respect to the reference system of the ski, to calculate the global ground reaction forces and ground reaction moments (*Figure 4.37*).

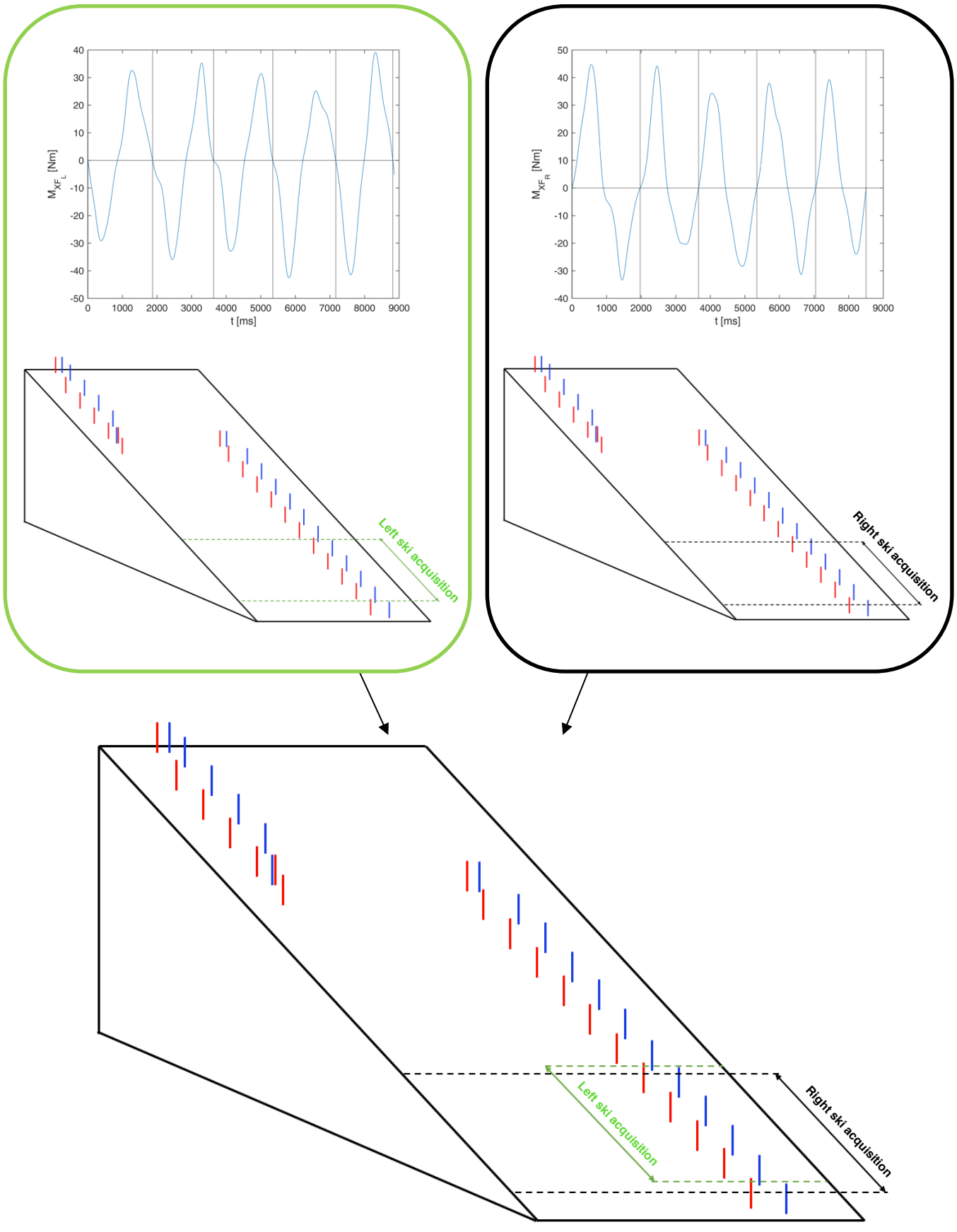

Figure 4.34. scheme of the stretch of slope used for data analysis on left and right ski

Figure 4.35. Mean Forces (left) and Mean Moments (right) acquired by the front cell (top graphs) and by the rear cell (bottom graphs) during a full slalom cycle from both left and right ski. SS3.4

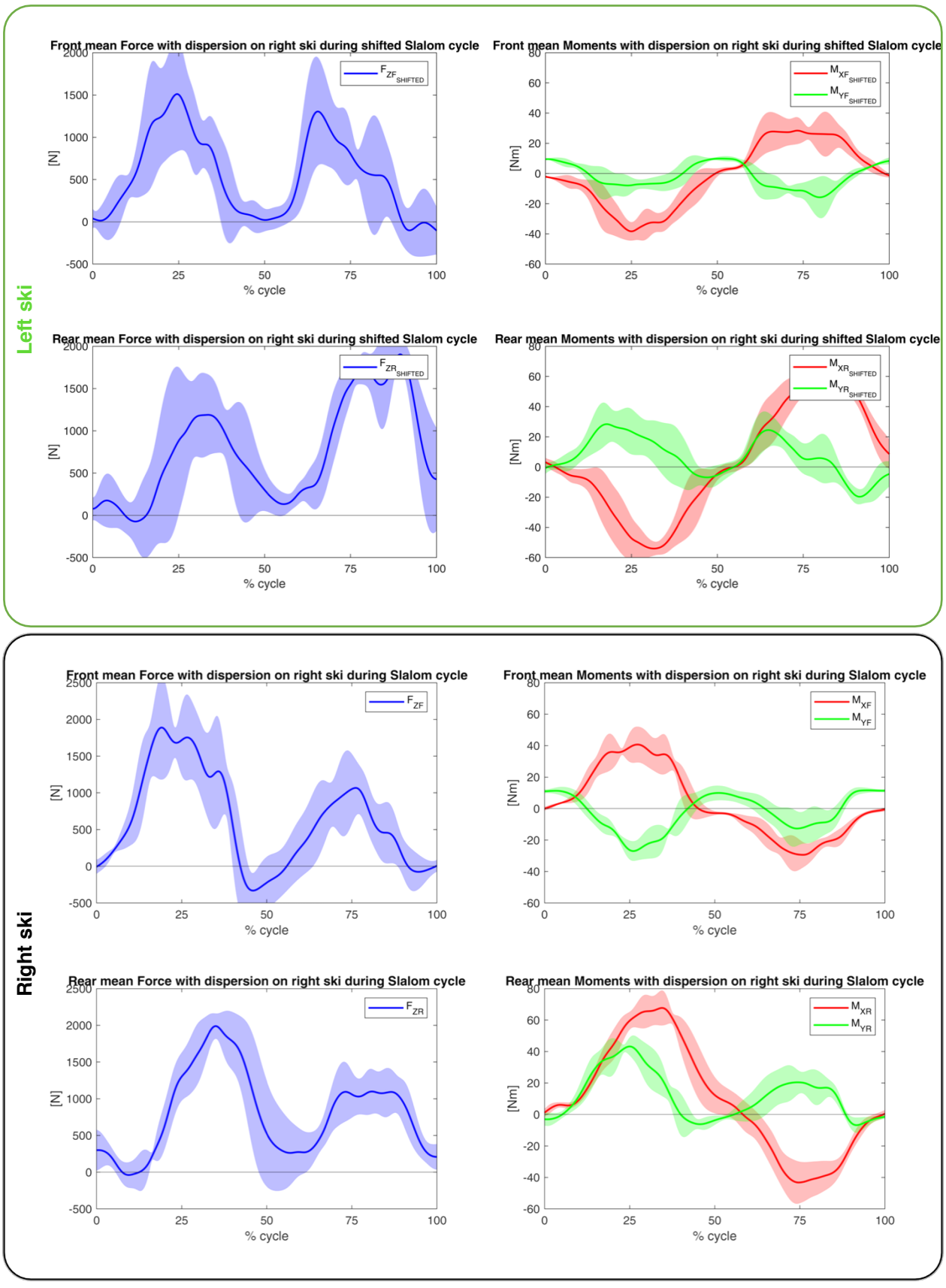

Figure 4.36. Mean Forces (left) and Mean Moments (right) acquired by the front cell (top graphs) and by the rear cell (bottom graphs) with dispersion during a full slalom cycle from both left and right ski. SS3.4

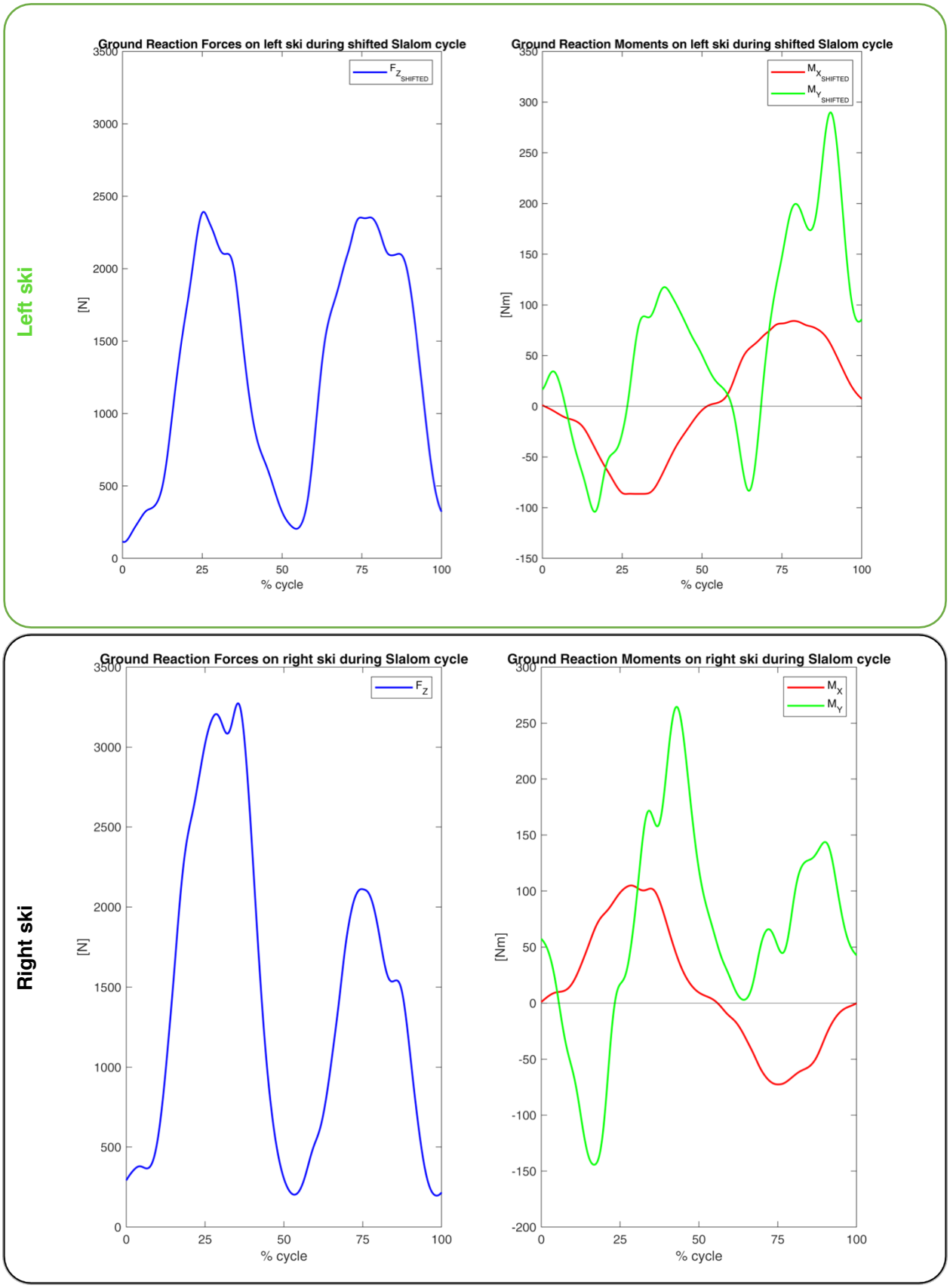

Figure 4.37. Global GRFs (left)and GRMs (right) during a full slalom cycle on left and right ski. SS3.4

The results were represented in the same graph and normalized by bodyweight BW which includes the weight of the athlete, of the acquisition system and of the ski equipment (*Figure 4.38*).

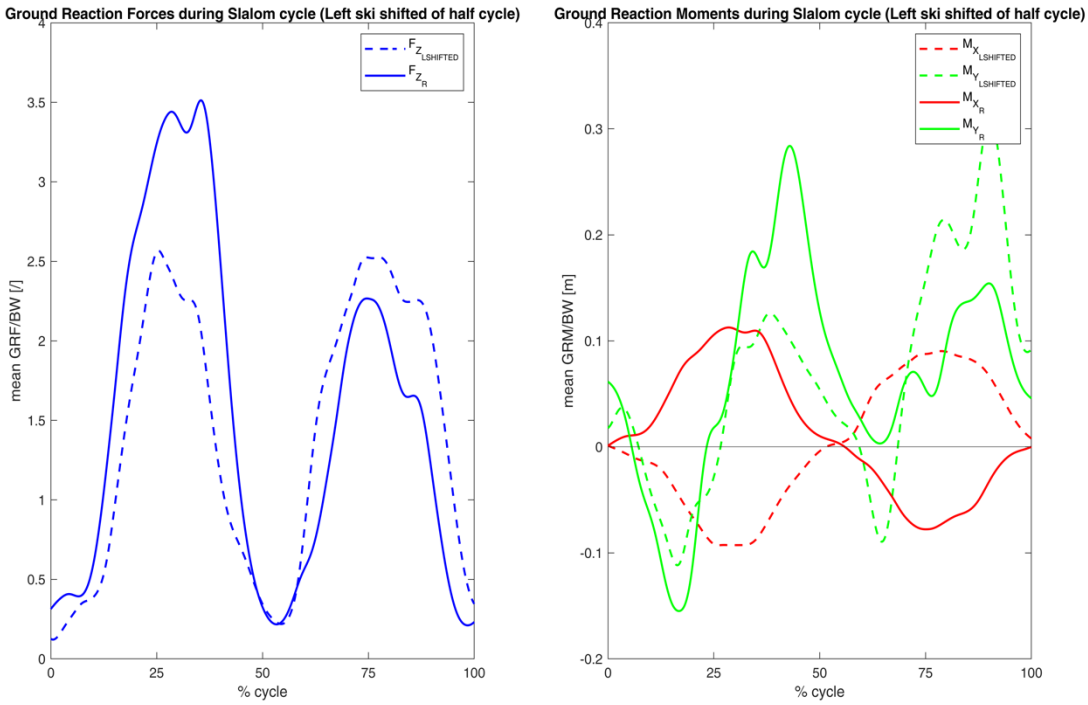

Figure 4.38. Confront of global GRFs (left)and GRMs (right) between left and right ski during a full slalom cycle. SS3.4

As previously mentioned, the cycle is different for left and right ski. The left ski cycle is composed of a right and left turn while the right ski cycles is composed of a left and a right turn. This was done to compare the loads acting on the two skis when both are in an external turn and later when both are in an internal turn.

From *Figure 4.38*, if we consider the values of F_Z is evident that the athlete can apply a greater force with his right leg then with his left leg when both are external. On the contrary, when the ski is internal the forces applied with the left and right leg are comparable. Moreover, the difference of F_Z among external and internal turns is considerable on his right leg while it's almost none on his left leg.

On the other hand, the ground reaction moments M_X and M_Y appear to be quite symmetrical between the two legs.

It's interesting to calculate the ratios between the maximum GRFs the athlete's legs can exert when they are both internal and both external. Another interesting ratio is the one between the GRFs that the athlete can exert when the same leg is internal and then external. These ratios can be considered as asymmetry indexes of the athlete.

$$\frac{F_{Z_R}\ at\ External\ peak}{F_{Z_{L\ shifted}}\ at\ External\ peak} = 1{,}414$$

$$\frac{F_{Z_R}\ at\ Internal\ peak}{F_{Z_{L\ shifted}}\ at\ Internal\ peak} = 0.897$$

$$\frac{F_{Z_R}\ at\ External\ peak}{F_{Z_R}\ at\ Internal\ peak} = 1{,}598$$

$$\frac{F_{Z_{L\ shifted}}\ at\ External\ peak}{F_{Z_{L\ shifted}}\ at\ Internal\ peak} = 1{,}012$$

These indexes can be used to improve the athlete's preparation, by identifying areas of strength and weakness and by creating specific training programs aimed to reduce these asymmetries.

Moving on, the center of pressure position during the slalom cycle was determined for both left and right skis (*Figure 4.39*). The whole cycle from 0% to 100% was considered.

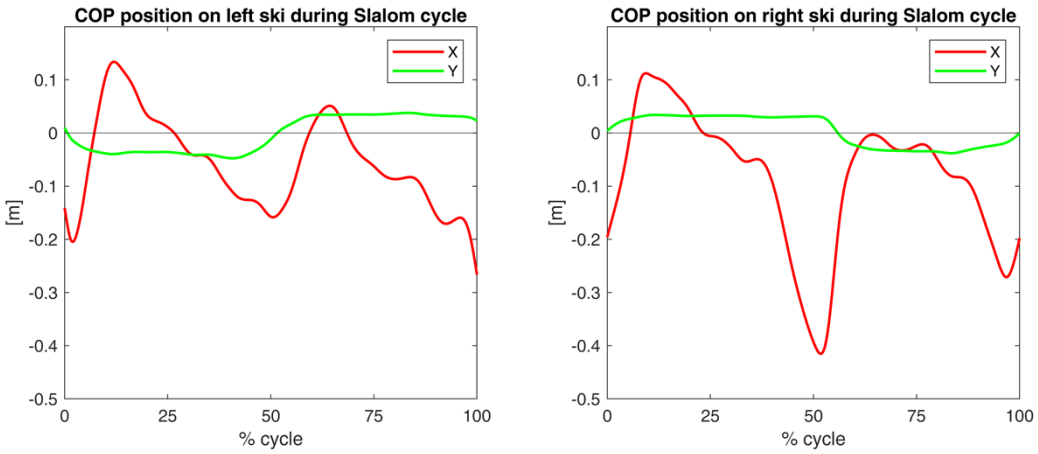

Figure 4.39. COP coordinates during the Slalom cycle on left and right. SS3.4

To get a better vision of the movement of the COP during one slalom cycle, in *Figure 4.40* its represented in the ski's XY plane. The different symbols and colors used in *Figure 4.40* represent the advancement of the cycle as shown in *Figure 4.41*.

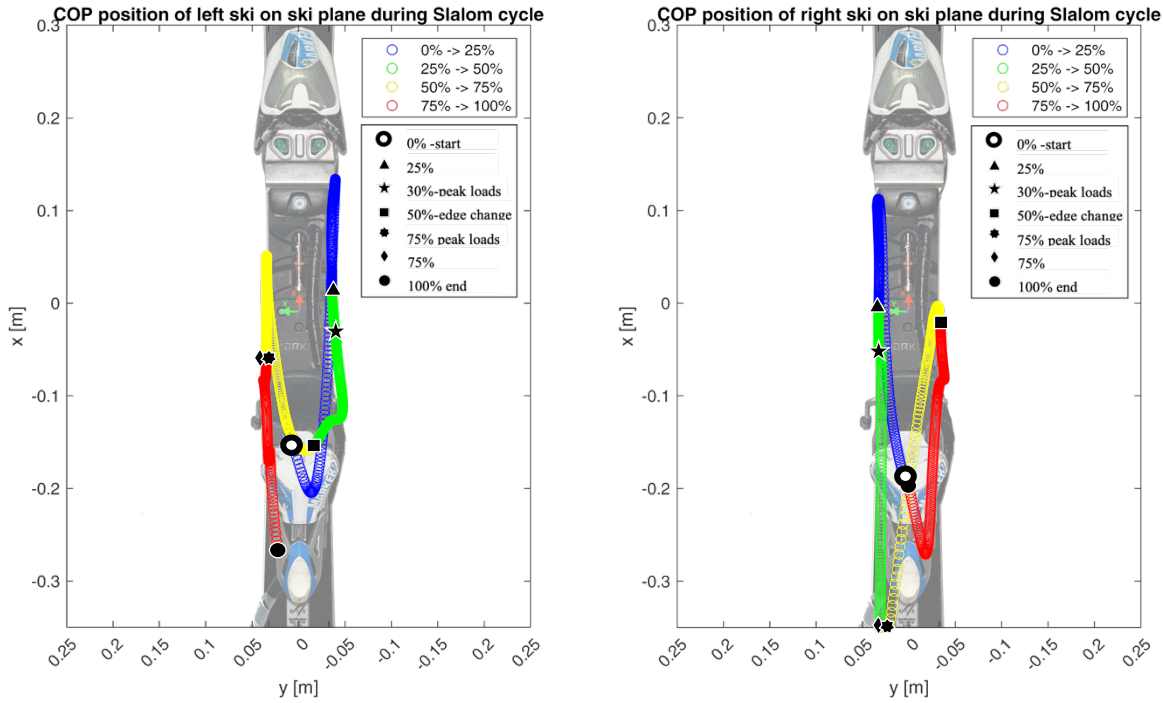

Figure 4.41. COP movement on left and right ski during Slalom cycle. SS3.4

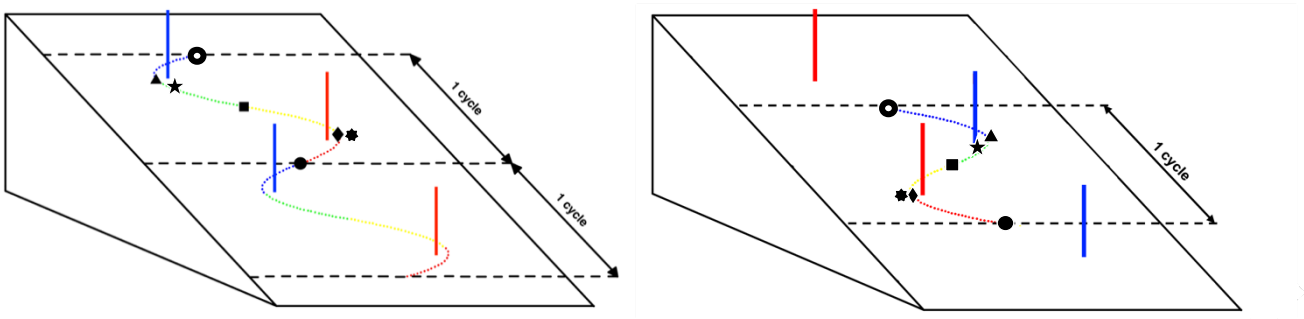

Figure 4.41. Space representation with markers

These test sessions confirm what was seen on the previous Slalom test session in Col Gallina. In both cases the peak of the loads were at 30% and at 75% of the cycle advancement, meaning that the difference with the GS could not be caused by the reconstruction of data. The athletes were different in the two test sessions so we can't say it with certainty.

The COP locus of points is also represented in isometric view in *Figure 4.42* with the corresponding value of F_Z.

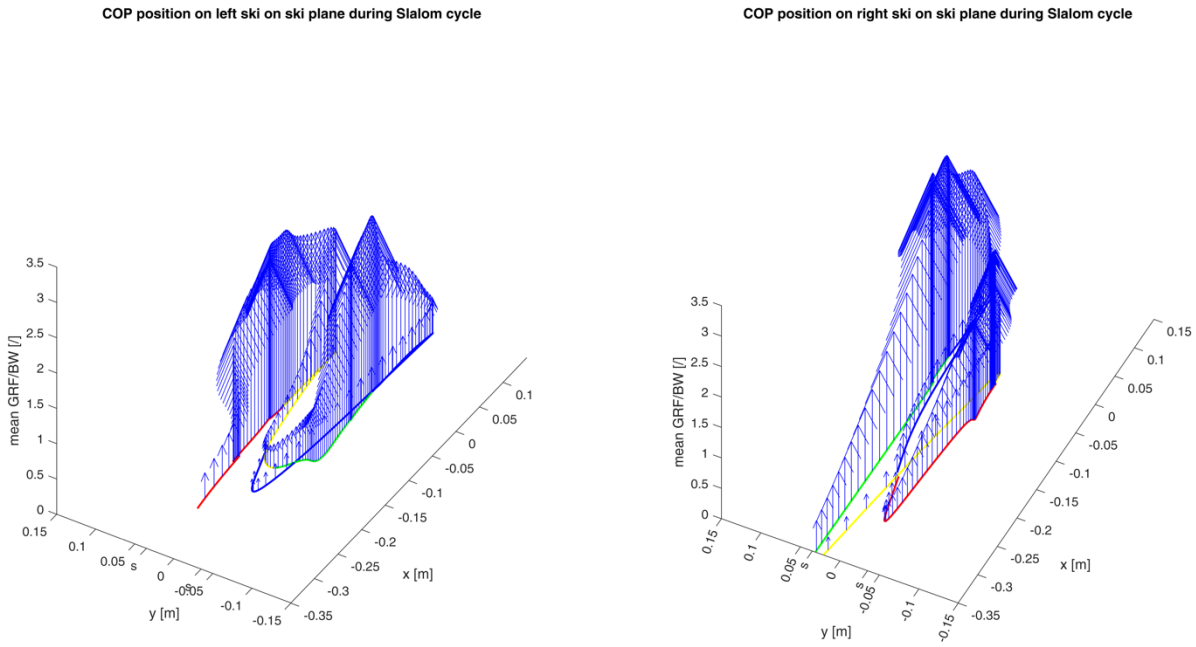

Figure 4.42. 3D plot of the COP with F_Z force value on left and right ski during Slalom cycle. SS3.4

The same analysis was done using data from the other four runs performed. All of them were done using the same portion of slope for the left and right ski. The results are showed below.

SS3.1

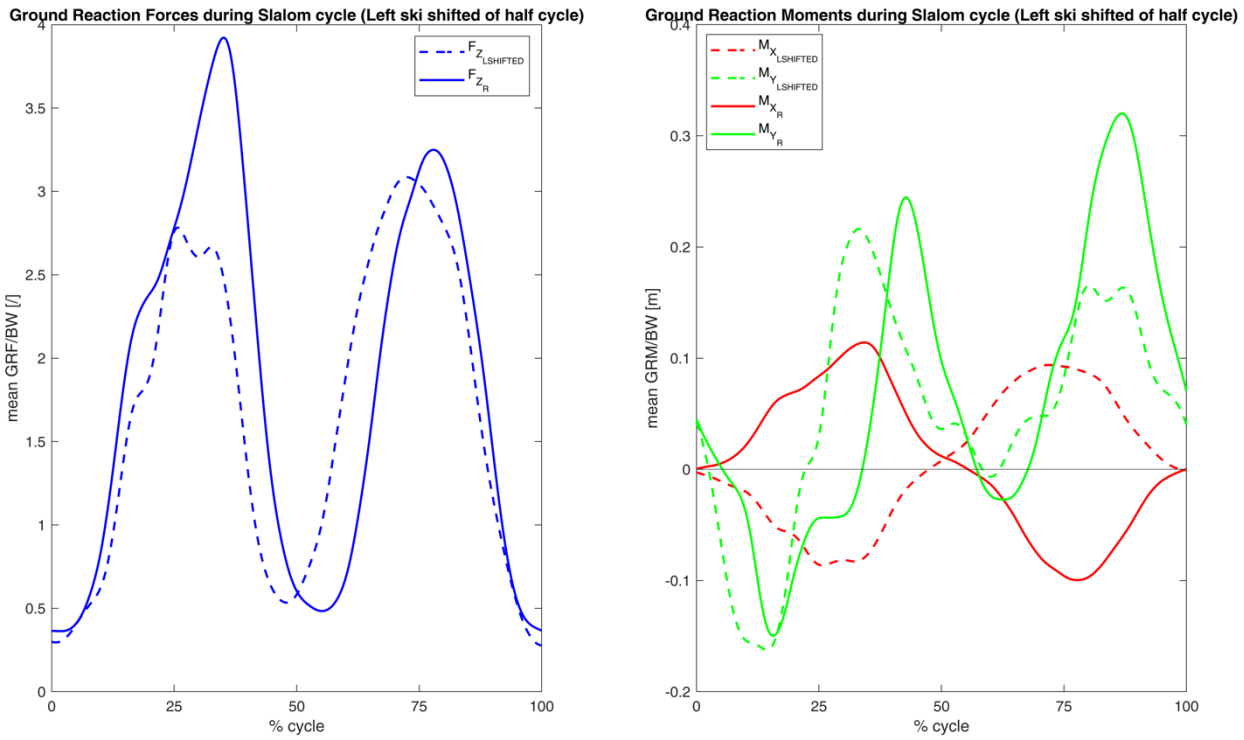

Figure 4.43. Confront of global GRFs (left)and GRMs (right) between left and right ski during a full slalom cycle. SS3.1

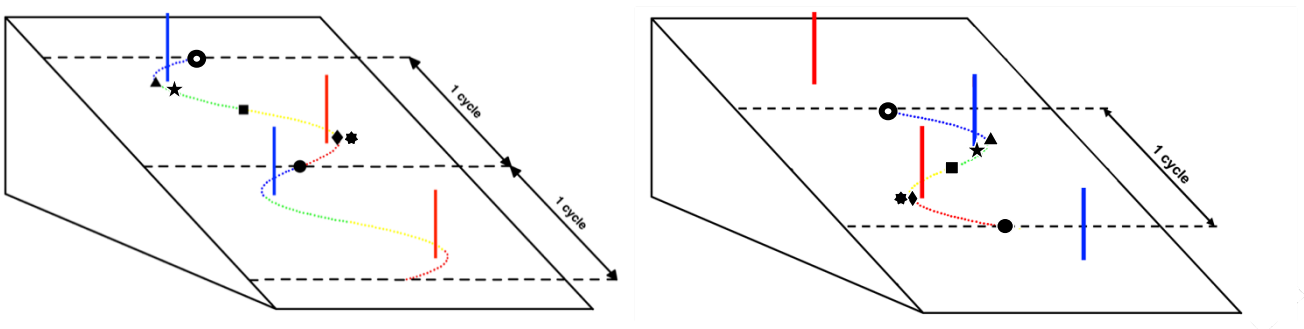

Figure 4.44. Space representation with markers

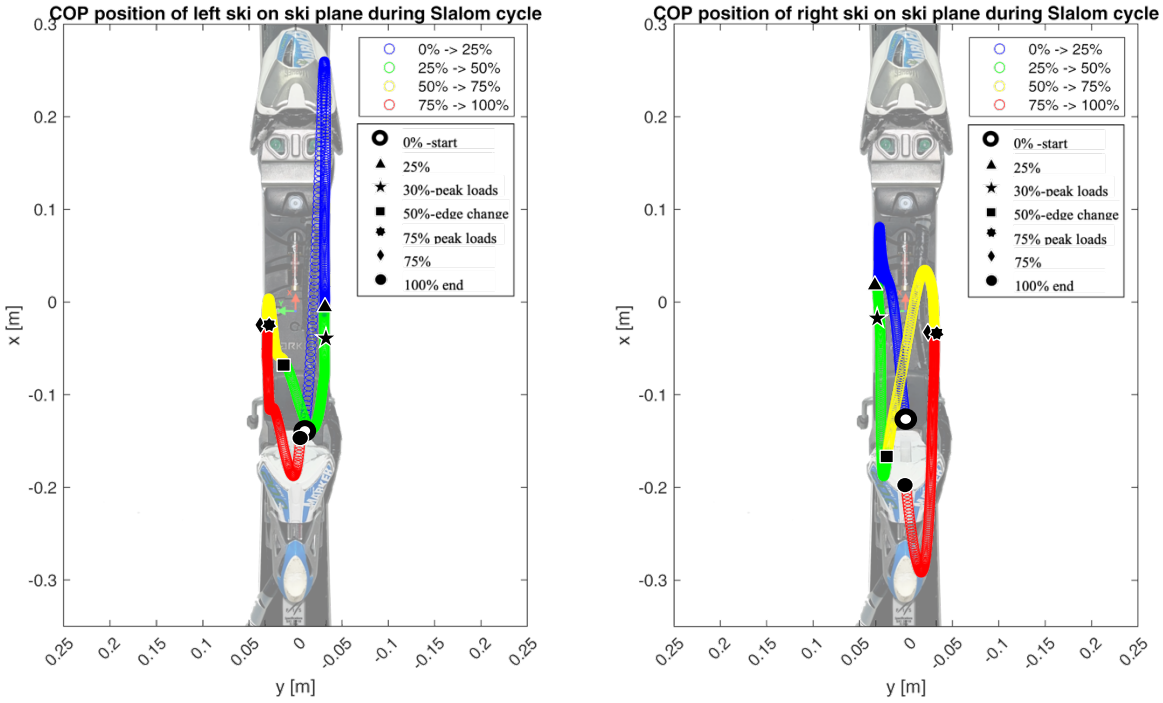

Figure 4.45. COP movement on left and right ski during Slalom cycle. SS3.1

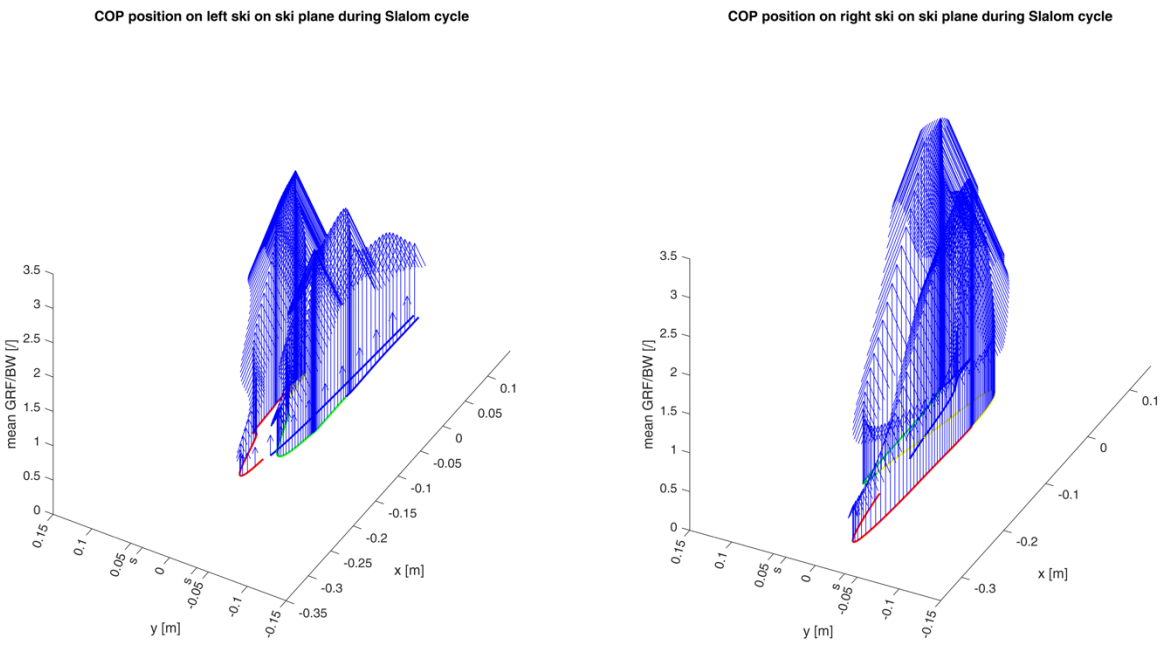

Figure 4.46. 3D plot of the COP with F_Z force value on left and right ski during Slalom cycle. SS3.1

SS3.2

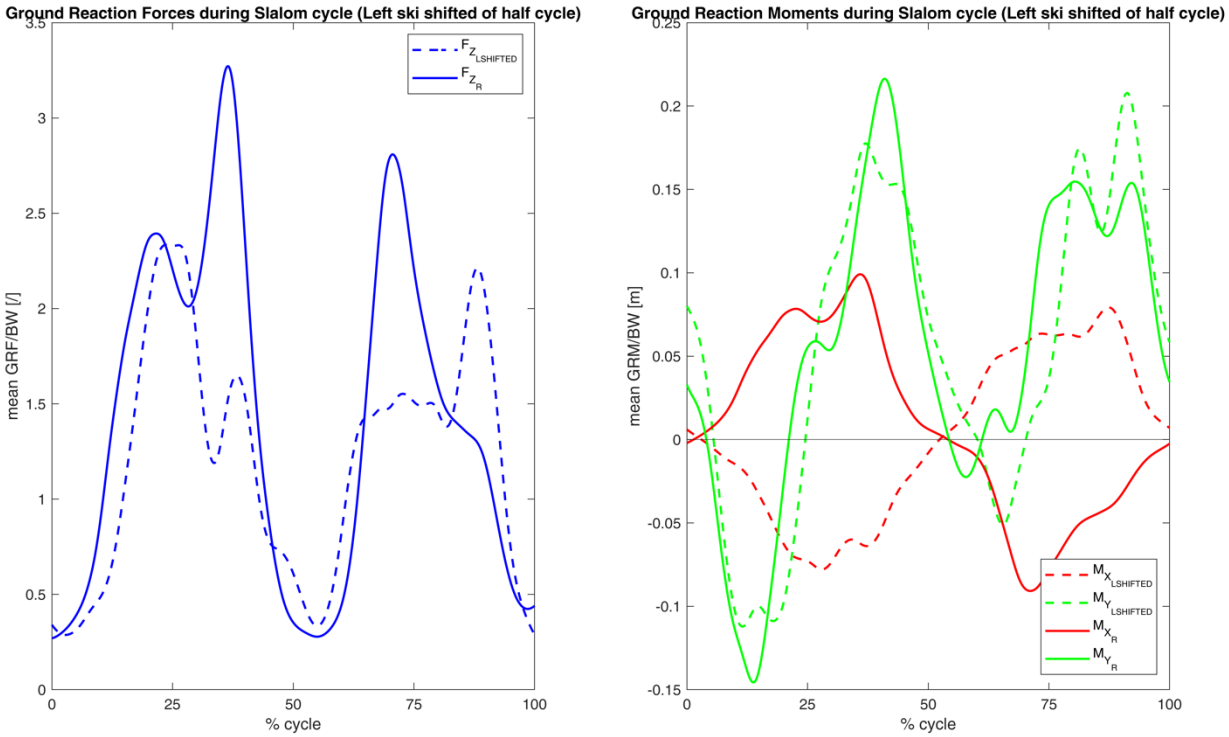

Figure 4.47. Confront of global GRFs (left)and GRMs (right) between left and right ski during a full slalom cycle. SS3.2

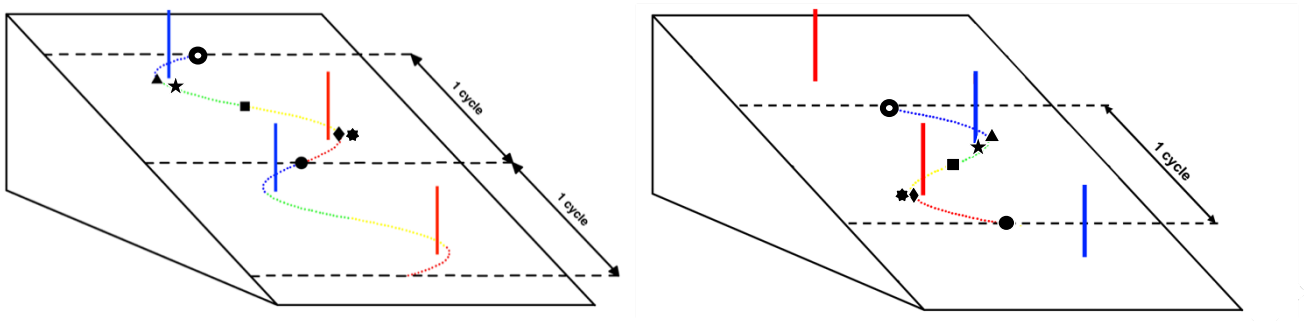

Figure 4.48. Space representation with markers

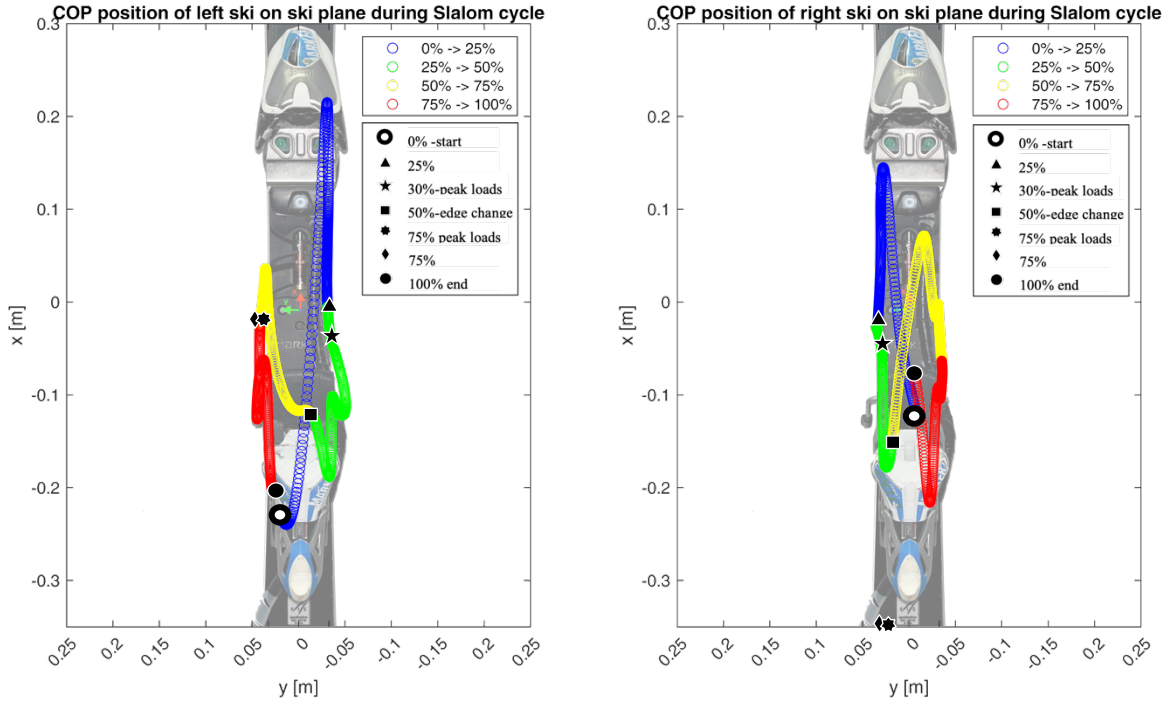

Figure 4.49. COP movement on left and right ski during Slalom cycle. SS3.22

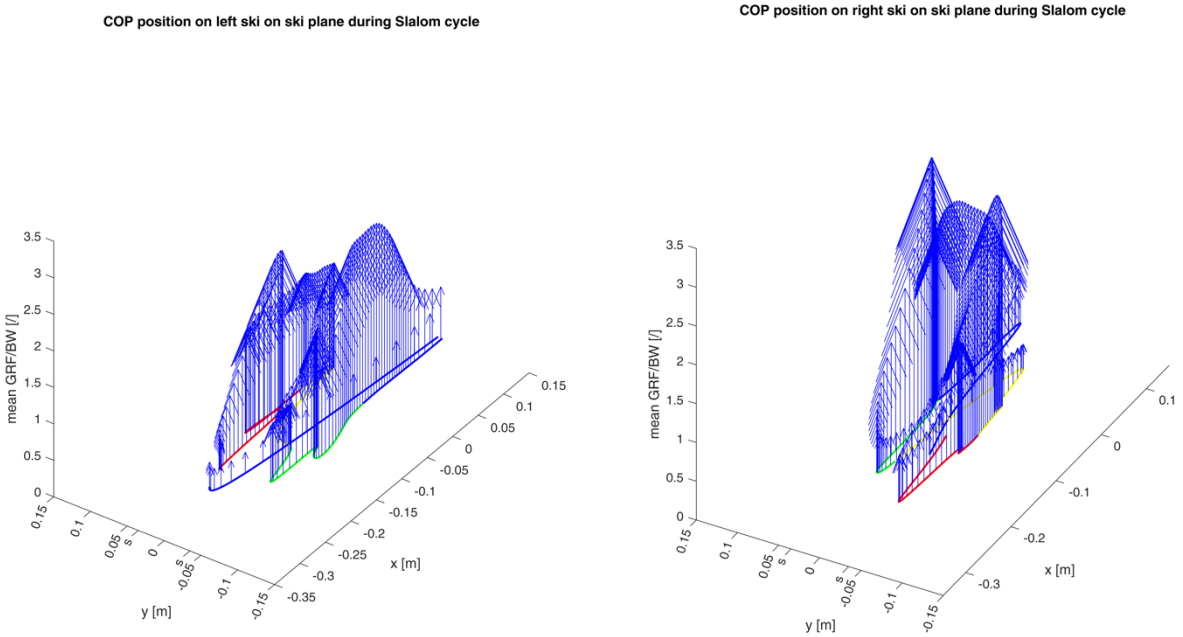

Figure 4.50. 3D plot of the COP with F_Z force value on left and right ski during Slalom cycle. SS3.2

SS3.3

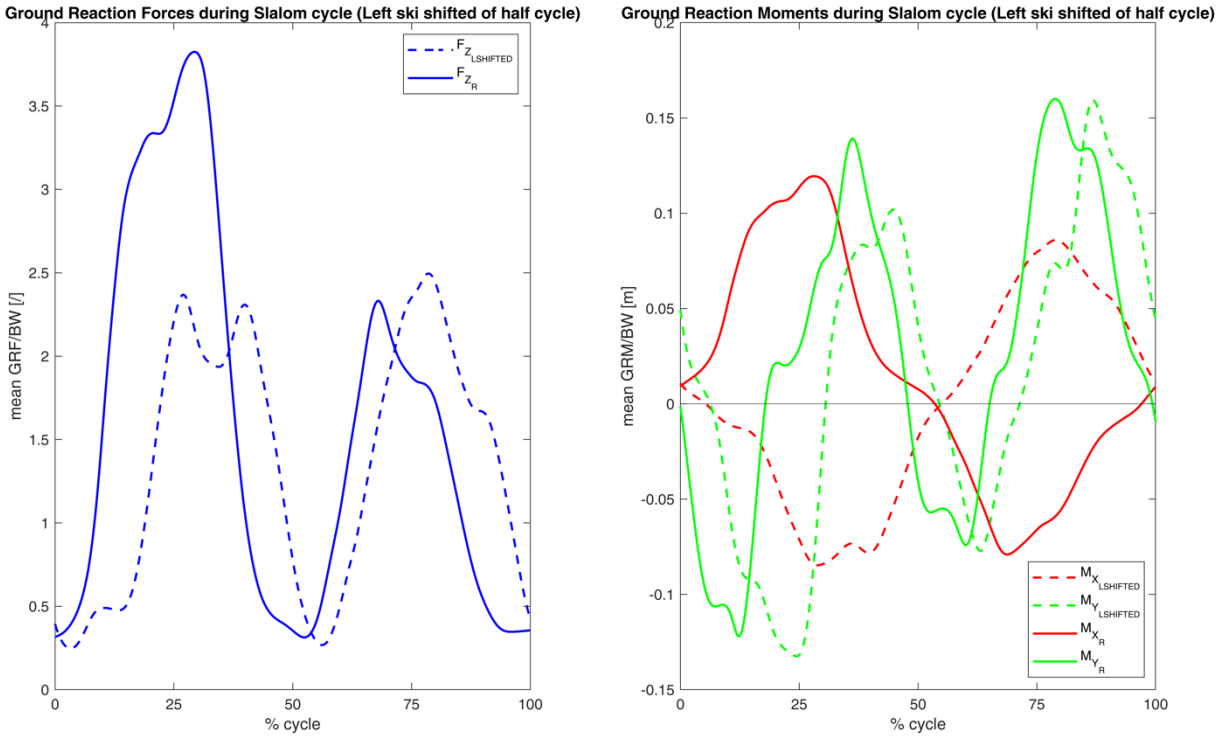

Figure 4.51. Confront of global GRFs (left)and GRMs (right) between left and right ski during a full slalom cycle. SS3.3

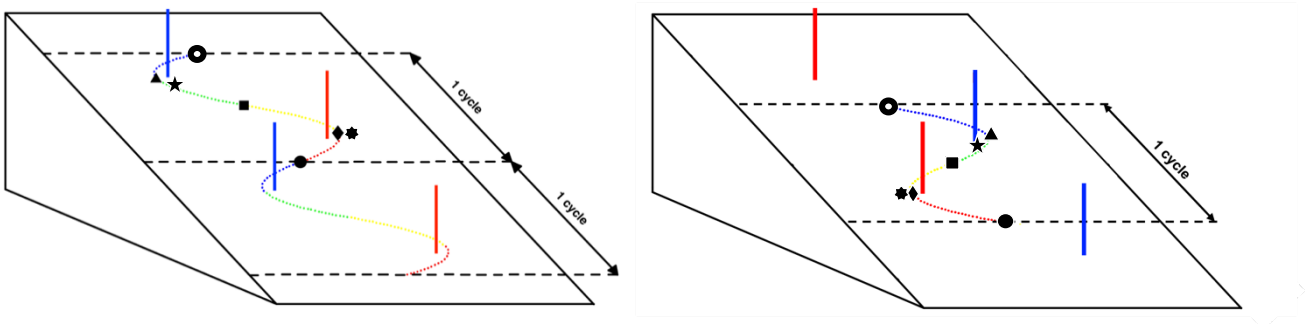

Figure 4.52. Space representation with markers

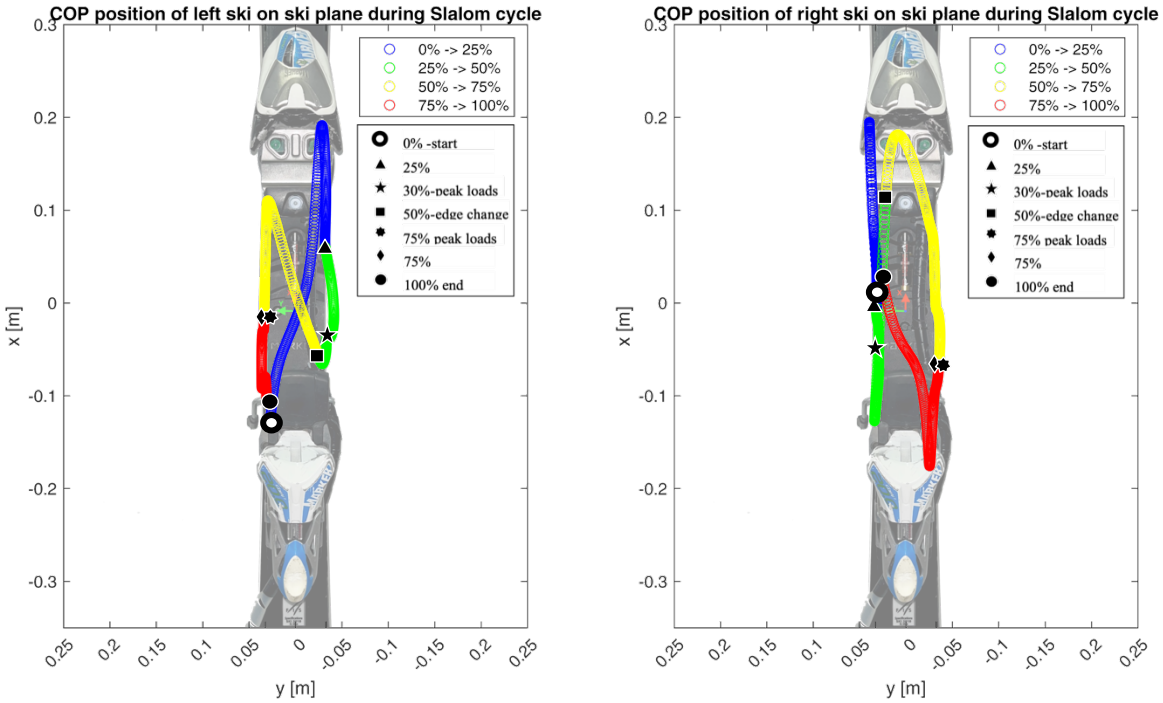

Figure 4.53. COP movement on left and right ski during Slalom cycle. SS3.3

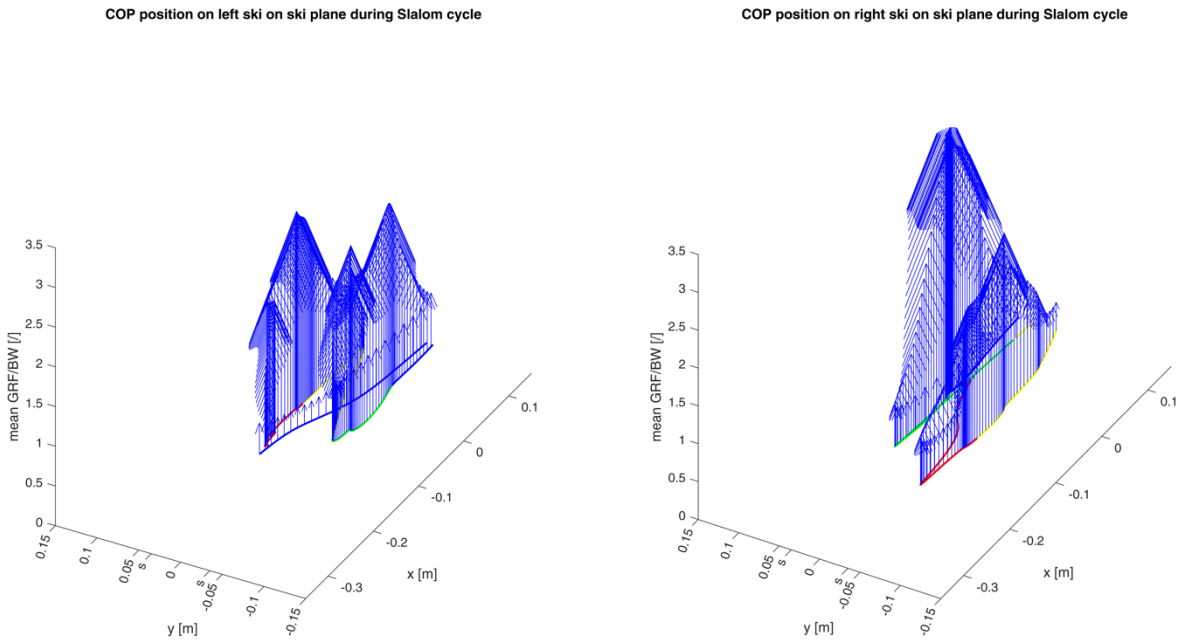

Figure 4.54. 3D plot of the COP with F_Z force value on left and right ski during Slalom cycle. SS3.3

SS3.5

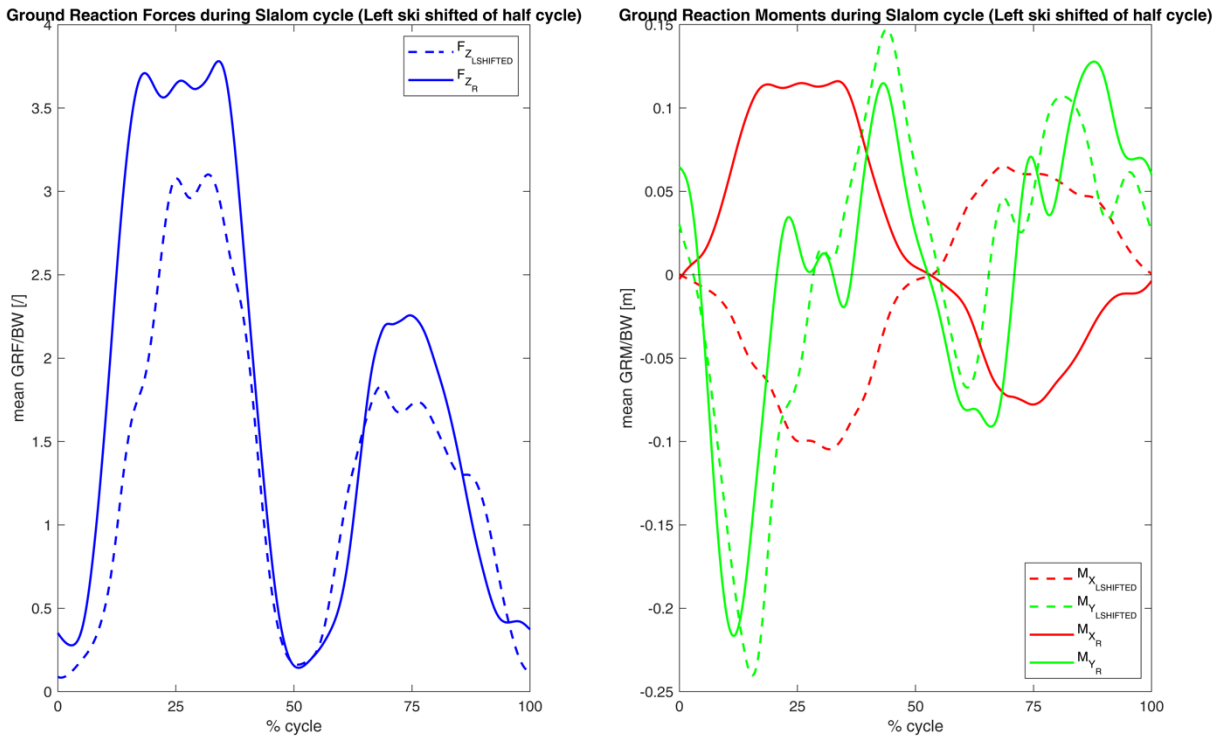

Figure 4.55. Confront of global GRFs (left)and GRMs (right) between left and right ski during a full slalom cycle. R SS3.5

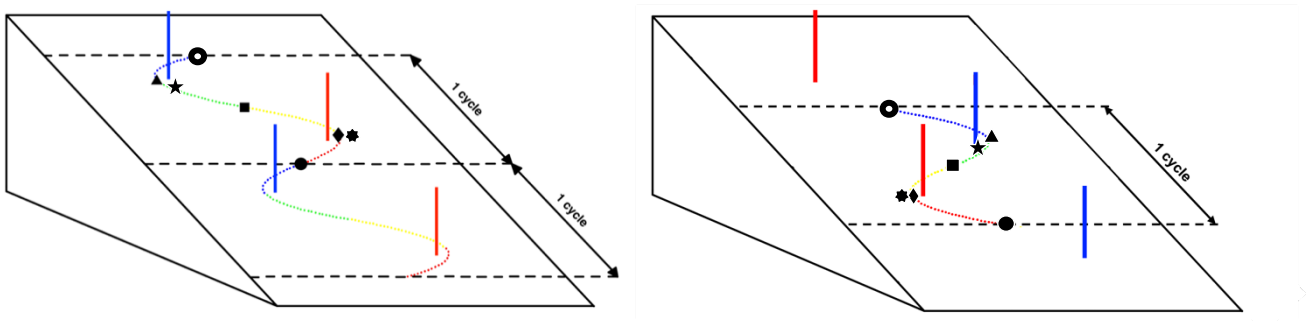

Figure 4.56. Space representation with markers

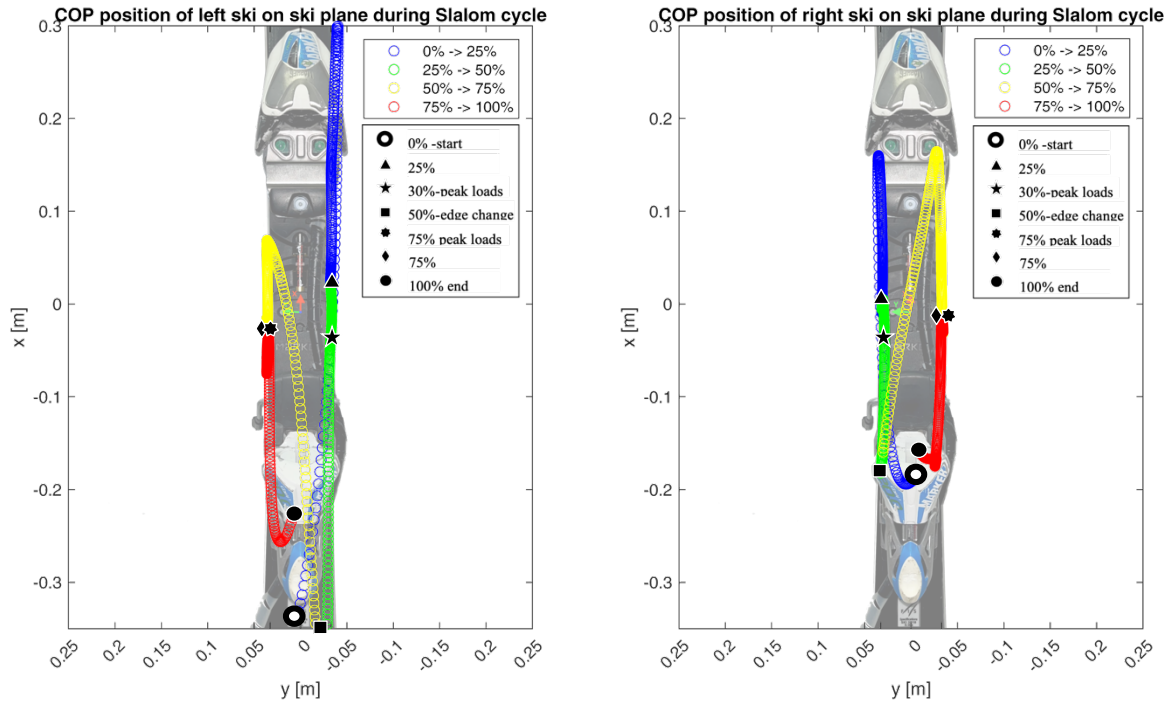

Figure 4.57. COP movement on left and right ski during Slalom cycle. SS3.5

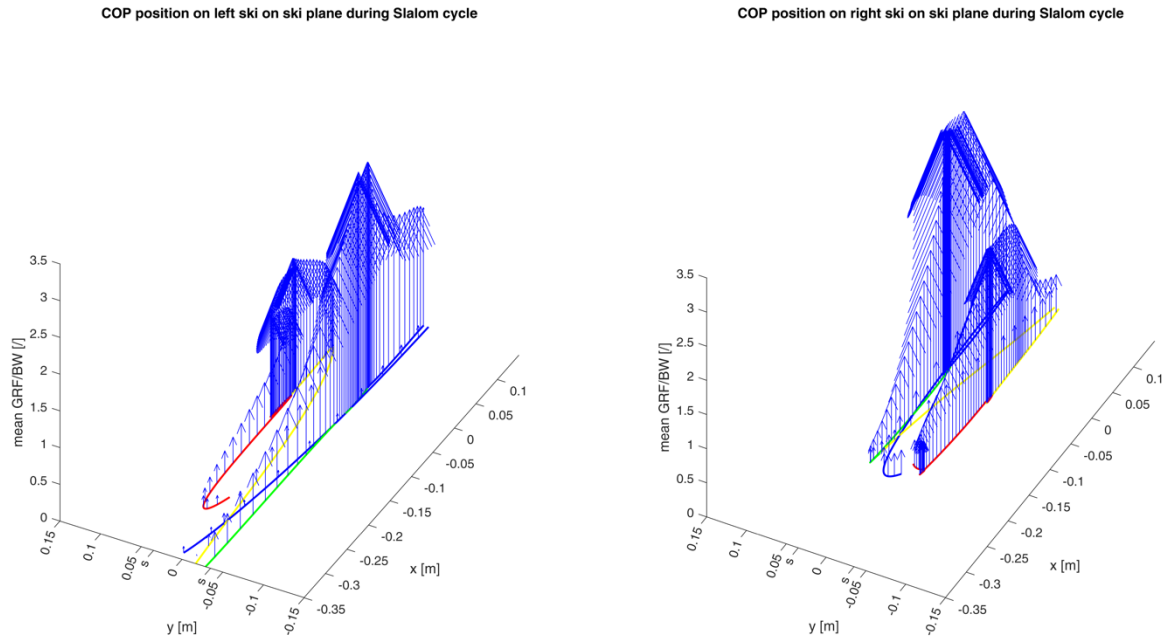

Figure 4.58. 3D plot of the COP with F_Z force value on left and right ski during Slalom cycle. SS3.5

All the other runs performed confirms what said for SS3.4. Every run is similar to the others in terms of loads and COP movement. It's interesting to see that even in the slower SS3.5, where there was less muscular activity involved, the loads are comparable if not greater to the intense SS3.4.

Overall, the athlete always applies a greater force with his right leg when it is on the extern. When the ski is internal the forces applied with the left and right leg are very similar.

The difference of F_Z among external and internal turns is considerable on his right leg while it's almost none on his left leg.

The ground reaction moments M_X and M_Y appear to be quite symmetrical between the two legs.

Also the COP is quite symmetrical, closing itself in a loop most of the times. This indicates consistency in the selected cycles and it also is an index of quality of the analysis. The right leg in general has a more compact locus of points, suggesting a greater control of the ski. On the contrary the COP of the left leg moves more in almost all runs.

5. Discussions and conclusions

The use of load measurement techniques in skiing can provide valuable insights on the loads transferred by the skier to the ground. Through a combination of laboratory-based experiments and field-based measurements, this study has investigated the loads at the snow - ski interface and at the ski - skier interface.

At the snow - ski interface the Edge Load Distribution of the Nordica prototypes and of the *Nordica SLWC* was determined for different inclinations and loads. The comparison of the resultant curves highlighted that the geometry of the skis has a deep influence on the Edge Load Distribution. It was also determined that, in general, with the increase of the inclination angle and of the applied load, the Edge Load Profile rises and its peak slides towards the tip of the ski. During the *Nordica SLWC* in vitro tests, data at the ski - leg interface were also collected. This allowed to compare the loads measured by the loadcells mounted on the ski with the applied force at the testbench. It was determined that at all inclination the loadcells values were inferior to the applied load.

The *Blizzard Firebirds GS* and *Nordica SLWC* instrumented skis were then used to measure real Giant Slalom and Slalom skiing loads. The Global Ground Reaction Forces and the Center of Pressure trends were determined during a normalized skiing cycle. The COP locus of points always showed results in accordance with the skiing experience and physical intuition.

When the *Nordica SLWC* were tested on the Edge Load Profile testbench, at 60 ° a 140 kgf load was applied. This load, as all the other loads in *Table 3.2*, come from the vectorial sum of the percentage of bodyweight that an average skier's leg can transfer to the ground (vertical component) and the centrifugal force calculated for speeds and turn radiuses compatible with the corresponding inclination (horizontal component). During the in-field tests the inclination angle was not measured, but analyzing the footage, when the skier is in full lean, a 60° inclination angle is plausible. The maximum lean occurs between 25% and 30% and between 75% and 80% of the Slalom cycle.

Considering SS3.4 as a reference, at these cycle percentages, the average values of F_Z are reported in *Figure 5.1.*

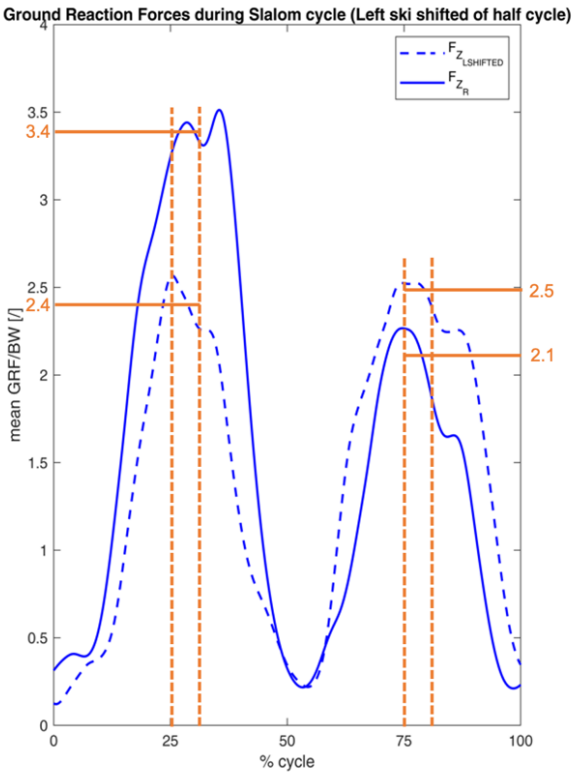

Figure 5.1. Confront of global GRFs (left) between left and right ski during a full slalom cycle. SS3.4

Recalling that the F_Z curves of the left ski are shifted of half cycle, so the 25% - 30% corresponds to 75% - 80% and vice versa, the resultant values are reported in *Table 5.1.*

	L	*R*
25% - 30%	2.5 N/BW	3.4 N/BW
	265 kgf	360.4 kgf
75%-80%	2.4 N/BW	2.1 N/BW
	254.4 kgf	222.6 kgf

Table 5.1. F_Z values on Left and Right ski at 25%-30% and 75%-80% of the Slalom cycle

The obtained values of F_Z are far from the 140 kgf applied on the Edge Load Profile testbench. This also applies for all the other test sessions. This suggests that the loads applied on the testbench of *Table 3.2* are more suitable for amateur skiing and that the obtained Edge Load Distributions are not representative of the competitive environment. Unfortunately, the in-field measured values of *Table 5.1* are impossible to apply at the testbench in the current state for both structural and power limitations. At 60° the ski flexes a lot and already at 140 kgf the central part is at risk of slipping out of the plate as visible in *Figure 5.2*.

Figure 5.2. Nordica SLWC on the ELP testbench at 60° inclination angle

A possible future development of this study could be the upgrade of the testbench to perform tests with applied loads closer to the in-field measured ones. An offset plate could be inserted between the swinging arm and the structure to allow a wider range of adjustment for the ski. This would allow the ski to be farther from the edge of the plate

during tests at 50° and 60° inclination angles. With this upgrade, tests with greater loads would be possible but the next limitation would be the power of the electric actuator. The actuator could be replaced with a more powerful one but under greater loads the ski would deform even more risking once again to slip out of the plate. Even with these two upgrades, the loads in *Table 5.1* wouldn't be reachable, but a more representative Edge Load Profile would be obtainable.

Another possible future development could be to consider the cross talk of the loadcells in the analysis in order to have more accurate measurements.

It would also be interesting to try the *Blizzard Firebird GS* on the testbench and in the 4 loadcells configuration. This would allow for a comprehensive comparison of the GRFs and COP in the Slalom and in the Giant Slalom.

Finally, when the *DTS Slice Nano* additional module will be purchased, it will be possible to acquire simultaneously all 6 channels of each cell in the 4 load cell configuration, without giving up to measure load components.

Overall, this study has demonstrated the potential of load measurement techniques improving our understanding of the forces involved in competitive skiing. By analyzing the Edge Load Profile and the Center of Pressure we have gained valuable information in the Slalom and the Giant Slalom. The methods implemented and the results obtained in this research could be used to create targeted training programs and to design optimized ski equipment. Hopefully the research in this field will keep going, analyzing in detail each and every aspect of this wonderful sport, providing more and better insights.

Bibliography

[1] T. Yoneyama, H. Kagawa, D. Tatsuno, M. Kitade, Kazutaka Osada, S. Shigehara (2021). Effect of flexural stiffness distribution of a ski on the ski–snow contact pressure in a carved turn. *Sports Engineering*, *24*.

[2] Zullo, G., Cibin, P., Bortolan, L., Botteon, M., & Petrone, N. (2023). An Innovative Compact System to Measure Skiing Ground Reaction Forces and Flexural Angles of Alpine and Touring Ski Boots. *Sensors*, *23*(2).

[3] Vaverka, F., Vodickova, S., & Elfmark, M. (2012). Kinetic Analysis of Ski Turns Based on Measured Ground Reaction Forces. In *Journal of Applied Biomechanics* (Vol. 28).

[4] L. Vanat, 2021 International Report on Snow & Mountain Tourism Overview of the key industry figures for ski resorts, no. April. 2021.

[5] A. Natri, B. D. Beynnon, C. F. Ettlinger, R. J. Johnson, and J. E. Shealy, "Alpine Ski Bindings and Injuries," Sport. Med., vol. 28, no. 1, pp. 35–48, 1999.

[6] V. Senner, F. I. Michel, S. Lehner, and O. Brügger, "Technical possibilities for optimising the ski-binding-boot functional unit to reduce knee injuries in recreational alpine skiing," Sport. Eng., vol. 16, no. 4, pp. 211–228, 2013.

[7] K. G. Shea et al., "Knee injuries in downhill skiers: A 6-year survey study," Orthop. J. Sport. Med., vol. 2, no. 1, pp. 1–6, 2014.

[8] J. Kröll, J. Spörri, M. Gilgien, H. Schwameder, and E. Müller, "Sidecut radius and kinetic energy: Equipment designed to reduce risk of severe traumatic knee injuries in alpine giant slalom ski racing," Br. J. Sports Med., vol. 50, no. 1, pp. 26–31, 2016.]

[9] M. Supej, V. Senner, N. Petrone, and H. C. Holmberg, "Reducing the risks for traumatic and overuse injury among competitive alpine skiers," Br. J. Sports Med., vol. 51, no. 1, pp. 1–2, 2017.

[10] F. Nimmervoll, R. Eckerstorfer, J. Braumann, A. Petutschnigg, and B. Sternad, “Method to Investigate Multi-Axis Release Action of Ski Safety Bindings: A New Approach for Testing in Research and Development,” Front. Sport. Act. Living, vol. 3, no. February, pp. 1–13, 2021.

[11] ISO, “ISO 9462 : 2014 Alpine ski-bindings — Requirements and test methods.” 2014.

[12] M. L. Hull and C. D. Mote, “Analysis of leg loading in snow skiing,” J. Dyn. Syst. Meas. Control. Trans. ASME, vol. 100, no. 3, pp. 177–186, 1978.

[13] N. Scott, T. Yoneyama, H. Kagawa, and M. Takahashi, “Measurement of joint motion and acting forces on a top athlete skiing,” Hubbard M Eng. Sport. vol 5. Int. Sport. Eng. Assoc., pp. 494–502, 2004.

[14] E. F. Moritz, S. Haake, M. Kiefmann, A.; Krinninger, U. Lindemann, V. Senner, and P. Spitzenpfeil, “A New Six Component Dynamometer for Measuring Ground Reaction Forces in Alpine Skiing,” Eng. Sport 6, 2006.

[15] M. Klous, E. Müller, and H. Schwameder, “Three-dimensional lower extremity joint loading in a carved Ski and snowboard turn: A pilot study,” Comput. Math. Methods Med., vol. 2014, 2014.

[16] F. Meyer, A. Prenleloup, and A. Schorderet, “Development of a New Embedded Dynamometer for the Measurement of Forces and Torques at the Ski-Binding Interface,” Sensors, pp. 1–11, 2019.

[17] N. Petrone, D. Vanzetto, G. Marcolin, B. Bruhin, and M. Gilgien, “The effect of foot setting on kinematic and kinetic skiing parameters during giant slalom: A single subject study on a Paralympic gold medalist sit skier.,” J. Sci. Med. Sport, vol. 24, no. 10, pp. 1049–1054, Oct. 2021.

[18] N. Petrone, G. Marcolin, E. Centofante, and B. Atzori, “Analysis of the structural behavior of an innovative reinforced ski boot,” Procedia Eng., vol. 2, no. 2, pp. 2599–2604, 2010.

[19] N. Petrone, G. Marcolin, and F. A. Panizzolo, “The effect of boot stiffness on field and laboratory flexural behavior of alpine ski boots,” Sport. Eng., vol. 16, no. 4, pp. 265–280, 2013.

[20] N. Petrone, G. Marcolin, M. Cognolato, P. Hofer, and W. Nachbauer, “The effect of buckle closure and temperature on the in-vivo flexibility of ski-boots: A pilot study,” Procedia Eng., vol. 72, pp. 630–635, 2014.

[21] G. Zullo, P. Cibin, and N. Petrone, “Torsion and bending loads on a ski-touring boot shell during uphill and downhill skiing [in press],” Sport. Eng.

[22] P. Rowe, C. Myles, S. Hillmann, and M. Hazlewood, “Validation of flexible electrogoniometry as a measure of joint kinematics,” Physiotherapy, vol. 87, no. 9, pp. 479–488, 2001.

[23] K. Nakazato, P. Scheiber, and E. Müller, “A comparison of ground reaction forces determined by portable force-plate and pressure-insole systems in alpine skiing,” J. Sport. Sci. Med., vol. 10, no. 4, pp. 754–762, 2011.